


Summer 2014

Hybrid nanomaterial and its applications: IR sensing and energy harvesting

Yi-Hsuan Tseng

Follow this and additional works at: <https://digitalcommons.latech.edu/dissertations>

 Part of the [Electrical and Computer Engineering Commons](#), and the [Nanoscience and Nanotechnology Commons](#)

**HYBRID NANOMATERIAL AND ITS APPLICATIONS:
IR SENSING AND ENERGY HARVESTING**

by

Yi-Hsuan Tseng, B.E, M.S.

A Dissertation Presented in Partial Fulfillment
of the Requirement of the Degree
Doctor of Philosophy

COLLEGE OF ENGINEERING AND SCIENCE
LOUISIANA TECH UNIVERSITY

August 2014

UMI Number: 3662462

All rights reserved

INFORMATION TO ALL USERS

The quality of this reproduction is dependent upon the quality of the copy submitted.

In the unlikely event that the author did not send a complete manuscript and there are missing pages, these will be noted. Also, if material had to be removed, a note will indicate the deletion.



UMI 3662462

Published by ProQuest LLC 2015. Copyright in the Dissertation held by the Author.

Microform Edition © ProQuest LLC.

All rights reserved. This work is protected against unauthorized copying under Title 17, United States Code.



ProQuest LLC
789 East Eisenhower Parkway
P.O. Box 1346
Ann Arbor, MI 48106-1346

LOUISIANA TECH UNIVERSITY

THE GRADUATE SCHOOL

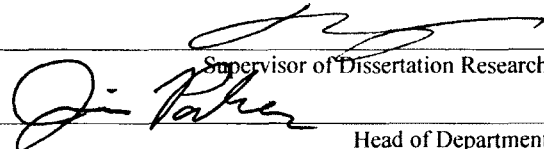
May 16, 2014

Date

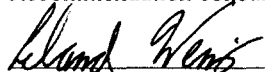
We hereby recommend that the dissertation prepared under our supervision
by Yi-Hsuan Tseng, MS


entitled Hybrid Nanomaterial and Its Applications: IR Sensing and Energy Harvesting

be accepted in partial fulfillment of the requirements for the Degree of
Ph.D in Engineering in Micro and Nanoscale Systems Concentration


Supervisor of Dissertation Research
Head of Department
Engineering
Department

Recommendation concurred in:





Sandra Zivanovic


Advisory Committee


Ji Fang (LO)

Approved:


Director of Graduate Studies

Approved:


Dean of the Graduate School


Dean of the College

ABSTRACT

In this dissertation, a hybrid nanomaterial, single-wall carbon nanotubes-copper sulfide nanoparticles (SWNTs-CuS NPs), was synthesized and its properties were analyzed. Due to its unique optical and thermal properties, the hybrid nanomaterial exhibited great potential for infrared (IR) sensing and energy harvesting.

The hybrid nanomaterial was synthesized with the non-covalent bond technique to functionalize the surface of the SWNTs and bind the CuS nanoparticles on the surface of the SWNTs. For testing and analyzing the hybrid nanomaterial, SWNTs-CuS nanoparticles were formed as a thin film structure using the vacuum filtration method. Two conductive wires were bound on the ends of the thin film to build a thin film device for measurements and analyses. Measurements found that the hybrid nanomaterial had a significantly increased light absorption (up to 80%) compared to the pure SWNTs. Moreover, the hybrid nanomaterial thin film devices exhibited a clear optical and thermal switching effect, which could be further enhanced up to ten times with asymmetric illumination of light and thermal radiation on the thin film devices instead of symmetric illumination. A simple prototype thermoelectric generator enabled by the hybrid nanomaterials was demonstrated, indicating a new route for achieving thermoelectricity. In addition, CuS nanoparticles have great optical absorption especially in the near-infrared region. Therefore, the hybrid nanomaterial thin films also have the potential for IR sensing applications.

The first application to be covered in this dissertation is the IR sensing application. IR thin film sensors based on the SWNTs-CuS nanoparticles hybrid nanomaterials were fabricated. The IR response in the photocurrent of the hybrid thin film sensor was significantly enhanced, increasing the photocurrent by 300% when the IR light illuminates the thin film device asymmetrically. The detection limit could be as low as 48mW mm^{-2} . The dramatically enhanced sensitivity and detection limit were due to the temperature difference between the two junctions formed by the nano hybrid thin film and copper-wire electrodes under asymmetric IR illumination, and the difference between the effective Seebeck coefficient of the nano hybrid thin film and that of the Cu wires. The IR sensor embedded in polydimethylsiloxane (PDMS) layers was also fabricated and tested to demonstrate its potential application as a flexible IR sensor.

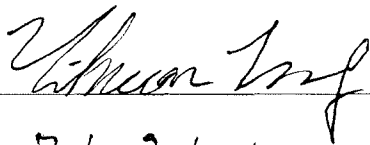
In another application, energy harvesting, a new type of thermoelectric microgenerator enabled with the SWNTs-CuS nanoparticles hybrid nanomaterial, was fabricated. This type of microgenerator did not require any cooling or heat sink element to maintain the temperature difference or gradient in the device. Instead, the integrated nanomaterials in the device enhanced the local temperature and thus produced and maintained an intrinsic temperature difference or gradient across the microgenerator, thereby converting light and heat directly into electricity. In order to enhance the maximum output voltage, the incoming light had to be focused on the thin film region. A tunable lens was fabricated to collect and focus the ambient light on the thin film to enhance the output voltage of the microgenerators. The tunable lens was fabricated with a flexible polymer, PDMS. Therefore, the focal length of the tunable lens can be adjusted by pumping oil into the lens chamber to deform a PDMS membrane, resulting in the

changed focus of the lens. In order to enhance the output power, two different arrays of thermoelectric generators in series and in parallel were fabricated. A hybrid nanomaterial thin film was also used to enhance the temperature gradient of the thermoelectric generators. For the devices in series, the generated voltage of all thermoelectric generators was combined together to enhance the output voltage. With the device in parallel, it can be used to combine all of the current of thermoelectric generators together to enhance the output current.

APPROVAL FOR SCHOLARLY DISSEMINATION

The author grants to the Prescott Memorial Library of Louisiana Tech University the right to reproduce, by appropriate methods, upon request, any or all portions of this Dissertation. It is understood that "proper request" consists of the agreement, on the part of the requesting party, that said reproduction is for his personal use and that subsequent reproduction will not occur without written approval of the author of this Dissertation. Further, any portions of the Dissertation used in books, papers, and other works must be appropriately referenced to this Dissertation.

Finally, the author of this Dissertation reserves the right to publish freely, in the literature, at any time, any or all portions of this Dissertation.

Author 
Date 7/27/2014

DEDICATION

This dissertation is dedicated to my parents for their love, endless support and encouragements.

TABLE OF CONTENTS

ABSTRACT.....	iii
DEDICATION	vii
LIST OF TABLES.....	xii
LIST OF FIGURES	xiii
ACKNOWLEDGEMENTS.....	xix
CHAPTER 1 INTRODUCTION.....	1
1.1 Nanomaterials	2
1.1.1 Graphene and CNTs	2
1.1.2 Nanoparticles	4
1.1.3 Hybrid Nanomaterials.....	6
1.2 Applications of Hybrid Nanomaterial.....	7
1.2.1 Infrared Sensing.....	7
1.2.2 Energy Harvesting	10
1.3 Previous Work and Problems.....	16
1.3.1 Infrared Sensing.....	16
1.3.2 Solar and Thermal Energy Harvesting.....	18
1.4 Dissertation Objectives.....	20
1.5 Organization of Dissertation.....	20

CHAPTER 2 CARBON NANOTUBES AND COPPER SULFIDE NANOPARTICLES	22
2.1 Carbon Nanotubes.....	22
2.2 Properties of Carbon Nanotube.....	23
2.2.1 Mechanical Properties of CNTs.....	24
2.2.2 Electronic Properties of CNTs.....	24
2.2.3 Thermal Properties of CNTs.....	27
2.2.4 Thermal Conductivity of CNTs	28
2.2.5 Optical Properties of CNTs.....	30
2.3 Nanoparticles.....	31
2.3.1 Surface Plasmon Resonances.....	32
2.3.2 Quantum Confinement.....	33
2.4 CuS Semiconducting Nanoparticles	34
2.4.1 CuS Nanoparticles Synthesis	34
2.4.2 Optical and Thermal Property.....	35
CHAPTER 3 OPTICAL AND THERMAL PROPERTIES OF SWNTs-CuS HYBRID NANOMATERIAL	38
3.1 Introduction.....	38
3.2 Experiments Setup and Measurements	41
3.2.1 Materials	41
3.2.2 Synthesis of SWNTs-CuS NP Hybrid Nanomaterials	41
3.2.3 Fabrication of Devices Based on SWNTs-CuS NPs Hybrid Nanomaterials	43
3.2.4 Synthesis the Hybrid Nanomaterial Thin Films.....	44
3.3 Results and Discussion	46

3.4 Summary	57
CHAPTER 4 ULTRASENSITIVE THIN FILM INFRARED SENSORS ENABLED BY HYBRID NANOMATERIALS	58
4.1 Introduction.....	58
4.2 Experiment Setup and Measurements.....	60
4.2.1 Fabrication of IR Sensors on a Glass Substrate	61
4.2.2 IR Light Source and IR Sensing Measurements	61
4.3 Results and Discussion	62
4.4 Summary	68
CHAPTER 5 USING NANOMATERIALS FOR LOCAL TEMPERATURE ENHANCEMENT FOR THERMOELECTRIC MICROGENERATORS	70
5.1 Introduction.....	70
5.2 Thermoelectric Microgenerators Embedded Hybrid Nanomaterial	72
5.2.1 Device and its Operation Principle	72
5.2.2 Fabrication Process of Thermoelectric Microgenerators	74
5.2.3 Experiment Setup and Measurements.....	76
5.3 Tunable Lens Fabrication and the Measurement Results	81
5.3.1 Measurement Setup and Results	82
5.4 Array of Thermoelectric Microgenerators Fabrication and the Measurement Results.....	85
5.4.1 Measurement Setup and Results	88
5.5 Summary	92
CHAPTER 6 CONCLUSIONS AND FUTURE WORK.....	93
6.1 Conclusions.....	93

6.2 Future Work	97
REFERENCES	101

LIST OF TABLES

Table 1-1	Basic structure properties of natural diamond, graphene, and CNTs at room temperature [22,23].....	2
Table 1-2	The brief descriptions of different IR regions [29]	9
Table 1-3	The IR wavelength division with ISO 20473	9
Table 1-4	Introducing the different types of green energies	11
Table 2-1	Important characteristics of CNTs [2].....	23
Table 2-2	The comparison of young's modulus and tensile strength between SWNT, MWNT, and stainless steel [10].....	24
Table 6-1	Simulation results of different thickness of isolator layer in thermoelectric generators.....	99

LIST OF FIGURES

Figure 1-1	A basic structure of CNTs thin film IR sensor and small image shows the surface of the thin film [35]	16
Figure 2-1	(A) shows a sketch of single SWNT and (B) shows a sketch of single MWNT [5]	23
Figure 2-2	The sp^2 hybridization structure of CNT [5]	25
Figure 2-3	(A) shows the definition of CNT geometry structure by change the rolling up vector of CNT; zigzagCNT ($\theta = 0$), chiral CNT (θ between 0 to 30), armchair CNT ($\theta = 30$). (Ba) is zigzag structure, (Bb) is chiral CNT, (Bc) is armchair CNT [11]	26
Figure 2-4	(8,0) shows CNT is metallic. (7,1) shows CNT is a narrow gap semiconductor. (5,5) shows CNTs is a wide gap semiconductor [12]	27
Figure 2-5	The simulation of the relation between the thermal conductivity of CNTs and temperature with different lengths of CNTs [14]	29
Figure 2-6	The simulation of the relation between the thermal conductivity of CNTs and temperature with shorter lengths of CNTs [14].....	29
Figure 2-7	The Relation between Temperature and thermal conductive in different electronic states of CNTs [13].....	30
Figure 2-8	The Raman spectroscopy of single-wall carbon nanotube.....	31
Figure 2-9	Color changed in different sizes of nanoparticles [18]	32
Figure 2-10	The sketch of the surface plasmon resonance effect on metal nanoparticles [21].....	33
Figure 2-11	The quantum confinement effect in (A) buck semiconductor and (B) nano-size semiconductor of the spatial electronic state [20]	34
Figure 2-12	The equipment for synthesize the CuS nanoparticles	35

Figure 2-13	A UV-vis-NIR absorption spectra of CuS nanoparticles [16]	36
Figure 2-14	A heat generating experiment to measure the temperature change in control and CuS nanoparticles solutions. The two solutions are exposed to NIR light in 15 min [16].....	37
Figure 3-1	The brief processes flows of synthesis SWNTs-CuS hybrid nanomaterial.....	42
Figure 3-2	(a) shows a 100ml of the SWNTs-CuS NPs hybrid nanomaterial solution. (b) shows the vacuum tube is drawing the liquid down to the bottom flask. (c) shows a SWNTs-CuS NPs thin film uniformly deposited on the top of the MCE membrane. (d) shows the MCE membrane with the SWNTs-CuS NPs thin film.....	45
Figure 3-3	(a) shows TEM image of SWNTs -CuS NPs hybrid nanomaterial. (b) shows SEM image of SWNTs-CuS NPs hybrid thin film. (c) shows Raman spectra of SWNTs-CuS NPs hybrid nanomaterial and SWNTs.....	47
Figure 3-4	(a)-(b) show reflectance measurements of a SWNTs thin film and three SWNTs-CuS NP hybrid thin films made by decorating SWNTs with three different amounts of CuS NPs (SWNTs-CuS 1: 10mg SWNTs decorated with 100 μ l CuS NPs solution; SWNTs-CuS 2: 10mg SWNTs decorated with 200 μ l CuS NPs solution; SWNTs-CuS 3: 10mg SWNsT decorated with 300 μ l CuS NPs solution) in the spectrum range from UV-visible to near IR. The inset in (a) shows the measurement setup: the light illuminates perpendicularly to the thin film/glass surface and the reflected light is measured.	48
Figure 3-5	(a) shows schematic of the nanohybrid thin film device. (b) shows photo of a SWNT-CuS NP hybrid thin film device on a glass substrate. (c) shows measured current when the light and heat source illuminates the nanohybrid thin film device at different regions	50

- Figure 3-6 (a) shows experimental setup: a source (e.g. light, heat or a lamp source) illuminates the thin film devices; the inset shows the electron creation and transfer from a CuS NP to a SWNTs. (b) show photon response: I-V curves of SWNTs and SWNTs-CuS NP nanohybrid thin film devices with light on and off. (c) shows modulated resistance (normalized to the resistance of the pure SWNTs thin film device) for different numbers of CuS NPs in the nanohybrids with light on and off; the inset shows that more and more CuS NPs are attached to SWNTs. (d) shows modulated photocurrent for the nanohybrid thin film device made of SWNTs-CuS 2 (10mg SWNTs decorated with 300 μ l CuS NPs solution) with light on and off using a SWNTs thin film device as a reference.....52
- Figure 3-7 (a) shows thermoresponse: I-V curves of SWNTs and SWNTs-CuS nanohybrid thin film devices with heat on and off. (b) shows modulated resistance for different numbers of CuS NPs in the hybrids. (c) shows modulated thermocurrent for the nanohybrid thin film device. (d) shows modulated hybrid current for the nanohybrid thin film device made.54
- Figure 3-8 (a) shows sketch and photo of a prototype thermoelectric generator. (b) shows measured current when the lamp illuminates the junction I region of the devices with and without nanohybrid thin film. (c) shows measured current when the lamp uniformly illuminates the devices with and without nanohybrid thin film. (d) shows measured power generation of the prototype thermoelectric generator.....56
- Figure 4-1 (a) shows sketch of a hybrid nanomaterial thin film IR sensor: Junction I and Junction II formed between the Cu-wire electrodes and the hybrid nanomaterial thin film. (b) shows photo of a fabricated thin film IR sensor on a glass substrate. (c) shows photo of a flexible IR sensor embedded in PDMS before and after deformation. The size of the thin film measures 20mm (length) \times 8mm (width) \times 25mm (thickness). (d) shows TEM image of the SWNTs-CuS NP hybrid. (e) shows SEM image of the hybrid nanomaterial thin film. (f) shows XRD patterns of the as-synthesized SWNTs-CuS NP composite thin film.63

- Figure 4-2 IR testing schemes: (a) shows symmetric illumination and (b) shows asymmetric illumination on a thin film IR sensor fabricated from Nanohybrid 3. (c) shows photocurrents for four different devices fabricated with pure SWNT and 3 different nanohybrids. For all cases, no voltage is applied on the IR sensor. (d) shows one representative photocurrent measurement before and after the IR light is on with different IR exposure times (10, 20, 30, 40, 50 sec, 60 s, 70 s). A voltage of 0.2mV is applied on the IR sensor and the IR light intensity is 7mW mm^{-2} . (e) shows the maximum photocurrent change under different IR light exposure times. IR testing schemes.....64
- Figure 4-3 No voltage is applied on the IR sensor for all the measurements: (a) shows measured photocurrent under different intensities of the IR source. (b) shows relationship between measured photocurrent vs. IR source intensity for a nanohybrid thin film IR sensor fabricated from Nanohybrid 3, showing good linearity. (c) shows detection limit: a representative measurement of the photocurrent by reducing the IR light density to 48mW mm^{-2} , suggesting that the detection limit of the IR sensor is about 48mW mm^{-2} . (d) shows flexible IR nanosensor: measured photocurrent after different cycles of bending of the IR sensor67
- Figure 5-1 A sketch of a thermoelectric microgenerator with integrated nanohybrid thin film: (top) angled topside view; (bottom) cross-section showing the Junction I and II formed between silicon substrate and Au layer73
- Figure 5-2 The basic structure of Seebeck effect device [103]74
- Figure 5-3 The fabrication process flow: (a) Start with p-type silicon wafer. (b) Au pattern is formed on the silicon substrate. (c) Silicon nitride is deposited and then patterned. (d) top Au pattern is formed. (e) SWNTs-CuS nanohybrid thin film is transferred on the substrate and SU8 layer is patterned. (f) the hybrid nanomaterial thin film is patterned using SU8 as a mask.76
- Figure 5-4 (left) the TEM image of SWNTs-CuS NPs hybrid nanomaterial; (right) the SEM image of the SWNTs- CuS NPs thin film.....77
- Figure 5-5 Photo of a fabricated thermoelectric microgenerator. The nanohybrid thin film was integrated in the Junction I region77
- Figure 5-6 The experimental setup for the measurements of voltages and currents by the thermoelectric microgenerators.....78

Figure 5-7	Measured open circuit voltage of a thermoelectric microgenerator with and without Nanohybrids under uniform lamp illumination	79
Figure 5-8	Measured open circuit voltage when the lamp illumination is only on the Nanohybrids region compared to a device without the integrated nanohybrids.....	79
Figure 5-9	Measured peak power by the thermoelectric microgenerator under different light intensity and temperature of the lamp by changing the gap between the device and the lamp	80
Figure 5-10	A tunable lens which the radius is 45mm with blue dyed water in the chamber.....	82
Figure 5-11	The tunable lens fabrication flows	82
Figure 5-12	The experimental setup with a tunable lens between a lamp and devices for the measurement of voltages and currents. A channel was connected with the syringe and the tunable lens, Oil flowed through the channel into the tunable lens	83
Figure 5-13	A contact angle measurement, when more oil is injected into the lens chamber, the angle of the tunable lens is increased	84
Figure 5-14	A Measured open circuit voltage when the lamp illumination is only on the hybrid nanomaterial thin film region with different amount of oil in the lens chamber	85
Figure 5-15	Top view of the fabrication steps for the thermoelectric microgenerators in series. a) 58 pieces of rectangle silicon sticks were formed on the top of the SiO ₂ layer. b) an Al layer was deposited on the silicon sticks to form the electrodes and connect all microdevices together in series. c) After the deposition of the Al electrodes, the hybrid nanomaterial thin films were directly bound on a junction and an SU8 layer was coated on the top of the thin film to protect the thin films.....	87
Figure 5-16	Top view for the fabrication steps for the thermoelectric microgenerators in parallel. a) 32 pieces of rectangle shape silicon sticks were formed on top of the SiO ₂ layer. b) An Al layer is deposited on the silicon sticks to form the electrodes and connect all microdevies together in series. c) After deposition of the Al electrodes, the hybrid nanomaterial thin films were directly bound on a junction and a SU8 layer was coated on the top of the thin film to protect the thin films.....	88

- Figure 5-17 An open circuit voltage measurement when the light source was only on illuminate on the hybrid nanomaterial thin films region compared to a device in series without the hybrid nanomaterial thin films.89
- Figure 5-18 An open circuit voltage measurement when the light source was only on illuminate on the hybrid nanomaterial thin films region compared to a device in parallel without the hybrid nanomaterial thin films.90
- Figure 5-19 A current measurement of a single thermoelectric generator and thermoelectric generators in parallel.....90
- Figure 5-20 a) shows the measurement setup. b) shows voltage measurement with and without a lens on the device (outdoor temperature was 30°C).....91
- Figure 6-1 A thermoelectric generator with a thermal isolator (SiO_2). Silicon and Au (red color) are used to form the generator. SWNTs-CuS thin film is used to enhance local temperature, and SU-8 layer is for protecting the thin film98
- Figure 6-2 A prototype thermoelectric generator with embedded thermal isolator.....99

ACKNOWLEDGEMENTS

I appreciate my mentor and advisor, Dr. Long Que, for his generous instruction and sacrifice for giving me this opportunity to learn and study in this great research environment. During my doctoral studying, he does not only encourage me to develop independent thinking and research skills but also teach me much life knowledge which I cannot learn from textbooks.

I am also very grateful for having exceptional doctoral committee members, Dr. Randal E. Null, Dr. Sandra Zivanovic, Dr. Leland Weiss, and Mr. Ji Fang for their generous advice and serving on my advisory committee for this dissertation.

I want to thank the IFM staff members, Mr. Ji Fang, Mr. Alfred Gunasekaran, Miss Debbie Wood, and Mr. Davis for the experimental support. Especially Mr. Ji Fang, as he gave me suggestions and ideas to design the layout of my research device. For my teammates, I am fortunate to have worked with them who are still studying here or graduated. When we faced some difficulties, we encouraged and helped each other to solve problems. They are my teammates and also my best friends. I would like to thank all of them, they are Dr. Zhongcheng Gong, Dr. Tianhua Zhang, Venu Kotipalli, Pushparaj Pathak, Yuan He, Xiang Li, and Shiva Vasiraju.

At the end, I would like to thank my family, my father, mother, and sister, they constantly support and encouraged me with their love and passion. Eventhough they live far away from here, they are still my mental mainstay to help me pass through any tough time in my life.

CHAPTER 1

INTRODUCTION

Nanotechnology is the science of synthesizing nanomaterials and functionalizing nanostructures [99,100]. Nanotechnology has been discovered since the 4th century [27]. The Roman Lycurgus cups are one of the examples. In ancient Rome, Artisans ground the gold or silver materials into very fine powders to form colloid gold or silver solutions which were then sealed into the transparent wall of glass cups to generate the various colors on the wall of the cups. According to the light emitting directions, the wall of the cups showed different translucent colors [27]. The attractive optical phenomenon of the nanomaterials was first presented by those finely ground material powders. In recent years, nanotechnology has become one of critical knowledge, more and more unique phenomenons are discovered and attract scientists to study. A lot of reports have indicated much unique potential for various applications.

Typically, nanomaterials are defined as the scale of one dimension between 1nm to 100nm. At that range, most physical properties of nanomaterials cannot be considered the same as bulk materials due to some important effects in the small scale, such as surface plasmon resonance, quantum confinement, and some quantum mechanical effects. Due to these effects, nanotechnology reveals many remarkable properties which have been used in many popular areas, such as IR sensing and energy harvesting applications.

1.1 Nanomaterials

According to the size, shape, and material differences, uncountable nanomaterials have been created and studied in recent years. Among them, two types of the nanomaterials, the fullerenes and nanoparticles, have been widely studied and related research is mostly reported. The fullerenes are pure carbon molecular structures in honeycombed order and can be formed in many different shapes, such as atom-size sheets (graphene) and cylindrical tubes (carbon nanonanotubes CNTs).

1.1.1 Graphene and CNTs

Graphene and CNTs are the most popular fullerenes for many applications and which have been investigated and discussed for many years due to their remarkable structures and electronic and optical properties. Table 1-1 shows Basic structure properties of natural diamond, graphene, and CNTs at room temperature.

Table 1-1 Basic structure properties of natural diamond, graphene, and CNTs at room temperature [22,23]

	Natural diamond	Graphene	Carbon nanotube
Thermal conductivity	$\sim 2200 \text{ Wm}^{-1}\text{k}^{-1}$	$2000\text{-}4000 \text{ Wm}^{-1}\text{k}^{-1}$	$\sim 3500 \text{ Wm}^{-1}\text{k}^{-1}$
Electron mobility	$2200 \text{ cm}^2/(\text{V}\cdot\text{s})$	$15000 \text{ cm}^2/(\text{V}\cdot\text{s})$	$100000 \text{ cm}^2/(\text{V}\cdot\text{s})$
Young's modulus	$\sim 1.2 \text{ TPa}$	$\sim 1 \text{ TPa}$	$1\text{-}5 \text{ TPa}$
Tensile strength	$\geq 1.2 \text{ GPa}$	130 GPa	$13\text{-}53 \text{ GPa}$

The basic structure of graphene is a two-dimension hexagonal carbon sheet formed as a fine sheet. The thickness of graphene is as thin as an atom and as light as 0.77 mg/m^2 . Although graphene is so thin that it is translucent, graphene has a very strong structure even better than natural diamond due to the carbon structure and very strong carbon covalent bonds. It shows almost 100 times the tensile strength of natural diamond

and three times that of CNTs [22][23]. On the other hand, the structure of CNTs is similar to graphene, but more like the graphene sheet rolled up and forming a cylindrical tube. In fullerenes, CNTs also have the strong carbon covalent bonds that make the CNTs stiff and straight. According to fabrication methods differences, the length of CNT can be fabricated up to millimeters and the width of CNT are only in 1 to 10 nanometers. The high ratio of the CNTs length to width causes the CNTs to be not only firm but also elastic [24].

The structure strength is not the only outstanding property of graphene and CNTs. They also exhibit remarkable electrical, optical and thermal properties. In comparing the electronic structures of graphene and CNTs, graphene is a semi-metal which has very good electrical conductivity and fast electron mobility. In addition, CNTs have different electronic structure than graphene. CNTs are formed by rolling up graphene sheets, and depending on the direction in which they are rolled up, the electronic structure of CNTs are changed to semi-metal, semiconductor, or semi-insulator. The geometrical structure can be indexed by the CNTs pair of atoms (n,m). If $n=m$, CNTs display no gap semiconductors the same as graphene. If $n-m$ is equal to a multiple of three, the gap of CNTs is closer and become narrow-gap semiconductors. In other situations, CNTs become wide-gap semiconductors [12].

For energy harvesting and optical sensing applications, graphene and CNTs exhibit excellent thermal and optical properties. There are many reports showing that both of them have excellent thermal conductivity, $2000-4000\text{Wm}^{-1}\text{k}^{-1}$ and $3500\text{Wm}^{-1}\text{k}^{-1}$, respectively, at room temperature. This high thermal conductivity shows the potential for harvesting thermoelectricity for transfer to useful energies. Moreover, graphene and

CNTs also have great optical absorption. In nanotechnology, graphene has only one atom-size thickness, but it is still able to absorb about 2.3% of light based on the Fine Structure Constant (FST). In this fine structure, the amount of absorption is able to congregate together. If two graphene thin films overlap together, the absorption value is increased almost as much as 2.3%. For CNTs, when large numbers of CNT congregate together to form a CNT thin film, the structure of the CNTs thin film is similar to a black body. Ideally, a pure black body exhibits 1.0 of absorptivity and emissivity over a wide range of wavelengths. In recent years, it has been reported that vertically aligned CNTs have great absorptivity and emissivity close to 0.99 over a wide wavelength from 200nm to 200 μ m [25].

1.1.2 Nanoparticles

In addition to fullerenes, a variety of nanoparticles are also of the scientific interest due to their wide potential applications, such as optical, electrical, and biomedical applications. Depending on the size scale and materials differences, nanoparticles exhibit remarkable property differences compared to bulk and molecular materials because of surface plasmon resonance and quantum confinement effects.

In biomedical science, some metallic nanoparticles, such as Au, Pt, and Ag nanoparticles (NPs), have been used in drug delivery, tumor detecting, optical sensing for DNA, and as photothermal agents. The nanoparticles have large surface to volume ratio and stable surface foundation that can be synthesized and functionalized with various chemical agents to allow them to be combined with antibodies, drugs, and ligands. For drug delivery, the delivery speed of drug-nanoparticles is fast because the nanoparticles,

such as colloidal gold, can uniformly suspend in solution very well. Therefore, the drugs can diffuse and reach the target fast rather than accumulate together.

Due to the localized surface plasmon resonance, metallic nanoparticles are of a size-dependent property. When the sizes of the Au nanoparticles are below 100nm, the absorption wavelength is shifted, so the colors of the nanoparticles become red instead of natural yellow. After the Au nanoparticles absorb the incoming light, the oscillatory plasmon is generated on the surface of the Au nanoparticles. The plasmon moves and decays along the surface of the nanoparticles cause a heat is generated on the surface [17].

Also, some metallic nanoparticles have magnetic properties, such as FeO, Fe₂O₃, and Fe₃O₄ nanoparticles. The nanoparticles are able to combine with chemical agents which can track tumors and be injected into the human body to detect the tumors by magnetic detectors [28].

Different from metallic nanoparticles, the semiconducting nanoparticles also have some unique electrical and optical properties due to the quantum confinement effect. When the sizes of the nanoparticles decrease to below 100nm, especially 10nm, the electron-hole pairs (excitons) are compressed resulting in the quantum confinement. The energy levels are discrete and the energy gap is increased. The electrons need higher energy to jump across the energy gap, so the nanoparticles have excellent light absorption and specific absorption peaks. For example, CuS NPs have specific absorption peaks at near infrared region. Moreover, the width of the energy gap is size-dependent. If the sizes of the nanoparticles are decreased, the absorption peak of nanoparticles exhibits a blue-shift [17].

1.1.3 Hybrid Nanomaterials

As aforementioned, for the past decades, many different nanomaterials and nanostructures have been synthesized and functionalized, such as metallic nanoparticles, semiconducting nanoparticles, graphene, and carbon nanotubes. Considering their unique and various properties, the nanoparticles exhibit great potential for biomedical, optical, and electrical applications. However, the use of a single nanomaterial has been studied over many years and it is hard to conspicuously improve the efficiencies. In order to enhance the efficiency of the nanomaterials, research has found that two different nanomaterials have the ability to combine together forming a new hybrid nanomaterial which can combine the unique properties of the two nanomaterials or even create new properties for scientific applications [35,55,89].

Due to the cylindrical structures of CNTs, the CNTs have the potential for attaching many nanomaterials on the surface of the CNTs to create new hybrid nanomaterials. Nanoparticles are one of the popular nanomaterials that have been used to combine with CNTs, because the nanoparticles have great catalytic properties for various chemical reactions. Moreover, various nanoparticles have their specific optical, thermal, and electrical characteristics to obtain more derivative properties for more applications.

In order to attach the nanoparticles on the surface of CNTs, there are several methods to deposit the different types of nanoparticles on the CNTs. For example, CNTs-based hybrid nanomaterials are often used as chemical agents to functionalize the surface of CNTs to form a charge to attract oppositely charged nanoparticles creating a strong force to stably attach the nanoparticles to the CNTs. This bonding method is called a non-covalent bond. The non-covalent bond presents a stable bonding structure and both atom

structures are not changed, so the bonding method does not destroy the characteristics of CNTs and nanoparticles.

According to the different materials of nanoparticles, the CNTs based hybrid anomaterials have various properties. For optical and energy harvesting applications, semiconducting nanoparticles, such as Copper Sulfide (CuS) nanoparticles, are an excellent nanoparticles to use to combine with CNTs to enhance the optical absorption value for harvesting from wider range of optical sources. The CuS NPs also exhibit an excellent optical absorption range at the near-infrared region which has the potential for detecting an infrared source [16].

1.2 Applications of Hybrid Nanomaterial

In recent years, the single-wall carbon nanotubes based nanoparticles (SWNTs-NPs) have been discovered with many excellent optical, thermal, and electrical properties that are even better than the SWNTs or the nanoparticles. The SWNTs-CuS nanoparticles (SWNTs-CuS NPs) are a great hybrid nanomaterial which exhibits fast electrons mobility, high optical absorption, specific optical absorption peaks at the near-infrared region, conversion of light to heat, and excellent thermal conductivity. Due to their unique properteies, SWNTs-CuS NPs have vast potential for many applications, especially infrared sensing and energy harvesting. For these applications, the SWNTs-NPs can also be fabricated as ultra-thin films to attach to the different micro\nano devices to create more functions or enhance the efficiency of the micro\nano devices.

1.2.1 Infrared Sensing

Light is electromagnetic radiation and human eyes can see or detect light energy between 400nm to 700nm wavelength. If the wavelength is over 700nm or 1mm, the

radiation is called infrared (IR) radiation. The range of wavelength also covers most thermal radiation. The history of the IR radiation was started in 1800, when Royal Society's William Herschel first discovered it in sunshine. He found the sun is generating not only visible light but also some invisible light with thermal energy [29].

The IR radiation can be found everywhere on the earth. Sunshine, humans, animals, and some objects have IR radiation. Generally, the IR radiation sources are broadly classified into four divisions: actinic range, hot object region, calorific region, and warm region. Table 1-2 shows brief descriptions of different IR regions [29]. In IR technology, IR sensing is the most critical science for the IR related devices. According to different IR targets, the sensitivity and detecting ranges of IR sensors must match the IR devices. Due to different ranges of IR radiation, the IR radiations have different characteristics. ISO 20473 divides IR radiation into three areas: near-infrared (NIR), middle-infrared (MIR), and far-infrared (FIR). Every IR region exhibits different characteristics which can be used in many different applications, such as scientific, industrial, military, and medical applications. Table 1-3 shows the IR wavelength division with ISO 20473.

Table 1-2 The brief descriptions of different IR regions [29]

IR sources	Descriptions
Actinic region	The radiation range is from visible light range to IR light. It is generated from actinic objects, such as Tungsten filament lamp and Sun. Actinic range is also called Photochemical reaction area.
Hot object region	The radiation is generated from non-actinic objects, such as electric iron and other heat generating devices. The average temperature is about 400°C.
Calorific region	The radiation is generated from boiling water and evaporating devices. Calorific region is also called non-actinic region. The average temperature is below 200°C.
Warm region	The radiation is generated from human bodies, animals, and terrestrial heat.

Table 1-3 The IR wavelength division with ISO 20473

IR regions	Wavelength	Purposes
Near-Infrared	0.78 μm – 3 μm	Fiber optical commutations and IR image intensifier
Middle-Infrared	3 μm – 50 μm	Guided missile technology and high temp. thermal image
Far-infrared	50 μm – 1000 μm	Far infrared laser

Because the IR radiation is invisible, the IR sensors are developed to detect the IR radiation and measure the heat of the objects. The related IR devices can be found everywhere, including TV remote, night vision, thermal imaging, and telecommunications. Typically, IR sensors can be separated into two major types, the thermal IR sensor and the photonic IR sensor [102].

The basic principle of a thermal IR sensor is detecting temperature change. The thermal IR sensor absorbs IR radiation to raise the temperature of the thermal element. According to the temperature change, the temperature-dependent thermal IR sensor can convert a thermal change to an IR radiation value. This thermal IR sensor can continue to

work without waiting to cool. However, the IR sensor has a longer response time because the thermal element has to wait until the photons convert to heat energy [101,102].

On the other hand, the photonic IR sensor works on photovoltaic and photoconductive effects. When a volume of incident photons excite the semiconducting material, the photons generate excitons (pairs of hole and electron) and the electrons move across the band gap to the conduction band to generate an electrical current or voltage. The electronic dependent photonic IR sensor can monitor IR radiation by the electrical current or voltage change. Because the photonic IR sensor can directly convert the photons into electronic signals, the photonic IR sensor is faster than the thermal IR sensor. However, temperature is the problem of the photonic IR sensor that affects the accuracy of the sensor. Therefore, the photonic IR sensor has to cool down for accurate measurements. [29,102]

1.2.2 Energy Harvesting

For many years, nuclear energy has been one of the major energy sources to supply electricity for human life because of its powerful and inexpensive properties. However, this powerful energy also brings with it an unstable factor to threaten the environment. The Fukushima Daiichi nuclear disaster is one of the terrible examples, the earthquake causing fatal radiation leak out from the nuclear power plant in 2011. The strong radiation exposed over ten km of surrounding area and affected over 300,000 people.

In order to avoid an accident happening again, searching for safe and stable energies instead of nuclear energy becomes the necessary issue. Many reports have indicated on green natural energies, such as solar, wind, heat, and tide, have great

potential to be the alternative energy because the green energies present clean and safe sources. Moreover, they are endless and everywhere on the Earth. Therefore, the topic of harvesting green energies has been attracting scientific interest for many years.

Typically, the major convertible types of green energy include light, thermal, and mechanical energies. According to the different energy sources, many suitable devices have been created to harvest the green energies and convert them into electricity or other useful energies. Even though the green energies are strong and endless, they still cannot totally replace nuclear and depleting energies due to some technical limitations of the harvesting devices. Table 1-4 shows introduction of different types of green energies

Table 1-4 Introducing the different types of green energies

Energy types	Sources
Light Energy	Sunshine and tungsten filament lamps.
Thermal Energy	Sunshine, Geothermal Energy, waste thermal energy, and heater.
Mechanical Energy	Vibration and mechanical stress or pressure.
Electromagnetic Energy	Solar radiation and inductor.
Fluid Energy	Ocean current and Wind flow.
Human body	Human body can generate both thermal and mechanical energy from the constant warm body and body actions such as running.
Other Energy	Bio-medical and chemical reactions.

According to the harvesting differences, engineering faces many issues concerning the increase in the efficiency of the energy harvesting devices. For the external issues, some green energies cannot support constant and strong power to drive the harvesting devices. Wind energy is one of the cases. If the local wind is too slow, a wind farm cannot be driven to generate electricity. Even some green energies, such as solar energy, which can support strong and endless energy in daytime, research still faces

some technical issues. For example, solar cell development is the hottest energy topic and it has been discovered and developed for many years due to strong and infinite light and thermal sources. However, development costs and solar-electricity conversion efficiency limitations restrict the ability of the solar cell. The conversion efficiency of common solar cells is still less than 50% and the higher efficiency of solar cells also has associated high costs. Therefore, how to reduce the development costs and increase the conversion efficiency becomes the biggest issue to develop green energies. Usually, the major optical energy harvesting devices work based on such mechanisms as piezoelectricity, electromagnetic induction, thermoelectric effect, and photovoltaic effect.

Piezoelectricity. Piezoelectricity was discovered by the French researchers Jacques and Pierre Curie in 1880. Based on the piezoelectric effect, piezoelectricity is described as the conversion between the electrical charge and mechanical stress in piezoelectric materials, such as quartz crystals. When the materials suffer external stress to deform the body structure, a polarized charge is generated on the surface resulting in a potential difference between two surfaces and generating voltage. In addition, piezoelectricity also exhibits reversible characteristic because the piezoelectric effect is mechanically converting the two energies in piezoelectric materials [30].

After piezoelectricity was discovered, over 20 species of natural piezoelectric materials were found and the efficiency of the material piezoelectricity was defined by piezoelectric constants using tensor analysis in 1910. During the World War I, the piezoelectric materials were used in submarines. They used piezoelectricity and hydrophone technologies to build the first ultrasonic submarine detector to emit a high-frequency sound and detect the returned echo from another submarine. In order to

enhance the detection efficiency in World War II, researchers fabricated the first synthetic piezoelectric material, ferroelectrics, which exhibit much higher piezoelectric efficiency than the natural materials. After the wars, piezoelectricity technology has continuously interested scientists to develop new materials and devices for wide application areas. Lead zirconate titanate (PZT) is one of the popular synthetic piezoelectric materials with a higher piezoelectric constant. Many reports have indicated that PZT has great potential for pressure sensors and pressure energy harvesting devices [30].

Electromagnetic Induction. The electromagnetic phenomenon was first reported by Michael Faraday in 1831. Electromagnetic induction is based on Faraday's Law. When a conductor is applied to an electromagnetic force, an electrical voltage is generated, and the electrical current follows the electromagnetic force and moves on the conductor [32]. The electromagnetic induction is the basic model to build some energy harvesting machines, such as turbine power generation for the wind or hydraulic power generators. For a wind power generator, when a strong wind continuously blows, the power generator is driven by spinning huge fans to generate an electromagnetic force and directly convert it to an electrical voltage or current which is then stored in high capacity cells.

Thermoelectric Effect. The thermoelectric effect was first discovered by Thomas Seebeck in 1821, so the thermoelectric effect is also called the Seebeck effect. The basic thermoelectric device uses two materials, which have different Seebeck coefficients, which are connected together forming junctions. When the junctions have a temperature difference, an electrical voltage is generated between the two junctions. The Seebeck

coefficient is defined by the potential difference (ΔV) developed per unit temperature difference (ΔT) between two end sides of a material [33]:

$$S = \frac{\Delta V}{\Delta T} \quad (1-1)$$

In considering the electronic movement of the thermoelectric effect, when a temperature gradient exists in the material, the temperature difference generates the electrical carriers. The electrons move from the hot end side to the cold end side generating a current flow in the material. In addition, the Seebeck coefficient could be either positive or negative due to the diffusion speed of the electrons. If the mean free path of the electrons is short, the Seebeck coefficient is positive because the higher lattice vibration results in electrons flipping back to the hot side. If the mean free path of electrons is long, the Seebeck coefficient is negative because the lower lattice vibration causes the electrons to accumulate at the cold end side. Generally, the thermoelectric generators use the thermoelectric effect to convert the heat into electricity directly. If the Seebeck coefficient difference between two joined materials is larger, the thermoelectric generator can generate larger electrical voltage. On the other hand, if the temperature difference between two junctions is higher, than the generated voltage also becomes larger. Equation 1-2 shows the relations between temperature, Seebeck coefficient and voltage [33]:

$$V = (S_{\text{material1}} - S_{\text{material2}}) \times (T_{\text{material1}} - T_{\text{material2}}) \quad (1-2)$$

Thermoelectric generators have been widely used to harvest heat energy. The generators can use the waste heat from furnaces, heaters, and consumer electronics to make a temperature gradient and generate electricity.

Photovoltaic Effect. The photovoltaic effect was first discovered by Edmund Bequerel in 1839. The photovoltaic device can harvest light and directly convert it to an electrical voltage or current without heat or other energy sources. The photovoltaic effect is based on the photoelectric effect. When sufficient light hits on the surface of the material, the valence band absorbs the photons and generates excitons (electron and hole pairs). The electrons gain enough energy and jump across the band gap to the conduction band becoming free electrons to generate an electrical current [34].

Since the first photovoltaic device was fabricated in 1880, related objects have attracted much scientific interest. In 1930, Walter Schottky and his group developed the first metal-semiconductor barrier called the Schottky barrier which can enhance the efficiency of photovoltaic devices. In 1950, the silicon wafer-based p-n junctions are fabricated leading to the formation of higher efficiency photovoltaic devices. Silicon-based solar cells are the most popular photovoltaic devices in the energy harvesting technology. The silicon-based solar cell started to be used to support power on low power consumption remote devices and satellites in space. During these times, the reports found the III-V compound semiconductor could enhance the solar cells more by the specific band structure. After 1970, more and more synthetic materials, such as polycrystalline silicon, amorphous silicon, and organic conductors, were fabricated for high efficiency and lower cost solar cells. Until now, research is still working on reducing the fabrication cost and to enhance the efficiency of solar cells for instant consumption and nuclear energies [34].

1.3 Previous Work and Problems

1.3.1 Infrared Sensing

As discussed above, IR sensing is the critical technology for a variety of applications, such as remote sensing, thermal imaging, night vision, thermal photovoltaics and optical communications. In nanotechnology, CNTs, graphene, CNTs nanoparticles, and CNTs composites have been used to develop thin film IR sensors to detect the near IR (NIR) region [35]. Figure 1-1 shows the rough structure of a thin film IR sensor. A micro-size thick thin film is formed with the nanomaterial which is sensitive to NIR. Two conductive wires are directly bound at two end sides of the thin film to form the electrodes to connect with the voltage meter. When the NIR radiation hits the surface of the thin film, a voltage is generated and measured by the voltage meter.

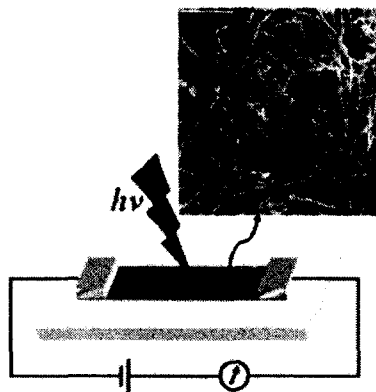


Figure 1-1 shows a basic structure of CNTs thin film IR sensor and the small image shows the surface of the thin film [35].

Reports have described how CNTs exhibit great potential to apply to optical devices to enhance the efficiency of the devices. CNTs thin film IR sensor is a remarkable device due to their unique optical properties. According to the black body effect, the CNTs thin film exhibits great optical absorption which can support a strong IR

radiation signal for the CNTs thin film IR sensors. Moreover, CNTs thin films have a fast photoresponse characteristic because the excitons which are generated from sufficient incoming photons are easily separated resulting in a fast transfer to other carriers in the CNTs electronic structure. A CNTs thin film IR sensor with 0.5mm width, 3.5mm length, and one μm thickness has been fabricated by Mikhail and his group. When a $0.12\mu\text{W}$ NIR radiation is exposed to the IR sensor, it shows a fast response time of about 502ms. Generally, the IR radiation also brings thermal energy. The thermal energy can also support extra energy to separate excitons and increase the photoconductivity. When the NIR radiation is exposed to the CNTs IR sensors, the resistance of the sensors is reduced by 0.7% [36].

When the IR radiation strikes the CNTs IR sensor, some of the electrical and thermal energies could diffuse out of the CNTs thin film to cause unnecessary energy waste. Therefore, Basudev Pradhan and his group report a new type of CNTs thin film IR sensor. They coated an electrical and thermal insulating polymer matrix on the CNTs to form CNTs-Polymer nanocomposite (CP) thin film IR sensors. This CP IR sensor whose thickness is about 25-60 μm , also exhibits fast response time, about 60ms under $0.7\text{mW}/\text{mm}^2$ NIR power and a strong conductivity change of about 4.26%. [35].

Due to the surface plasmon resonance and quantum confinement effect, the nanoparticles have also shown potentials for IR sensors. Longyan and his group used the carbon nanoparticles embedded in Polydimethylsiloxane (PDMS) substrate to form a flexible IR sensor. The flexible IR sensor has a very elastic structure because the PDMS substrate is a transparent and flexible polymer. Therefore the flexible IR sensor shows the advantage which can be integrated with different shaped devices. Moreover, the flexible

IR sensor exhibits a stronger current change than the CNTs and CP IR sensors, the highest current change being about 52.9%, which is 75 times larger than a CNTs IR sensor in vacuum and 12 times larger than a CP IR sensor. It can detect the IR power as low as $58\mu\text{W mm}^2$ [37].

However, for IR sensing, the existing carbon nanomaterials thin film IR sensors have intrinsic limitations. Firstly, the carbon element has great optical wavelength absorption. The wavelength is not only the NIR wavelength, but also the visible wavelength. The IR sensors are not very sensitive to the NIR region. Secondly, the current change rate of the thin film IR sensors still has room to be improved. Increasing the current change rate can also improve the efficiency of the thin film IR sensor and the IR detecting limit.

1.3.2 Solar and Thermal Energy Harvesting

As can be seen from the history of energy harvesting, scientists are continuously seeking to improve the efficiency of existing harvesting devices and to develop new devices. In order to harvest different green energies, various energy harvesting devices have been fabricated. For optical energy harvesting, solar cells are the main photovoltaic product which can be classified into three generations by the cost and efficiency of the solar cells.

The first generation of the solar cell exhibits higher light-electricity conversion efficiency than the Shockley-Queisser solar cell but also higher fabrication cost. In the Shockley-Queisser limit of a single-junction solar cell, the solar conversion rate is about 31% to 41% depending on the concentration of the incoming light source [38]. The first

generation solar cell uses extremely pure silicon material to fabricate the single-junction solar cell, so the fabrication cost is more expensive.

Since the pure silicon material is expensive to market, the next generation of solar cells was fabricated in 1970 and used semiconducting material to fabricate a thin film by the deposition process rather than the expensive pure silicon. This solar cell successfully reduced the fabrication cost, but it was not produced as much as the first generation due to its low efficiency. It is only suitable for a large area to absorb enough light energy [39]. The third generation is fabricated based on a p-n junction solar cell. The efficiency of the solar cells is limited by the Shockley-Queisser limit. So the efficiency is only about 33.7%, if the band gap of the solar cell is 1.1eV. However, the third generation is fabricated in a nano-scale to enhance its efficiency over the Shockley-Queisser limit. The new type of solar cells include intermediate-band, hot carrier, and multi-junction cells [40].

For thermal energy harvesting, the thermoelectric generators basically rely on the thermoelectric effect. Since the first thermoelectric generator was fabricated in 1960, scientists have been trying to improve the generator. However, the efficiency of general thermoelectric generators is still within the range of μW and mW which is lower than other energy harvesting devices. In recent years, scientists have focused on synthesizing new material to improve thermoelectric generators. They found that when the sizes of the materials are reduced to the nano-scale, nanomaterials exhibit better thermoelectric efficiency which can be used to improve thermoelectric generators.

In order to replace those high consumption energies, such as petroleum, coal and nuclear energy, harvesting clean and endless green energies is the first priority. Scientists

continuously improve the efficiency of energy harvesting devices. In recent years, research has found some nanomaterials that have the ability to absorb not only light energy but also thermal energy to increase the efficiency of energy harvesting devices.

1.4 Dissertation Objectives

The aim of this dissertation research is to develop and investigate a novel hybrid nanomaterial with unique optical properties to improve sensitivity of thin film IR sensing and to enhance the efficiency of green energy harvesting applications. In the beginning, a hybrid nanomaterial, single-wall carbon nanotubes-copper sulfide nanoparticles (SWNTs-CuS NPs), will be introduced to exhibit its potential for these applications. Then, the hybrid nanomaterial is used to form a thin film ultra-sensitive IR sensor to demonstrate the thin film IR sensor's characteristics. After that, micro thermoelectric generators will be fabricated and the hybrid nanomaterial thin film will be embedded on the generators to enhance the efficiency of the generators. Further considerations for how to optimize the devices and improve their efficiencies will be analyzed.

1.5 Organization of Dissertation

Chapter 1 introduces nanomaterials and the potential applications of IR sensing and energy harvesting. Some common nanomaterials, such as CNTs, graphene, metallic nanoparticles, semiconducting nanoparticles, and hybrid nanomaterials are introduced. The next section reviews IR sensing and the two major types of IR sensors: photoelectric and thermoelectric IR sensors. After that, is a review of energy harvesting and introduction to the major types of energy harvesting mechanisms: piezoelectricity, electromagnetic induction, thermoelectric effect, and photovoltaic effect. The last section

is to analyze the advantages and the disadvantages of the existing thin film IR sensors and green energy harvesting devices.

Chapter 2 will go deep into the knowledge and the unique properties of CNTs and nanoparticles. The outstanding structure and, electronic, optical, and thermal properties of CNTs are covered and discussed. The next section is to explain two major phenomena in nano-scale: quantum confinement and surface plasmon resonance effects and discuss the size-dependent properties of metallic and semiconducting nanoparticles.

Chapter 3 will introduce a new hybrid nanomaterial, carbon nanotubes-copper sulfide nanoparticles (SWNTs-CuS NPs). Methods for synthesis of the SWNTs-CuS NPs hybrid nanomaterial and fabricating of SWNTs and SWNTs-CuS NPs thin films are introduced. The unique optical and thermal properties of the hybrid nanomaterial are discovered and discussed which shows the great potential for IR sensing and energy harvesting applications.

Chapter 4 will discuss the first application: IR sensing. An ultrasensitive SWNTs-CuS NPs thin film IR sensor is discovered and introduced. The methods of fabricating the thin film and flexible thin film IR sensors and the measurement set up are explained. After that, the results of the measurements are discussed.

Chapter 5 will discuss second application: energy harvesting. A new type of thermoelectric microgenerator based on SWNTs-CuS NPs thin film is fabricated and introduced. Its fabrication process and measurement results of the micro-scale energy harvesting device are discussed.

Chapter 6 will have a conclusion and summary for the whole dissertation. Suggestions for future work will be further discussed.

CHAPTER 2

CARBON NANOTUBES AND COPPER

SULFIDE NANOPARTICLES

2.1 Carbon Nanotubes

Since the discovery of carbon nanotubes (CNTs) in 1991, CNTs have been attractive to study because of their unique properties, such as extremely high thermal and electrical conductivity, strong mechanical strength, and high optical absorption, all of which show the great potential for many useful applications [1]. Table 2-1 shows the basic physical characteristics of CNTs. Basically, CNTs have two common structures; single-wall carbon nanotubes (SWNTs) in Figure 2-1A and multi-wall carbon nanotubes (MWNTs) in Figure 2-1B. A CNT can form with a rolled up graphene; the structure is similar to a hollow cylinder structure with long micro-scale lengths and extremely narrow nano-scale widths. Chemical vapor deposition (CVD), laser vaporization, and electrical arc to co-vaporization are commonly used to fabricate CNTs [3]. For the quality of the CNTs, the CVD process can make purer and longer CNTs than the laser vaporization process. The electrical arc to co-vaporization process requires higher temperature than other processes and both laser vaporization and electrical arc to co-vaporization processes are difficult to control the chirality and purity of CNTs [3].

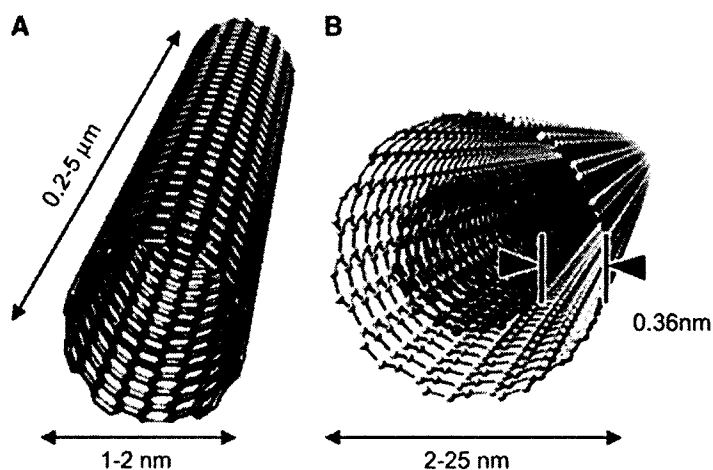


Figure 2-1(A) shows a sketch of single SWNT and (B) shows a sketch of single MWNT [5].

Table 2-1 Important characteristics of CNTs [2]

Electrical conductive	Metallic or semiconducting
Electrical transport	Ballistic, no scattering
Maximum current density	$\sim 10^{10} \text{ A/cm}^2$
Thermal conductivity	$600 \text{ W} \cdot \text{K}^{-1}$
Diameter	1nm to 100nm
Length	Up to millimeter

2.2 Properties of Carbon Nanotubes

The outstanding properties of CNTs can be classified as mechanical, electrical, thermal, and optical properties. Every unique property has been deeply studied and reported since 1991 and applied to many different application fields, such as energy harvesting devices, micro-sensors, micro-probe, hydrogen storage for batteries, field emission devices, nano-electrical devices, and electrochemical devices [6]. The structure of a single CNT is like a graphene sheet but rolled up to become a tube. According to different fabrication processes, the CNTs have two different types: single-wall (SWNT) and multi-wall CNT (MWNT). SWNT only has a single wall to form the tube and the diameter is about 0.2nm. MWNT has 2 to 20 walls which overlap together to form a

multi-wall tube and the diameter can reach from 5nm to 100nm. In some cases, the two ends can be capped for some different applications.

2.2.1 Mechanical Properties of CNT

CNTs are an allotrope like carbon fullerene, but unlike the ball style. A CNT is rolled up with 2-D graphene sheet. The atomic structure of a graphene sheet is a carbon-carbon bond which is the strongest bonding type in the world, as strong as diamond. Hence, many applications, such as composite reinforcement or lubrication, are using CNTs to enhance the structure strength. The ratio of their width to length can achieve 1:1000[3]. In some specific cases, the length of CNTs can be made as long as 18.5cm by the CVD process [7]. Usually, metals which have strong structure are inflexible in use; however, CNT has extremely strong structures, but also is more flexible than other hard metals because of the remarkable hollow cylinder structure, strong but flexible [8]. Compared with stainless steel, CNTs exhibit an extremely firm body but also have great tensile strength. Table 2-2 shows the comparison of young's modulus and tensile strength between SWNT, MWNT, and stainless steel [10].

Table 2-2 The comparison of young's modulus and tensile strength between SWNT, MWNT, and stainless steel [10].

	Young's modulus(TPa)	Tensile strength(GPa)
SWNT	2.8~3.6	13~52
MWNT	1.7~2.4	11~63
Stainless steel	0.18	0.86

2.2.2 Electronic Properties of CNT

A CNT presents unique electronic structures similar to a one-dimensional graphene sheet, but rolled up to becomes a hollow cylindrical body. CNT is the sp^2

hybridization structure; each carbon atom is bonded with three other neighbor carbon atoms to form a honeycomb structure and extend the same structure periodically to build up a CNT. Figure 2-2 shows the typical the sp^2 hybridization structure of CNT. Compared with a single carbon atom structure, the sp^2 hybridization structure of CNTs gives totally different electronic properties [10].

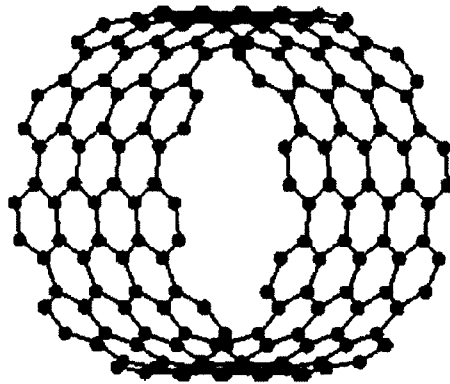


Figure 2-2 The sp^2 hybridization structure of CNT [5]

The carbon atom bonding structure of a CNT and a graphene sheet are almost the same, but a CNT has a cylinder structure rather than a sheet. For the electronic CNT property, the rolled up vector of CNTs could affect the electronic property and become different from a graphene sheet. Equation 2-1 shows the relation between the vector and the electronic property change. r is the rolling up vector, a and b are the linear pair in the lattice structure, and n and m are the pair of atoms[10].

$$r = na + mb \quad (2-1)$$

According to the vector of pair atoms (n and m) difference, the CNT shows three different geometry structures; zigzag, armchair, and chiral, which is shown in Figure 2-3A [11]. When $m=0$, the CNT is called zigzag CNT, as shown in Figure 2-3Ba. When $n=m$, the CNT is called armchair CNT, as shown in Figure 2-3Bb. In another situation,

the CNT is called chiral CNT, as shown in Figure 2-3Bc [11]. For the electronic property of CNT, the rolled up vector also affects the energy gap of CNT causing the CNT to be a metallic or semiconductor structure. When the $n=m$ (armchair), the electronic property of the CNT is similar to metal which has great conductivity because the CNT has no energy gap. When $n-m$ =multiple of 3(chiral), the energy gap of the CNTs is very close; therefore, the CNT becomes a semiconductor. In other situations (zigzag), CNTs become wide-gap semiconductors because the energy gap of CNT is larger than the chiral structure [12]. Figure 2-4 shows three different electronic states of CNT, a zigzag CNT (8, 0), a chiral CNT (7, 1), and an armchair CNT (8, 0) [12].

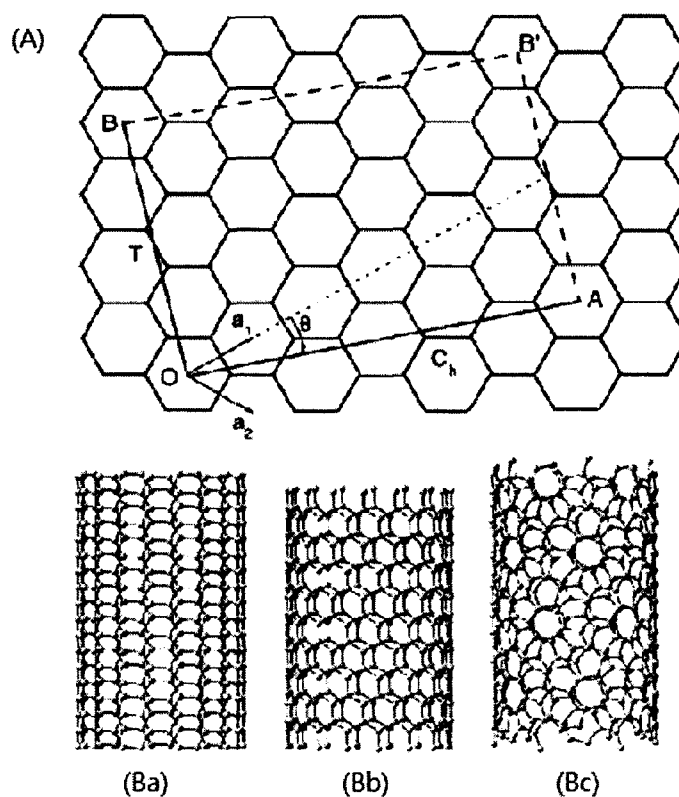


Figure 2-3(A) shows the definition of CNT geometry structure by change the rolling up vector of CNT; zigzagCNT ($\theta = 0$), chiral CNT (θ between 0 to 30), armchair CNT ($\theta = 30$). (Ba) is zigzag structure, (Bb) is chiral CNT, (Bc) is armchair CNT [11].

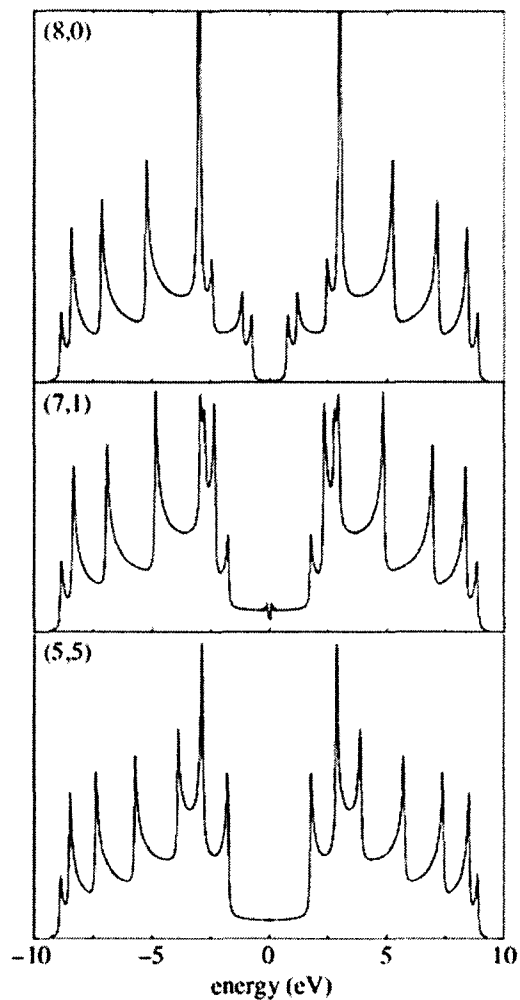


Figure 2-4 (8,0) shows CNT is metallic. (7,1) shows CNT is a narrow gap semiconductor. (5,5) shows CNTs is a wide gap semiconductor [12].

2.2.3 Thermal Properties

Due to the tiny size and sp^2 hybridization structure, the CNT presents unique thermal properties which include variable thermal conductivity, thermal expansion, and thermopower. The thermal properties of CNT depend on temperature, tube length, diameter, and rolling up vector [12] [13].

2.2.4 Thermal Conductivity

Due to the hollow cylinder sp^2 structure, the thermal conductivity of a CNT is greater than the in-plane thermal conductivity of graphite [12], and the thermal conductivity of CNT is depending on the heat transfer (photon transfer) rather than electron transport. Therefore, there is no specific effect between the electrical and temperature conductivity of CNT. The main parameters that can affect the temperature conductivity of CNTs are changed in temperature, dimension, and the crystal rolling up vector rather than electrical characteristics. Figure 2-5 shows the relation between the thermal conductivity of CNTs and temperature in longer lengths of CNT. Longer lengths of CNTs have higher thermal conductivity at around 500K. Thermal conductivity will achieve saturation when the photons start colliding in CNTs. Depending on the temperature change, only long wavelength photons can be excited at low temperature; moreover longer CNTs can suffer more photon collisions than short CNTs at low temperature. Hence, when temperature becomes higher, the thermal conductivity of longer CNTs have no bigger difference than with short CNTs. Figure 2-6 shows the simulation of the relation between the thermal conductivity of CNTs and temperature with shorter lengths of CNTs [14].

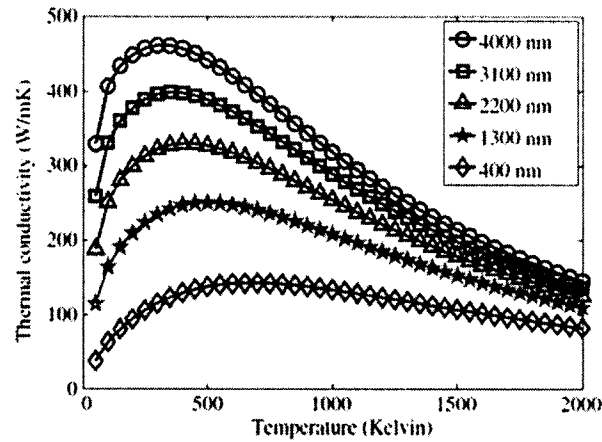


Figure 2-5 The simulation of the relation between the thermal conductivity of CNTs and temperature with different lengths of CNTs [14]

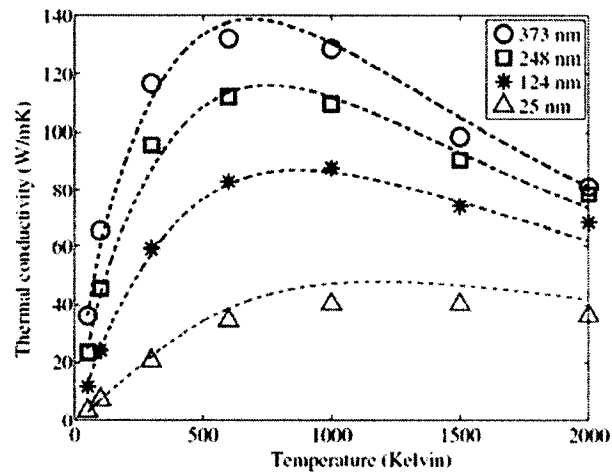


Figure 2-6 The simulation of the relation between the thermal conductivity of CNTs and temperature with shorter lengths of CNTs [14]

Besides, the different geometry structures of CNTs which are zigzag (20,0), chiral (10,13), and armchair (11,11), can also affect the thermal conductivity change. Figure 2-7 shows the relation between temperature and thermal conductivity for different geometry structures of CNTs [13]

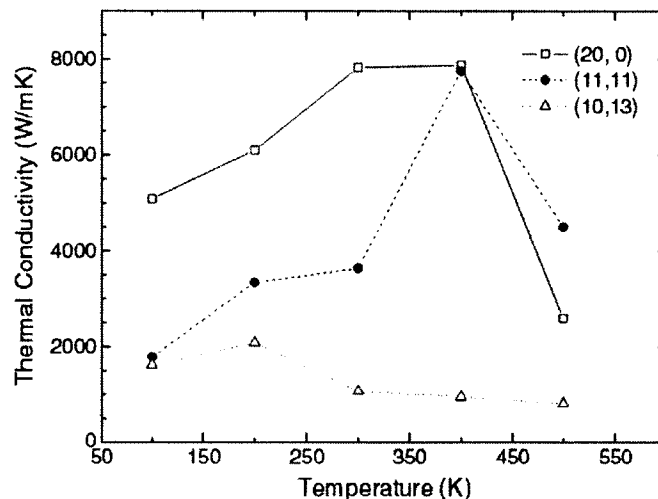


Figure 2-7 The relation between Temperature and thermal conductive in different CNT structures [13]

2.2.5 Optical Properties of CNTs

The optical properties of CNTs can be specifically described by absorption and Raman spectroscopy. Raman spectroscopy is the better way to detect and measure the CNTs. It has perfect spatial resolution and sensitivity to CNTs. In Raman spectroscopy, the CNTs are shown in the two different regions in Figure 2-8. At the region 1500 to 1600, it called G mode or G-band. The G-band can split into several peaks, because it depends on the structure of CNTs and excitation state. The G-band also can estimate the tube diameter and whether the tube is metallic or semiconducting.

In addition, the zigzag and chiral semiconducting structure of CNTs also present the photovoltaic property as a solar cell. When stronger energy photons, which can cross the band gap, excite the CNTs and generate pairs of electrons and holes, electrons will be able to jump cross the band gap and generating direct current electricity.

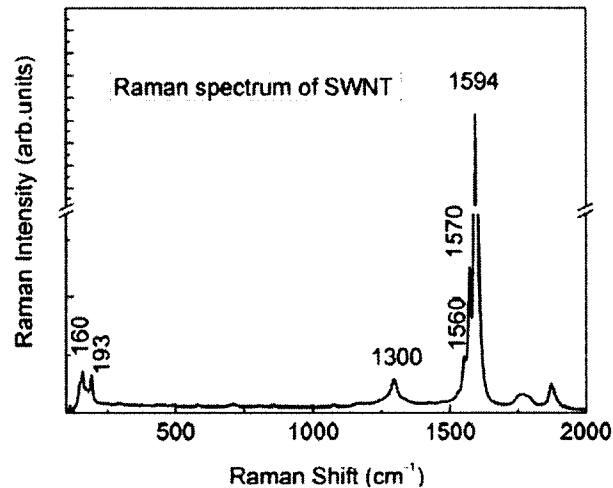


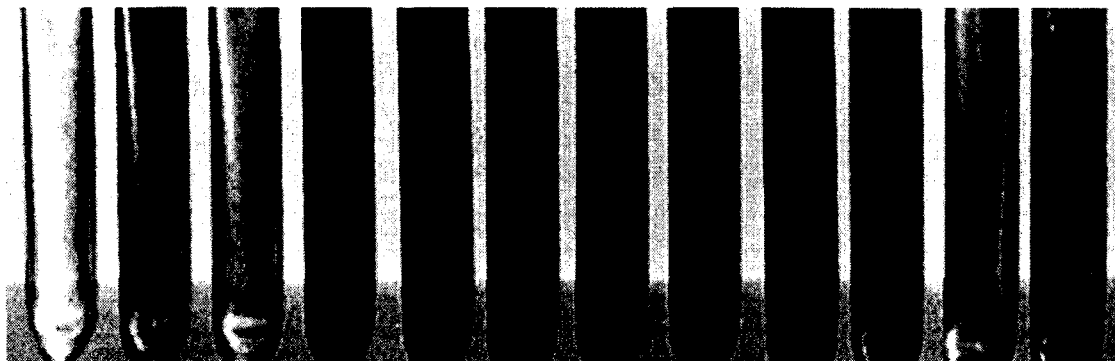
Figure 2-8 The Raman spectroscopy of single-wall carbon nanotube

2.3 Nanoparticles

Since 1994, the first publication describes the applications of nanoparticles. They show remarkable properties which are different than bulk or molecular materials and interested researchers in focusing on this brand-new research direction in nanotechnology.

For the fabrication, the lithographic and chemical methods are used to synthesize nanoparticles. Usually, the chemical method is the newer technology and can work on smaller size nanoparticle synthesis. In nanotechnology, when the sizes of materials are formed between 100nm to 1nm, they are called nanoparticles. Quantum dots specifically define the size of nanoparticles below 10nm. When the sizes of the nanoparticles become smaller, the quantum confinement and surface plasmon resonance effects occur in the nanoparticles, the electronic structure of nanoparticles are changed to affect the optical and electrical properties of the nanoparticles. The properties are size-dependent. For example, when the sizes of the nanoparticles are smaller, the colloidal nanoparticles show the different emission colors, because a blue-shift of the optical wavelength absorption occurs in the nanoparticles. The Figure 2-9 shows the Ag nanoparticles in solution

[16][17]. Every tube has different sizes of Ag nanoparticles. The left tube has bigger Ag nanoparticles and the right tube has smaller Ag nanoparticles.



Figures 2-9 Color changed in different sizes of nanoparticles [18].

2.3.1 Surface Plasmon Resonances

Another critical phenomenon that affects the size-dependent properties is surface plasmon resonances. This phenomenon occurs frequently on the surface dielectric/metal or vacuum/metal interfaces. When photons emit and stimulate the surface, the surface electromagnetic waves are generated and oscillate coherently along the interface [21].

For metal nanoparticles, when photons stimulate the surface of the nanoparticles, the surface electromagnetic waves lead the conduction electrons to oscillate collectively with the waves. Figure 2-10 shows the sketch of the surface plasmon resonance effect on metal nanoparticles [21]. Moreover, the surface plasmon resonances can efficiently enhance the optical absorption in colloidal metal nanoparticles. Comparing the bulk metal to metal nanoparticles, the metal nanoparticles have much larger surface area than the bulk surface area for the same volume. When the photons irradiate on the nanoparticles, the nanoparticles can absorb more incoming wavelength on the surface.

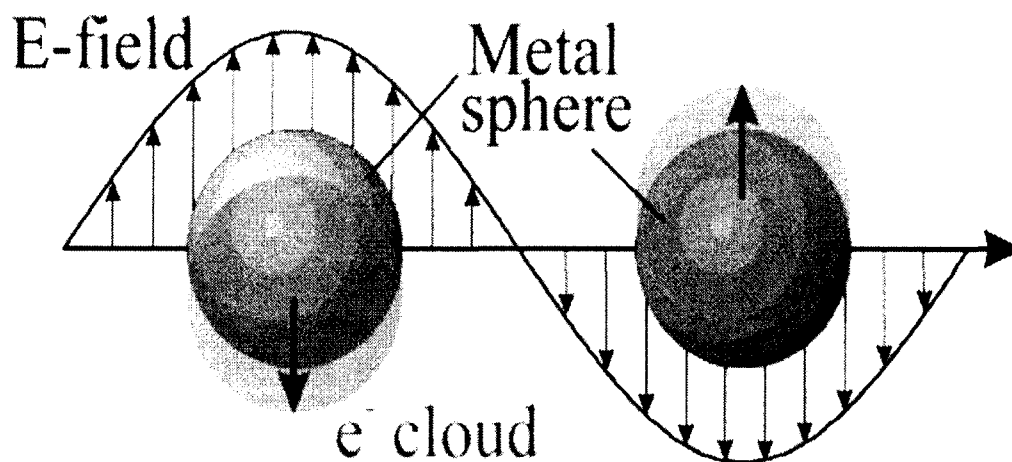


Figure 2-10 The sketch of the surface plasmon resonance effect on metal nanoparticles [21].

2.3.2 Quantum Confinement

One of the reasons, the nanoparticles are size-dependent and different compared to bulk and molecular materials, which is because the quantum confinement affects the semiconductor nanoparticles, such as Si, CdSe, or CuS nanoparticles. In CdS nanoparticles, when the sizes of the CdS nanoparticles reduce from 4.15nm to 0.6nm, the emission wavelength has a blue-shift from red color to blue color and the optical absorption is stronger. Moreover, the bandgap energy become higher from 1.88eV to 3.02eV and the electrons need more energy to jump from the valence band to the conduction band [19].

For the macro-size semiconductor, the bound state of the electronic exciton (electron-hole pair) is unrestricted because the dimension of the macro-size semiconductor crystallite is much larger than the exciton Bohr radius. When the size of the semiconductor reduces to nano-size, the dimension of the nano-size semiconductor is smaller than the exciton Bohr radius which results in the exciton being squeezed and confined into one dimension. This phenomenon is called the quantum confinement effect.

Due to the quantum confinement effect, the energy level becomes discrete and the energy band-gap becomes larger to generate a blue-shift in the optical emission. Figure 2-11 shows the quantum confinement effect in bulk semiconductors and nano-size semiconductors [20].

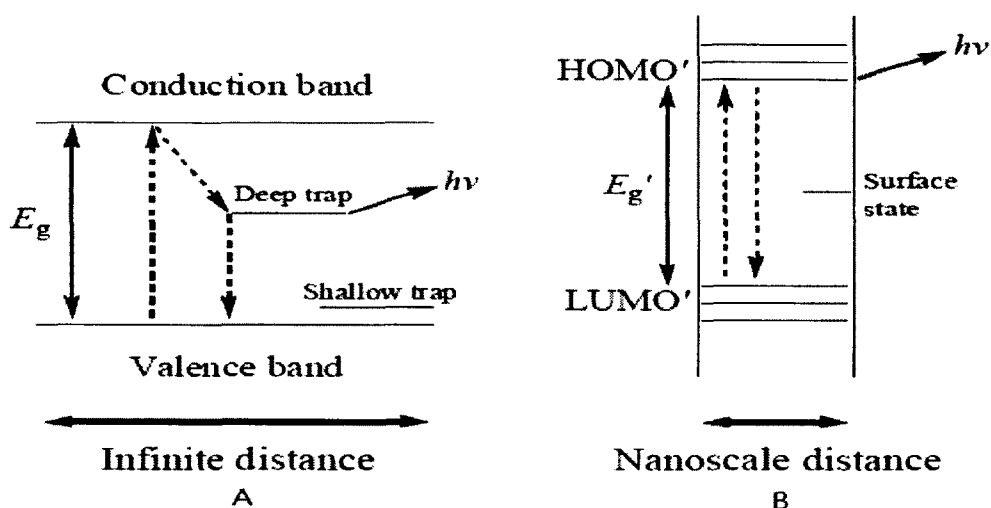


Figure 2-11 The quantum confinement effect in (A) bulk semiconductor and (B) nano-size semiconductor of the spatial electronic state [20].

2.4 CuS Semiconducting Nanoparticles

Generally, nanoparticles can be divided into two groups: metal and semiconductor nanoparticles. Copper sulfide nanoparticles (CuS nanoparticles) are one of the semiconductor nanoparticles which exhibit unique optical, thermal, and structural properties because of the quantum confinement effect and other nano-phenomena. Due to these properties, CuS nanoparticles have great potentials to benefit cancer therapy, optical sensing, and renewable energy applications [16].

2.4.1 CuS Nanoparticles Synthesis

In the beginning, 17mg of Copper(II) chloride ($\text{CuCl}_2 \cdot 2\text{H}_2\text{O}$) and 14.2 μl of thioglycolic acid ($\text{HSCH}_2\text{CO}_2\text{H}$) were added into 100ml of distilled water (DI water).

Thioglycolic acid is an organic compound that is used to stabilize the chemical reaction of CuS nanoparticles synthesis. A small amount of 1M NaOH solution was added into the Copper(II) chloride solution with stirring until the pH value reached 9.0 and then using argon bubbling degasification to promote the reaction for 20 min. After the bubbling degasification, the solution was mixed with 8 mg of thioacetamide which is dissolved into 20ml of DI water and heated up at 60°C for two hours for CuS nanoparticles to form [16]. Figure 2-12 shows the basic equipment to synthesize the CuS nanoparticles.

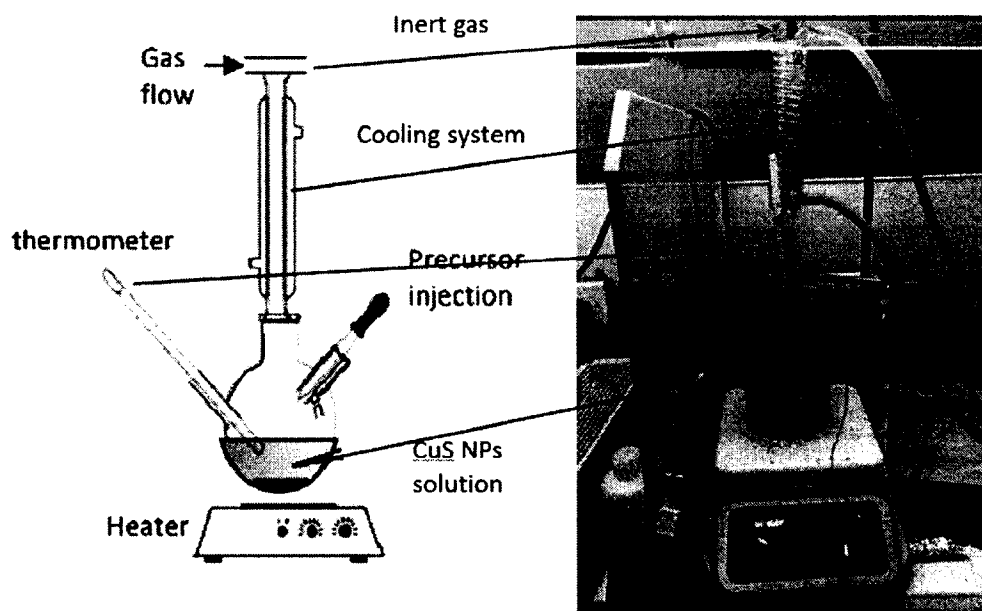


Figure 2-12 The equipment for synthesizing the CuS nanoparticles.

2.4.2 Optical and Thermal Property

Particle-wave duality is the fundamental phenomenon used to explain why the nanoparticles properties differ from bulk materials. Every particle exhibits particle and wave characteristics. In a macro-size, particle characteristics are easily observed but their wave characteristics, because the wavelength is in the nano-scale which is much smaller than the particle size, the wave characteristic is very difficult to perceive. When the

particle size reduces to nano-scale and the wavelength function is larger than the particle size, the wave characteristics become easier to observe than the particle characteristics. When the particle sizes are smaller than the wavelength, the free electrons are confined in the structure resulting in the free electrons needing stronger energy to cross the energy gap and a blueshift of the absorption wavelength in semiconductor nanoparticles [17][20]. Figure 2-13 shows a UV-vis-NIR absorption spectrum of CuS nanoparticles in which the particle sizes are about 3nm [16]. A blueshift can be observed in the CuS nanoparticles. The minimum light absorption location shifts from approximately 600nm (bulk CuS) to 500nm wavelength (CuS nanoparticles) [16][21]. The CuS nanoparticles exhibit great light absorption range from 450nm to 1050nm. Especially in the near-infrared (NIR) range, the maximum absorption of the CuS nanoparticles is at 900nm wavelength [16].

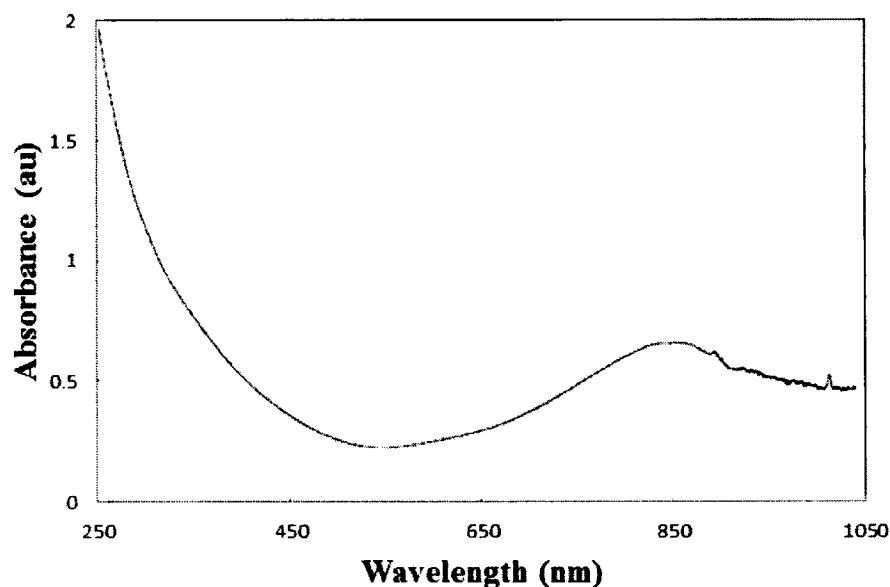


Figure 2-13 A UV-vis-NIR absorption spectra of CuS nanoparticles [16].

As a nanostructure, CuS nanoparticles can absorb the wavelength and generate the specific heat. In Figure 2-14, an experiment shows the CuS nanoparticles have a unique

thermal property. The gray points are the control solution (pure DI water) and the dark green points are DI water with amount of CuS nanoparticles. Both solutions are exposed to NIR light (808nm) for 15 min. The temperature of the CuS nanoparticles solution is increased 12.7°C, which is much higher than the control solution. According to the optical and thermal properties of CuS nanoparticles, the CuS nanoparticles have great potential to apply to energy harvesting devices and IR sensing detectors [16].

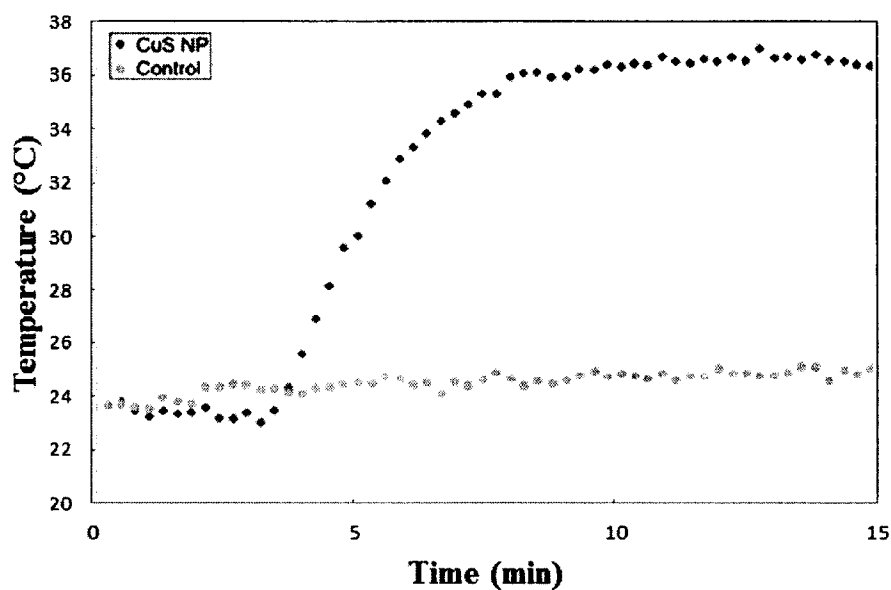


Figure 2-14 A heat generating experiment to measure the temperature change in control and CuS nanoparticles solutions. The two solutions are exposed to NIR light for 15 min [16].

CHAPTER 3

OPTICAL AND THERMAL PROPERTIES OF SWNTs-CuS HYBRID NANOMATERIAL

3.1 Introduction

Carbon nanotubes (CNTs), particularly a single-walled carbon nanotubes (SWNTs) thin film, shows excellent absorption of light and thermal radiation, which can be potentially used as the basis for constructing light and thermal energy cells [46–48]. The light and thermal absorption of the SWNTs and its thin film can be possibly further modified, optimized and enhanced by attaching some other nanomaterials (e.g. nanoparticles (NPs)) to the SWNT. In the past few years, a variety of SWNTs and NPs hybrid nanomaterials have been synthesized [49–58], mainly being achieved by utilizing either covalent or non-covalent binding mechanisms between NPs and SWNTs. Among these approaches, the non-covalent approach to synthesize the SWNTs-NPs hybrid nanomaterials is quite attractive since the attached NPs essentially do not change much the electronic structure of the SWNTs [49], while the covalent approach might induce some tremendous changes. The properties, particularly their optical properties, of this type of hybrid nanomaterials have been extensively studied, indicating their potential as the basic building blocks for tunable optoelectronic devices, thin film optic switches, optical chemical sensors and solar cells [49–53]. Recent work also found that

upon exposure to light and thermal radiation, the SWNT film can be used as a local temperature enhancer for the generation of thermoelectric power [46]. Nevertheless, little work has been done to evaluate the thermal (e.g. IR radiation) response of this type of hybrid nanomaterial. Hence, studies of the thermal response of the hybrid nanomaterials become necessary for the design and optimization of thermoelectric power generation and IR sensing applications.

This type of hybrid nanomaterial usually uses expensive noble metal NPs, such as Pt, Au or Ag NPs being attached to SWNTs, thereby modifying the electric and optical properties of SWNTs [49, 50]. These types of metal NPs clearly are unfavorable for synthesizing inexpensive hybrid nanomaterials for lowcost applications. To this end, some other compounds and relatively inexpensive nanomaterials, such as CdSe, CdS and PdS NPs have been utilized to replace noble metal NPs [55,57,58]. However, the toxic and harmful properties of cadmium, lead and their compounds are not favorable for the synthesis of 'green' hybrid nanomaterials, hence it is becoming critical to have low-cost and environment-friendly nanomaterials to replace these expensive or toxic ones.

One of the ideal and promising materials is copper sulfide (CuS) NPs, which are both eco-friendly and inexpensive. In addition, CuS NPs have a broad absorption of light from 400 to 1100nm [59, 60]. Some CuS-based hybrid nanomaterials, such as CuS=ZnS and CuS=ZnO heterostructures, have been synthesized and their optical properties have been evaluated, exhibiting remarkable photocatalytic stability [51,55]. The photoresponse of multi-walled carbon nanotubes–copper sulfide (MWNT-CuS) hybrid nanomaterials has also been reported [53]. In this case, the hybrid nanomaterials were formed by using acid-functionalized MWNTs as templates, copper sulfate pentahydrate ($\text{CuSO}_4 \cdot 5\text{H}_2\text{O}$)

and thiourea ($\text{N}_2\text{H}_4\text{SC}$) as a copper source and a sulfur source, respectively. Using a hydrothermal method, MWNTs-CuS hybrid nanomaterials have been synthesized.

Experiments found that the hybrids can generate significant photocurrent while pure MWNTs and CuS NPs alone do not show any light responses, suggesting that the photocurrent only results from the combined effect of MWNTs and CuS NPs. Experiments also found that the hybrids show a clear rectifying effect, indicating that Schottky junctions are formed between MWNTs and CuS NPs. However, the rectifying characteristics might limit the applications of the as-synthesized MWNTs-CuS hybrid nanomaterials, especially as the building blocks for constructing some electronic and optoelectronic devices [61]. Additionally, similar to other hybrid nanomaterials, the thermal or IR response of this type of hybrid nanomaterial has not been studied either.

Finally, to the best of our knowledge, there is no report on the optical and thermal response of the SWNTs-CuS hybrid nanomaterials, especially the SWNTs-CuS hybrid nanomaterials without rectifying effects. Herein, synthesis of SWNTs-CuS NPs hybrids of metal-like electrical conductivity by simple non-covalent chemical route using oleylamine molecules as the linker molecules is reported. Studies of the photoresponse and thermoresponse of the hybrid nanomaterials compared to SWNTs thin film under light illumination and thermal radiation are reported. In addition, as a technical demonstration, a prototype thermoelectric generator enabled by the SWNTs-CuS NP nano hybrids is also reported.

3.2 Experiments Setup and Measurements

3.2.1 Materials

SWNTs powder was purchased from Carbon Solutions, Inc. and used without any further purification. Toluene solution was purchased from Sigma-Aldrich, Inc. (MO, USA). Oleylamine was purchased from Fluka (Sigma-Aldrich, MO, USA). Thioglycolic acid (TGA), $\text{CuCl}_2 \cdot 2\text{H}_2\text{O}$ and thioacetamide were purchased from Sigma-Aldrich (MO, USA). CuS nanoparticles were synthesized using a procedure similar to previously reported approach from other research groups [59,62]. Specifically [59], a certain amount (0.017048 g) of $\text{CuCl}_2 \cdot 2\text{H}_2\text{O}$ was dissolved within 100ml distilled water, followed by adding 0.2 mmol of TGA under constant stirring. The solution's pH was adjusted to 9.0 by adding a 1M solution of NaOH. The solution, contained in a three-necked flask fitted with a septum and valves, was degassed for 20 min by argon bubbling, followed by adding a solution containing 8.0mg thioacetamide in 20ml distilled water. The mixture was then heated at 50°C for two hours to promote CuS nanoparticle growth.

3.2.2 Synthesis of SWNTs-CuS NPs Hybrid Nanomaterial

For the synthesis of the SWNTs-CuS NPs hybrid nanomaterial, oleylamine molecules were used. The oleylamine molecules allowed for the functionalization of the surface of the SWNTs. This process allows for the creation of an electrical charge on the surface of the SWNTs. This charge attracts the CuS NPs (due to their opposite electrical charge). The process used 10mg of SWNTs powder that was mixed in a solution of 150 μl of oleylamine molecules and 100ml of toluene. This solution was stirred under a pure nitrogen atmosphere overnight to functionalize the surface of the SWNTs. After the completion of chemical reaction, the functionalized SWNTs (f-SWNTs) solution was

placed in a centrifuge (5000 r.p.m. for 30 min) to separate the f-SWNTs powder and the toluene solution. Next, the f-SWNTs powder had to be washed two times in 100ml of isopropyl alcohol (IPA) and sonicated for one hour to clean the f-SWNTs and remove any of residual oleylamine. After two cycles of IPA cleaning, the f-SWNTs powder was mixed again with a new solution of 100ml toluene solution. The f-SWNTs powder was uniformly suspended in toluene solution under sonication for one hour. Now, the f-SWNTs solution is ready to be bonded with the CuS NPs. The prepared CuS NPs solution can be directly added and suspended in the f-SWNTs solution, which can then be sonicated overnight to form the SWNTs-CuS NPs hybrid nanomaterial solution. Then, the SWNTs-CuS NPs hybrid nanomaterial was precipitated by adding a small amount of methanol [22]. Figure 3-1 shows the brief processes of synthesis SWNTs-CuS NPs.

In this dissertation, three different SWNTs-CuS NPs hybrid nanomaterial solutions were prepared. For the preparation of the SWNTs-CuS NPs solutions, the same amount of the functionalized SWNTs was dispersed in 100ml toluene in three beakers separately, followed by adding three different concentrations (100, 200, 300 μ l) of CuS NPs solution to the three beakers to obtain three types of hybrid nanomaterials.

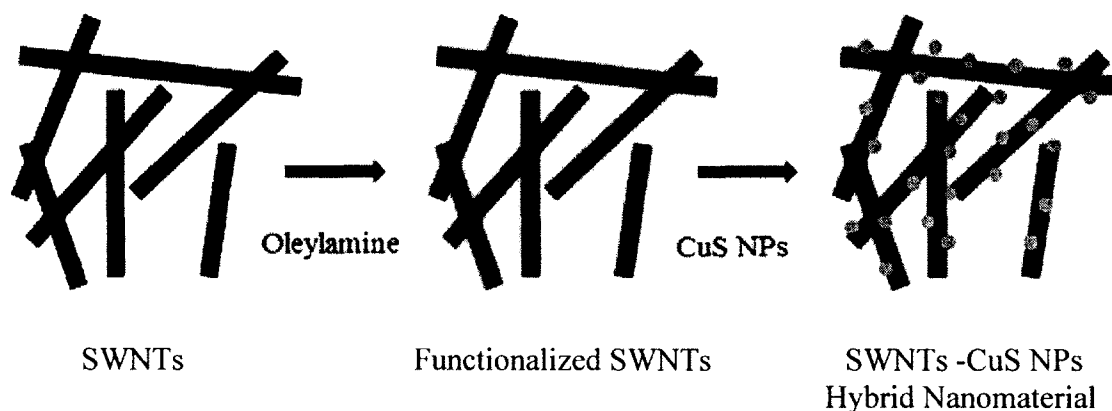


Figure 3-1 The brief processes of synthesis SWNTs-CuS NPs

3.2.3 Fabrication of Devices Based on SWNTs-CuS NPs Hybrid Nanomaterials

Thin films of both SWNTs-CuS NPs hybrid nanomaterials and SWNTs were prepared on a mixed cellulose ester (MCE) membrane using a vacuum filtration method published in the literature[53]. Briefly, the nanohybrid and SWNTs suspensions were vacuum filtered separately through a mixed cellulose ester (MCE) filter (47mm in diameter). The resulting thin film on the filter was rinsed twice with isopropyl alcohol and deionized water and then dried at 80°C for two hours to remove any remaining organic residues in the film. After drying, the thin film sheet can then be either peeled off the filter or transferred onto a solid or flexible substrate after being cut into desirable sizes.

Two-Terminal Thin Film Devices. The thin film, measuring 1.5cm (length) × 1.0cm (width) × 25μm (thickness), was anchored on a glass substrate, with two ends connected with Cu wires using Cu conductive glue forming two electrodes (Anders Product, Inc). The thin film devices were then measured under different light and thermal (heat) radiations.

Prototype Thermoelectric Generator Devices. Cu strips and Si strips diced from a p-type silicon wafer with 500μm thickness were used to construct prototype thermoelectric generator devices on a glass substrate. The Seebeck coefficient of Cu is ~1:84μV K⁻¹ and the Seebeck coefficient of Si (the p-type Si doped with boron at a concentration in the range of 3×10^{18} to 2×10^{19} cm⁻³) is ~300μV K⁻¹ [19]. Cu strips and a Si strip were connected by Cu conductive glue (Anders Product, Inc.). One junction between the Cu and Si strip was embedded in the SWNTs-CuS nanohybrid thin film,

while the other junction was exposed to air. For comparison, other devices with the same dimensions were fabricated, but with both junctions exposed to air.

3.2.4 Synthesis the Hybrid Nanomaterial Thin Films

For different applications, both the SWNTs and the SWNTs-CuS NPs nanomaterial can be formed into thin film structures by the vacuum filtration method. The preparation of the SWNTs-CuS NPs solutions has been explained in Section 3.2.2. Figure 3-2 (a) shows the synthesized SWNTs-CuS NPs solutions. For the SWNTs solutions, the SWNTs powder can directly mix with isopropyl alcohol (IPA) to synthesize the SWNTs solution. 10mg of SWNTs powder and 100ml of IPA can synthesize about a 20-25 μ m thick SWNTs thin film. The thicknesses of the thin films are able to be increased by increasing the volume of SWNTs used. Before the synthesis of the SWNTs or SWNTs-CuS NPs thin films, the mixture solutions had to be sonicated overnight to make uniformly mixed SWNTs or SWNTs-CuS NPs solutions. For the setup of the vacuum filtration, which is shown in Figure 3-2 (b), a Whatman ME-24 mixed cellulose ester (MCE) membrane was mounted between two flasks; the diameter of the MCE is 48mm and has pore size of about 200nm. A vacuum pump was connected to the bottom flask by a plastic tube to draw the solution down into the bottom flask. For forming the thin film, the solution was poured into the top flask and the vacuum pump draws the liquid down into the bottom flask and only leaves the SWNTs or SWNTs CuS NPs hybrid nanomaterial to deposit a uniform and tight thin film on the MCE membrane. Figure 3-2 (c) shows the top view of the top flask and (d) shows the SWNTs CuS NPs hybrid nanomaterial thin film deposited on the MCE membrane.

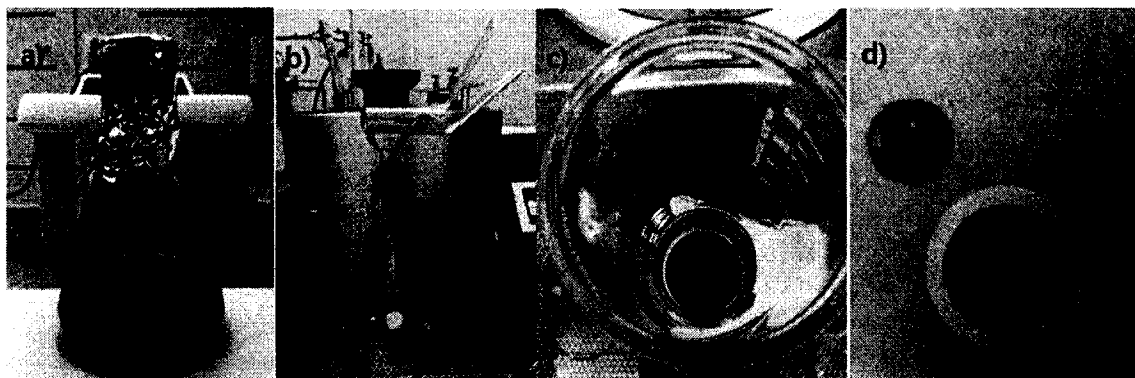


Figure 3-2 (a) shows a 100ml of the SWNTs-CuS NPs hybrid nanomaterial solution. (b) shows the vacuum tube is drawing the liquid down to the bottom flask. (c) shows a SWNTs-CuS NPs thin film uniformly deposited on the top of the MCE membrane. (d) shows the MCE membrane with the SWNTs-CuS NPs thin film.

3.2.5 Characterizations

The surface morphology of the samples was characterized using a scanning electron microscope (SEM, HITACHI S-4800) and a transmission electron microscope (TEM, ZEISS Libra 120). The chemical composition of the samples was analyzed from the Raman spectra using a SENTERRA Raman Microscope (Bruker Optics, Inc.). The reflectance spectra were recorded using optic-fiber-based reflectance measurement system (Ocean Optics, Inc.). The light and thermal radiation source used in the experiments was the Olympus TL-2 incandescent lamp. The cold light source used in the experiment was an XD-301 series 150W halogen lamp cold light source. The light power was measured using a CCD optical power meter (Thorlabs PM100). The light intensity was calculated by the measured light power divided by the CCD sensing area. The temperature from the lamp was measured with a thermocouple (Omega HH306). The current–voltage (I-V) curves of the thin film devices were measured using an electrical measurement probe station (Keithley Instruments). The currents or voltages generated by the thin film devices and prototype thermoelectric generator devices upon exposure to a

lamp, or a cold light, or a heat source were measured using a digital multimeter (Agilent U1253B). Based on these measurements, the power generated by the prototype thermoelectric generator was obtained.

3.3 Results and Discussion

The TEM images of the hybrid nanomaterials are given in Figure 3-3(a). It is clear that the CuS NPs are attached to the SWNTs, which provide and facilitate the direct pathways for charge transfer between NPs and SWNTs. The SEM image of the SWNTs-CuS NP nanohybrid thin film is shown in Figure 3-3(b). It also reveals that the SWNTs are decorated with CuS NPs. Raman spectra of the SWNTs-CuS NP hybrid nanomaterial and the SWNTs are shown in Figure 3-3(c). As expected, the major spectra between nanohybrids and pure SWNTs show little difference, suggesting that the electronic structure of the SWNTs remains essentially unchanged, thus the electrical property of the nanohybrids should be similar to that of the SWNTs but definitely different from that of the SWNT-CuS NPs hybrid nanomaterials that were synthesized differently [53].

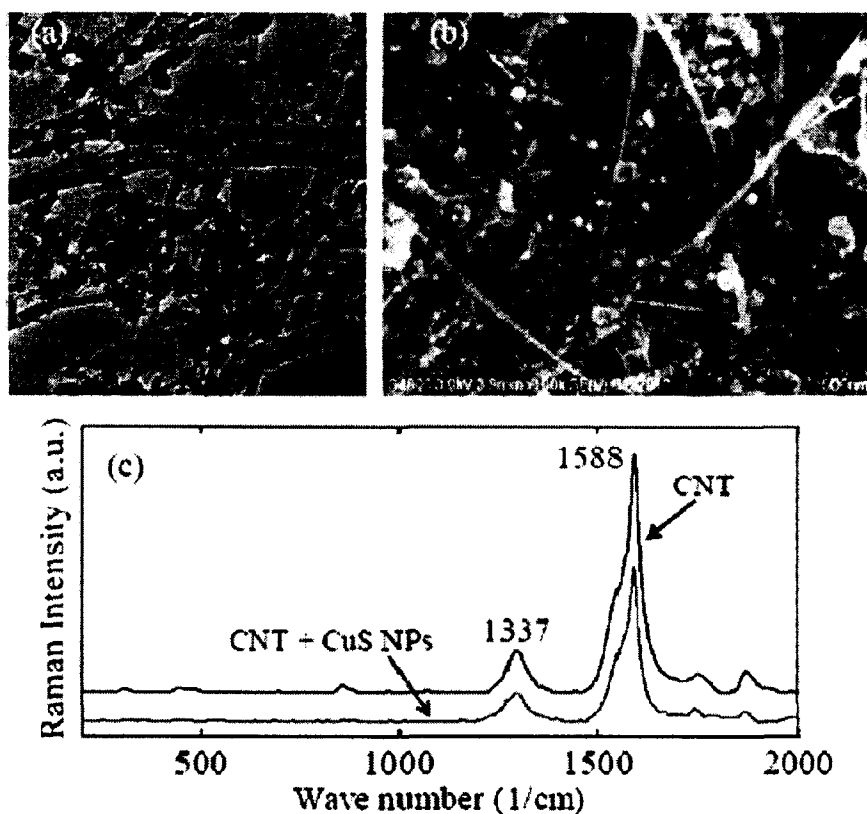


Figure 3-3 (a) shows TEM image of SWNTs-CuS NPs hybrid nanomaterial. (b) shows SEM image of SWNT-CuS NPs hybrid thin film. (c) shows Raman spectra of SWNTs-CuS NPs hybrid nanomaterial and SWNTs.

The light absorption capability of the nanohybrid thin film has been evaluated. The measured reflectance from different thin films on glass substrates is shown in Figure 3-4. The reflectance from the SWNT thin film and the nanohybrid thin films of the same thickness of $\sim 25\mu\text{m}$ decreases tremendously, indicating the strong absorption of the visible and near IR light by the SWNTs thin film [47] and the nanohybrid thin films. In addition, it was found that the reflectance further decreases, thus the absorption of the light further increases, with the increased amount of the CuS NPs decorated with SWNTs as compared to the pure SWNTs, which is as shown in Figure 3-4(b). The enhanced absorption of the photons by the hybrid nanomaterial is due to the strong absorption of the photons by the CuS NPs attached to SWNTs from the visible to the near IR range (e.g.

400-1100nm) [59, 50]. Hence, it is anticipated that the heat generated by the nanohybrids due to the quantum effect of the NPs and the unique thermal properties of SWNTs can be further enhanced, as compared to a pure SWNTs thin film [65, 66].

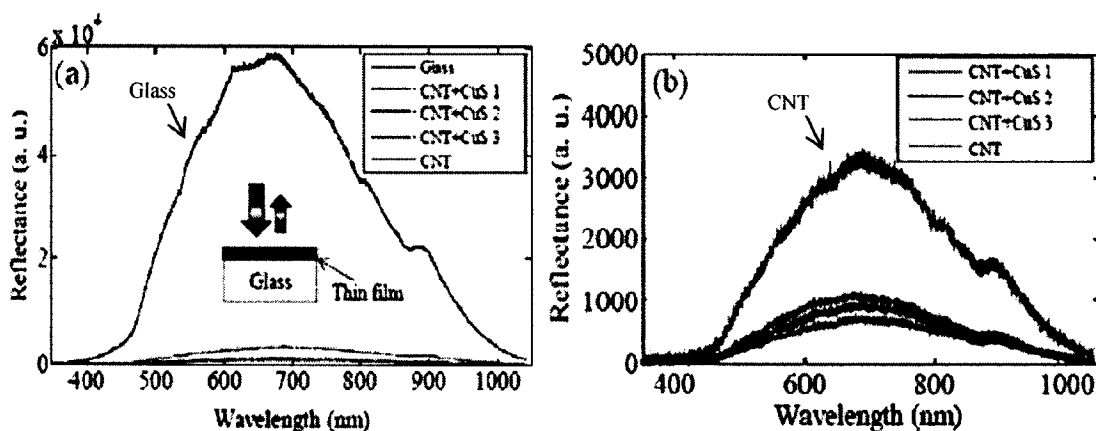


Figure 3-4. (a)-(b) show reflectance measurements of a SWNTs thin film and three SWNTs-CuS NP hybrid thin films made by decorating SWNTs with three different amounts of CuS NPs (SWNTs-CuS 1: 10mg SWNTs decorated with 100 μ l CuS NPs solution; SWNTs-CuS 2: 10mg SWNTs decorated with 200 μ l CuS NPs solution; SWNTs-CuS 3: 10mg SWNT decorated with 300 μ l CuS NPs solution) in the spectrum range from UV-visible to near IR. The inset in (a) shows the measurement setup: the light illuminates perpendicularly to the thin film/glass surface and the reflected light is measured.

A schematic and a photo of a hybrid nanomaterial thin film device on a glass substrate are shown in Figures 3-5(a)–(b), which has two Cu-wire electrodes connected to both ends to form a two-terminal device. The current generated by the thin film device, when a lamp (Olympus TL-2 incandescent lamp) is positioned to illuminate different regions of the device, has been measured, as shown in Figure 3-5(c). In addition, the current generated, when one electrode is covered by a polydimethylsiloxane (PDMS) slab, has also been measured. The measured current is zero before the lamp is turned on. When the lamp is positioned at and illuminates the center of the device, as illustrated in Figure 3-5(c-1), a stable current is generated and is stable at about 0.31 μ A. This current is due to

the photovoltaic and thermovoltaic effect of the nanohybrid thin film, since no temperature difference exists between the two electrodes [48, 67]. When the lamp is off and removed, the current returns to zero. However, when one electrode is covered by a 4mm thick PDMS slab, as show in Figure 3-5(c-2), under the same experimental conditions, the generated current measured to be about $0.50\mu\text{A}$ after the lamp is on but, eventually the current decreases and reaches the same level as that of the device without the PDMS slab. This observed phenomenon suggests that the temperature at the electrode covered by a PDMS slab is a little lower than that of the other electrode at the beginning when the lamp is first turned on. Thus, a thermoelectric voltage is also generated [35] and added to the voltage generated only by the nanohybrid thin film, resulting in an increase in the current (i.e. from 0.31 to $0.50\mu\text{A}$). After a certain time, when the heat diffuses through the PDMS layer and reaches the electrode underneath, the temperature difference between the two electrodes decreases. As a result, the thermoelectric voltage also decreases as well. Eventually the current becomes the same level as that of the device without a PDMS slab. When the lamp is removed, the current drops and becomes about $-0.24\mu\text{A}$ for a while before the current returns to zero. This is due to the fact that for the electrode covered by the PDMS slab, its temperature is maintained and is higher than that at the other electrode for sometime before the two electrodes reach the same temperature. If the lamp is positioned at and illuminates one of the electrode regions of the device without applying a PDMS slab, the so-called asymmetric illumination in Figures 3-5(c-3), the measured current is about $3.6\mu\text{A}$, which is about one order of magnitude larger than that of the aforementioned case (i.e. $0.31\mu\text{A}$), suggesting that the asymmetric illumination can greatly enhance the current generation, thereby improving the sensitivity of the

nanohybrid thin film devices. The light intensity is 1.0mW mm^{-2} and thermal radiation (temperature change) is 17.6°C for all three experiments.

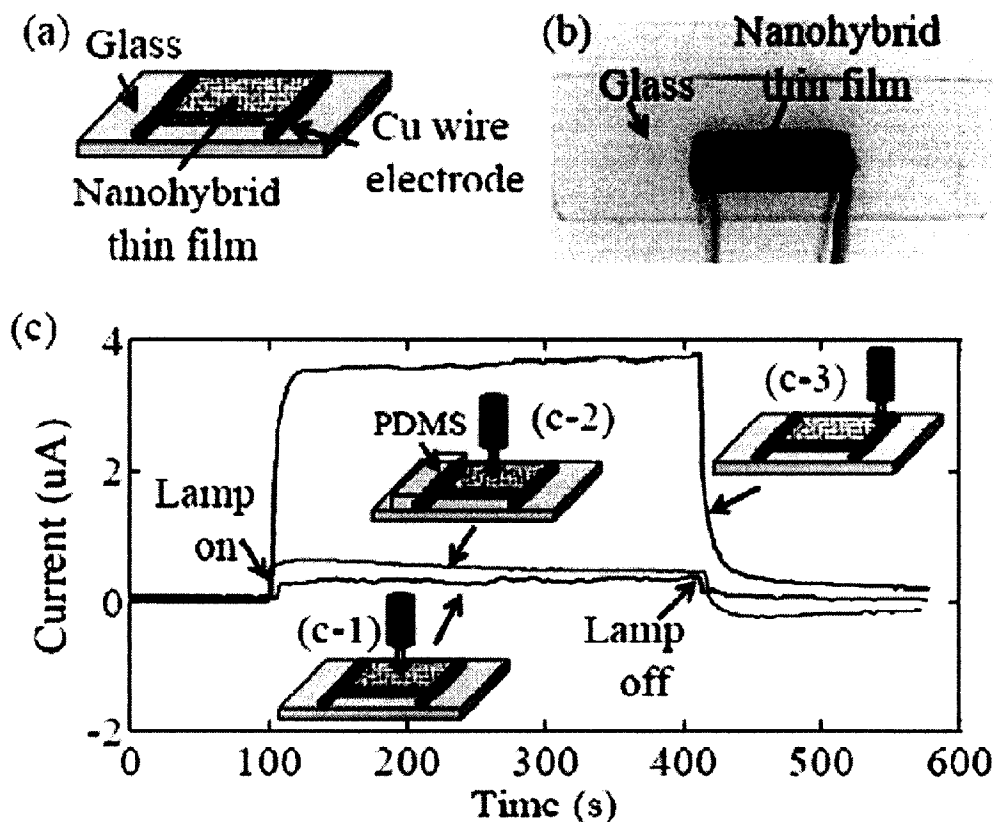


Figure 3-5 (a) shows schematic of the nanohybrid thin film device. (b) shows photo of a SWNTs-CuS NP hybrid thin film device on a glass substrate. (c) shows measured current when the light and heat source illuminates the nanohybrid thin film device at different regions.

In the following, the asymmetric illumination technique has been utilized to evaluate the optical and thermal response of the nanohybrid thin film device. The setup for evaluating the photoresponse, thermoresponse and photothermoresponse of the thin film devices is illustrated in Figure 3-6(a). In order to analyze the photoresponse of the nanohybrids, the photocurrents of the thin film device have been measured using a cold light source with light intensity of 0.57mW mm^{-2} and a thermal radiation (temperature

change) of 2.4°C. In this case, the thermal radiation from the light source is minimized. Thus, the optical effect on the nano hybrids is dominant and can be evaluated. I-V measurements of the SWNTs-CuS NPs nano hybrid and the pure SWNTs-based thin film devices are shown in Figure 3-6(b). The measured I-V curves exhibit high linearity, confirming the metal-like electrical properties of nano hybrids. It has been found that the I-V slope (conductance) increases when the optical source is turned on and will go back to its original position if the optical source is off, with excellent repeatability.

For the pure SWNTs thin film device, the conductivity change before and after turning on the light is quite small at about 4.3%, which is consistent with the results previously reported in the literatures [53, 55], while the changes for the nano hybrid thin film devices are much larger, in the range of 28.7% to 57.2%. Basically, the more the CuS NPs are decorated with SWNTs, the larger the conductivity. In other words, the resistance of the thin film devices decreases when the light is on compared to when the light is off. The resistance further decreases when the light is on if the number of CuS NPs decorated with SWNTs increases, as shown in Figure 3-6(c). The aforementioned optical switching characteristics of the nano hybrid material have been further observed and are shown in Figure 3-6(d). In these measurements, no voltage is applied on the thin film device and the light source is turned on and off periodically with varied duration. The photocurrent shows clear modulation and switching characteristics. It is well known that the origin of the photocurrent involves the following process: absorption of photons, creation of excitons (electron-hole pairs) and transfer of charges [69]. As previously reported, the functionalization of SWNTs with oleylamine molecules makes it an n-type material, thereby making the electrons the major carriers in the hybrid nanomaterial [55,

56]. The optical switching behavior of the hybrid nanomaterial under light illumination is thus due to these aforementioned processes in CuS NPs and SWNTs [69]. Specifically, upon light illumination, excitons (electron-hole pairs) are generated in CuS NPs and SWNTs. While the holes would remain in the CuS NPs, the electrons will transfer to the SWNTs. As a result, an enhanced photocurrent is generated and enhanced conductivity of the hybrid nanomaterial is achieved.

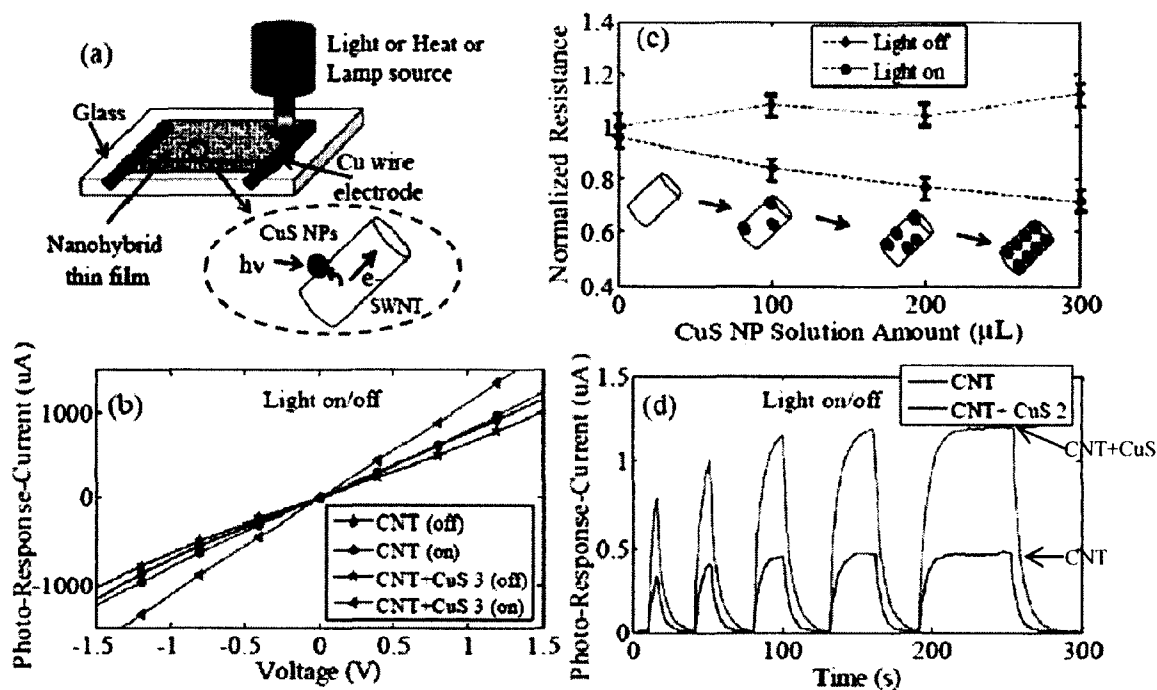


Figure 3-6 (a) shows experimental setup: a source (e.g. light, heat or a lamp source) illuminates the thin film devices; the inset shows the electron creation and transfer from a CuS NP to a SWNTs. (b) show photon response: I-V curves of SWNTs and SWNTs-CuS NP nanohybrid thin film devices with light on and off. (c) shows modulated resistance (normalized to the resistance of the pure SWNTs thin film device) for different numbers of CuS NPs in the nanohybrids with light on and off; the inset shows that more and more CuS NPs are attached to SWNTs. (d) shows modulated photocurrent for the nanohybrid thin film device made of SWNTs-CuS 2 (10mg SWNTs decorated with 300 μ l CuS NPs solution) with light on and off using a SWNTs thin film device as a reference.

The thermoresponse from the nanohybrids has also been evaluated experimentally.

The thin film devices for the experiments are the same as those in the optical experiments.

In this case, the lamp is covered with Al foil, thus only the thermal radiation will reach the devices. The thermal radiation (temperature change) is 18.0°C for the experiments. Thermocurrent measurements of nanohybrid and SWNTs thin film devices are shown in Figures 3-7(a)-(c). The observed I-V behaviors of the devices are similar to those of the photoresponse, but the conductivity change is much larger. Specifically, the change is about 90.5% for SWNTs and from ~110.2% to ~166.3% for nanohybrids. Correspondingly, the resistance of both the SWNTs and the nanohybrid thin film devices decreases dramatically when the heat is turned on. The resistance of the nanohybrid thin film devices further decreases with SWNTs that are decorated with the increased amount of CuS NPs. All these measurements show the thermal switching behavior of the SWNTs and nanohybrids. This unique behavior of this type of nanohybrid suggests that their sensitive response to the thermal illumination can be potentially used for infrared (IR) sensing applications [35]. The origin of the thermocurrent in the SWNTs and the hybrid nanomaterial thin film devices should involve phonon absorption and exciton (electron-hole pair) creation and dissociation, resulting in free electrons and holes and charge transfer [70, 71]. As previous report, the change in conductivity or resistivity of SWNTs thin film is largely due to the temperature change in the thin film, but not due to the presence of photoexcited holes and electrons [70]. This phenomenon has also been observed in our nanohybrid material system.

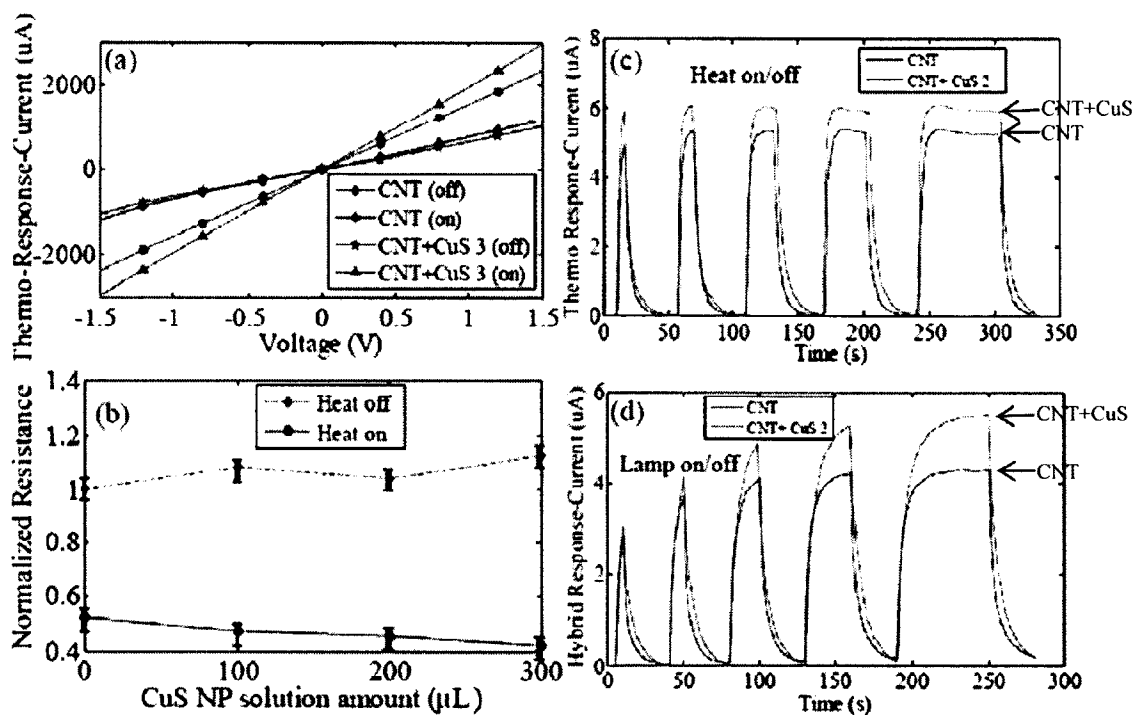


Figure 3-7 (a) shows thermoresponse: I-V curves of SWNTs and SWNTs-CuS nanohybrid thin film devices with heat on and off. (b) shows modulated resistance (normalized to the resistance of the pure SWNTs thin film device) for different numbers of CuS NPs in the hybrids with heat on and off. (c) shows modulated thermocurrent for the nanohybrid thin film device made of SWNTs-CuS 2 (10mg SWNTs decorated with 300µl CuS NPs solution) with heat on and off using a SWNTs thin film device as a reference. (d) shows modulated hybrid current for the nanohybrid thin film device made of SWNTs-CuS 2 (10mg SWNTs decorated with 300µl CuS NPs solution) with lamp light and heat on and off using a SWNTs thin film device as a reference.

For instance, compared to the measured resistance change on the same thin film device in Figures 3-6(c) and 3-7(b), the resistance change shows a big difference under light and thermal (IR) illumination, respectively. Under light illumination, the resistance change of an SWNTs thin film device is only about 4.3%. In contrast, the change is much more significant, at about 47.5%, under thermal irradiation. This is due to the fact that under light illumination, even though electrons and holes can be efficiently generated in SWNTs, the temperature in the SWNTs thin film only has a small change, resulting in a very small change in resistance [70]. However, even under light illumination, but with the

increased amount of CuS NPs attached to SWNTs, the resistance change becomes larger (Figure 3-6(c)) since the temperature of the thin film increases more due to the increased amount of CuS NPs.

This suggests that the optical sensitivity of the nanohybrid thin film devices can be improved dramatically by attaching NPs to the SWNTs. The photo-thermoreponse of the nanohybrid thin film has also been evaluated. In this case, the lamp is used to provide a source of both light and heat. It was found that there was a similar response for the photoresponse and thermoresponse of the thin film devices, as shown in Figure 3-7(d). Obviously, in this case, the nanohybrid thin film interacts with both the light and thermal radiation, and thus the generated current results from the combined effects from photons and thermal radiation.

Usually, in order to build a thermoelectric generator to convert thermal/heat energy into electricity, a temperature difference or gradient needs to be formed and maintained across the device [68, 72]. Ideally, a temperature difference or gradient across a thermoelectric generator can be self-maintained when it is exposed to a light or a thermal radiation source. As a technical demonstration, a prototype thermoelectric generator enabled by the SWNTs-CuS NPs hybrid nanomaterials has been designed, constructed and tested. The prototype device, shown in Figure 3-8(a), consists of Junction I formed by a Cu and a silicon strip embedded in the hybrid nanomaterial thin film, and Junction II formed by a Cu and a silicon strip open to the air. Since there is a difference between the Seebeck coefficients of Si and Cu, a voltage will be generated if the temperature between Junctions I and II is different. When a light source is uniformly illuminated on the whole device, the two junctions have an intrinsic temperature

difference due to the higher local temperature at Junction I embedded in the hybrid nanomaterial. As a result, a voltage will be generated.

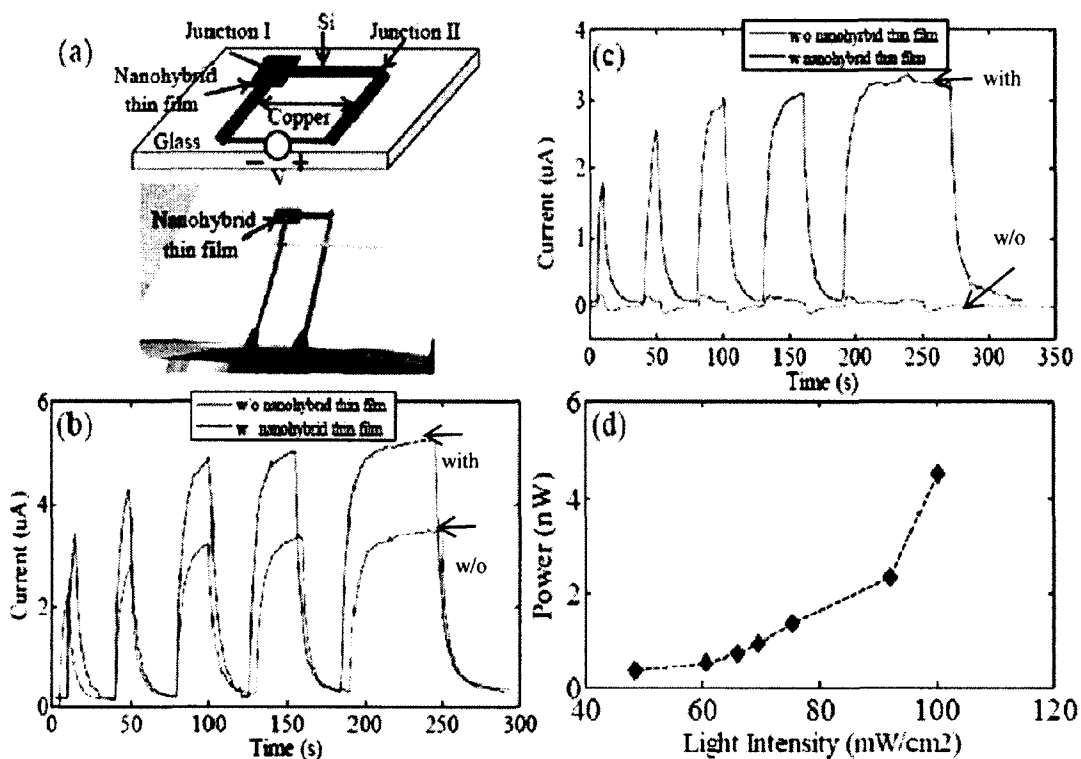


Figure 3-8 (a) shows sketch and photo of a prototype thermoelectric generator. (b) shows measured current when the lamp illuminates the Junction I region of the devices with and without nanohybrid thin film. (c) shows measured current when the lamp uniformly illuminates the devices with and without nanohybrid thin film. (d) shows measured power generation of the prototype thermoelectric generator.

For comparison, two 'identical' devices have been fabricated except that one has nanohybrid material and the other does not. In Figure 3-8(b), the measured current when the illumination of a lamp is focused on the Junction I region is given. As can be seen, for both devices, the currents have been clearly generated but the current is larger for the device with the integrated nanohybrid in the Junction I region than that without the nanohybrids. In Figure 3-8(c), the lamp uniformly illuminates the whole device. As can be seen, the device with integrated nanohybrids has much larger current generation than

that without nanohybrids, which has essentially negligible current generation since the temperature difference between Junctions I and II is close to zero. In contrast, for the device with nanohybrids, the temperature difference exists intrinsically between the two junctions due to the significant thermoresponse and photoresponse of the nanohybrids. The measured power generation of the prototype device, as shown in Figure 3-6(d), is in the range of nano-watts, which can be scaled up to the range of micro-watts or even milliwatts by cascading a series of these types of structures. This technical demonstration indicates that this new route for designing thermoelectric generators requires no heat-sink and cooling components, but the temperature difference in the generators can be formed and thus intrinsically maintained by integrated nanomaterials or nanostructures.

3.4 Summary

In summary, single-walled carbon nanotube–copper sulfide nanoparticle (SWNTs-CuS NP) hybrid nanomaterials have been synthesized and their properties have been characterized. Compared to the SWNTs thin film devices, the hybrid nanomaterial thin film devices exhibit clearly enhanced optical and thermal switching characteristics, light absorption, photocurrent and thermocurrent generation under light illumination or/and thermal radiation. A prototype thermoelectric generator enabled by the hybrid nanomaterials has been designed and demonstrated, providing a new route to obtain thermoelectricity without any cooling or heat-sink component.

CHAPTER 4

ULTRASENSITIVE THIN FILM INFRARED

SENSORS ENABLED BY HYBRID

NANOMATERIALS

4.1 Introduction

Infrared (IR) sensing is an important technology for a variety of applications in energy, environmental science, and medical engineering, such as energy metering [73], pollutant monitoring in environments [74,75], remote sensing [76], thermal imaging [77], night vision [78], thermal photovoltaic [79], medical imaging [80] and optical communication [81]. Silicon and some organic materials are sensitive to IR but not sensitive beyond 800nm. In order to extend the IR detection range, some nanomaterials, such as carbon nanotubes (CNTs), CNT composites, carbon nanoparticles and graphene thin films have been explored for IR sensing. The reported sensitivity of nanomaterial-based IR sensors is in the range of 0.7% to 52.9% [82,35,37,83,84]. Specifically, Haddon and his co-workers have evaluated the IR sensing ability of a suspended pure CNTs thin film. It was found that the IR response can be greatly improved if the CNTs film is suspended in a vacuum, which is about a 0.7% change in its resistance [82]. Chen and co-workers have utilized CNTs composites to build a thin film IR sensor; experiments found that IR response in terms of conductivity change is about 4.26% [35]. Recently, Wang

and co-workers have developed a simple way to fabricate carbon nanoparticle thin film IR sensors and experimental results demonstrate a photocurrent change of up to 52.9%, and the lowest IR intensity which can be detected is $\sim 45 \mu\text{Wmm}^{-2}$ [37].

Due to their unique optical, electrical and thermal properties, CNTs and their thin films have been used for a great number of applications, including light and thermal energy harvesting [84,47,48]. Previous research also found that the optical and electrical properties of CNTs and their films can be modified, optimized and enhanced by decorating CNTs with some other nanomaterials, such as nanoparticles. Over the past years, a variety of CNTs and nanoparticle hybrid nanomaterials have been synthesized by either a covalent or non-covalent bonding mechanism between nanoparticles and CNTs [92,50,51]. The widely used nanoparticles are Pt, Au NPs. However, these metallic nanoparticles are not favorable in the UV to visible light absorption range of 350nm to 600nm [85,86]. Additionally, these types of metallic nanoparticles clearly are unfavorable for synthesizing inexpensive hybrid nanomaterials for low cost applications. Recently, some other compounds and relatively inexpensive nanomaterials, such as CdSe, CdS, and PdS have been utilized to decorate the CNTs [55,57,87]. These nanoparticles are also mainly favorable for UV and visible light absorption from 250nm to 500nm [88,89]. In addition, the toxic property of cadmium, lead and their compounds are unfavorable for synthesis of “green” hybrid nanomaterials. Excellent IR light absorption and being nontoxic, would be an ideal choice. One of the promising materials is copper sulfide (CuS) nanoparticles, which are both eco-friendly and inexpensive. Moreover, CuS NPs have a broad near IR absorption from 800nm to 1400nm [45]. Herein, a new type of IR sensor based on SWNTs-CuS hybrid nanomaterials offering up

to 300% sensitivity is reported. The IR response of this type of IR sensor has been significantly enhanced by using hybrid nanomaterials and an asymmetric IR illumination strategy.

4.2 Experiment Setup and Measurements

The hybrid nanomaterials were prepared by using oleylamine molecules as the linker molecules between SWNTs (Carbon Solutions, Inc.) and CuS NPs. 10mg of the SWNTs in 100ml toluene solution containing 0.1% (v/v) oleylamine was sonicated in a nitrogen atmosphere and consequently stirred overnight. The oleylamine-functionalized SWNTs were isolated by centrifugation and rinsed with ethanol. The same amount of the functionalized SWNTs was dispersed in 100ml toluene in three beakers separately, followed by adding solutions of CuS nanoparticles with three different amounts (100, 200, 300 μ l) to three beakers to obtain three types of hybrid nanomaterials. Each of the three mixtures was again gently sonicated for 1.5 hours at room temperature. Then the SWNTs-CuS NP hybrid nanomaterials were precipitated by adding a small amount of methanol. Specifically, three types of nanohybrids have been synthesized including Nanohybrid 1 (10mg SWNTs+100 μ l CuS NPs), Nanohybrid 2 (10mg SWNTs+200 μ l CuS NPs), and Nanohybrid 3 (10mg SWNTs+300 μ l CuS NPs). Thin films of both SWNT-CuS NP hybrid nanomaterials and SWNTs were prepared on a mixed cellulose ester (MCE) membrane using the vacuum filtration method [14,16]. Briefly, the nanohybrid nanomaterial and SWNTs suspensions were vacuum-filtered through a mixed cellulose ester (MCE) filter (47mm in diameter), separately. The resulting thin film on the filter was rinsed twice with isopropyl alcohol and deionized water and then dried at 80°C for two hours to remove any remaining organic residues in the film. After drying,

the thin film sheet can be either peeled off the filter or transferred onto a solid or flexible substrate after being cut into desirable sizes.

4.2.1 Fabrication of IR Sensors on a Glass Substrate

The hybrid nanomaterial thin film with a size of 2 cm (length) \times 0.8 cm (width) \times 25 μ m (thickness) was attracted to a glass substrate, with two ends connected with Cu wires using Cu conductive glue forming two Cu-wire electrodes (Anders Product, Inc).

Fabrication of Flexible IR Sensors Embedded in PDMS. A piece of PDMS layer is formed on a glass substrate and then peeled off from the substrate. A hybrid nanomaterial thin film with a size of 2cm (length) \times 0.8cm (width) \times 25mm (thickness) is placed on the PDMS layer, with two ends connected with Cu wires using Cu conductive glue to form two Cu-wire electrodes (Anders Product, Inc). Then, PDMS is poured on the thin film and cured. As a result, the flexible IR sensor is embedded in PDMS.

4.2.2 IR Light Source and IR Sensing Measurements

The IR light source is provided by a xenon light bulb (XNiteFlashSTG, LDP, LLC) filtered by a long-pass, near IR filter (X-Nite 1000nm filter) with 1000nm cutoff at 50% and 1300nm passband >90%. The power of the IR radiation is measured by a Newport power meter model 1918-C with an IR detector 918DIR- OD3. All measurements were carried out when the IR radiation was perpendicular to the surface of the IR detector. Unless otherwise mentioned, no voltage was applied on the IR sensor for the measurements. In this case, the photocurrents generated by the IR sensors upon exposure to an IR source were measured using a digital multimeter (Agilent U1253B). To determine the photocurrent change of the IR sensor under IR radiation, a voltage of

0.2mV was applied to the IR sensor. In this case, the current-time curves of the IR sensors were measured using an electrical measurement probe station (Keithley Instruments).

4.3 Results and Discussion

The sketch of the hybrid nanomaterial thin film IR sensor is given in Figure 4-1(a). A photo of a fabricated device on a glass substrate is given in Figure 4-1(b) and a photo of a fabricated device embedded in PDMS is shown in Figure 4-1(c), which is a prototype of a flexible IR sensor. For both types of the IR sensors, the size of the hybrid nanomaterial thin film measures 20mm (length) \times 8mm (width) \times 25mm (thickness). The TEM images of the hybrid nanomaterials are given in Figure 4-1(d). It is clear that the CuS NPs are attached to SWNTs, which provide and facilitate the direct pathways for charge transfer between NPs and SWNTs. The SEM image of SWNTs-CuS NP nanohybrid thin films with 25mm thickness is shown in Figure 4-1(e). The SWNTs are clearly decorated with CuS NPs. CuS NP aggregation is clearly observable, [55] which can be mitigated by diluting the concentration of CuS NPs during the synthesis of the hybrid nanomaterial.

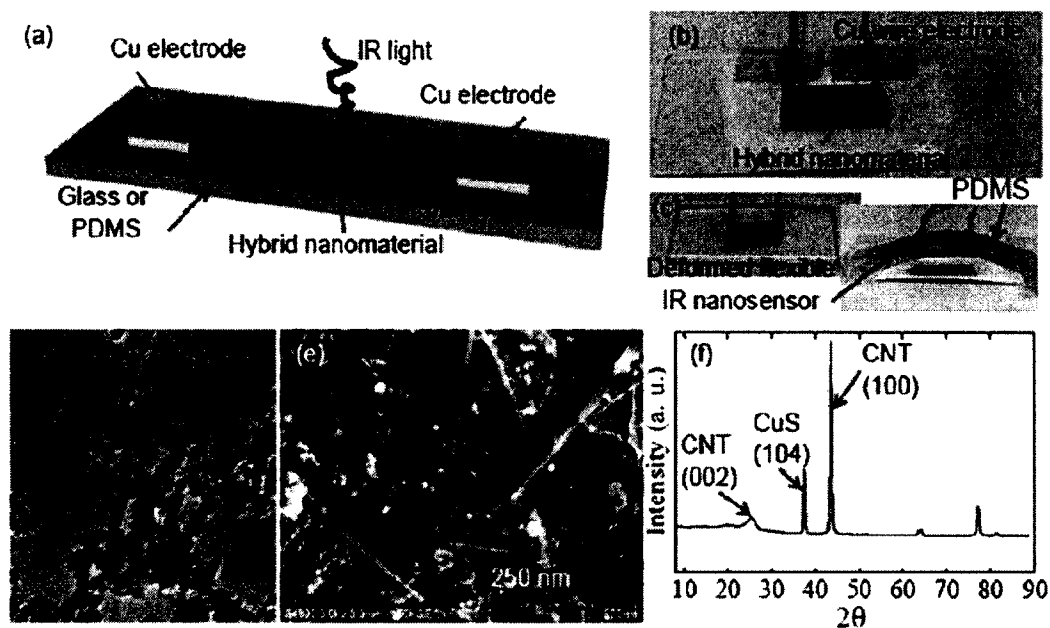


Figure 4-1 (a) shows sketch of a hybrid nanomaterial thin film IR sensor: Junction I and Junction II formed between the Cu-wire electrodes and the hybrid nanomaterial thin film. (b) shows photo of a fabricated thin film IR sensor on a glass substrate. (c) shows photo of a flexible IR sensor embedded in PDMS before and after deformation. The size of the thin film measures 20mm (length) \times 8mm (width) \times 25mm (thickness). (d) shows TEM image of the SWNTs-CuS NP hybrid. (e) shows SEM image of the hybrid nanomaterial thin film. (f) shows XRD patterns of the as-synthesized SWNTs-CuS NP composite thin film.

The X-ray diffraction (XRD) patterns of the as synthesized SWNTs-CuS nanocomposite using an X-Ray Diffractometer (D8 DISCOVER, Bruker) are given in Figure 4-1(f). The XRD patterns have mixed characteristic peaks of carbon nanotubes [93] and CuS NPs,[16] indicating that the SWNTs have been indeed decorated with CuS NPs.

Usually for the thin film IR sensor devices, the IR illumination on the device is symmetric, which means all regions of the device are uniformly exposed to an IR source or only the center of the thin film sensor is exposed to an IR source [35,37,82,83]. In our experiments, two IR illumination schemes on the IR sensor have been examined. As

shown in Figure 4-2(a) and (b), the measured photocurrents of the same IR sensor, without applying any voltage, under symmetric and asymmetric IR illumination are given.

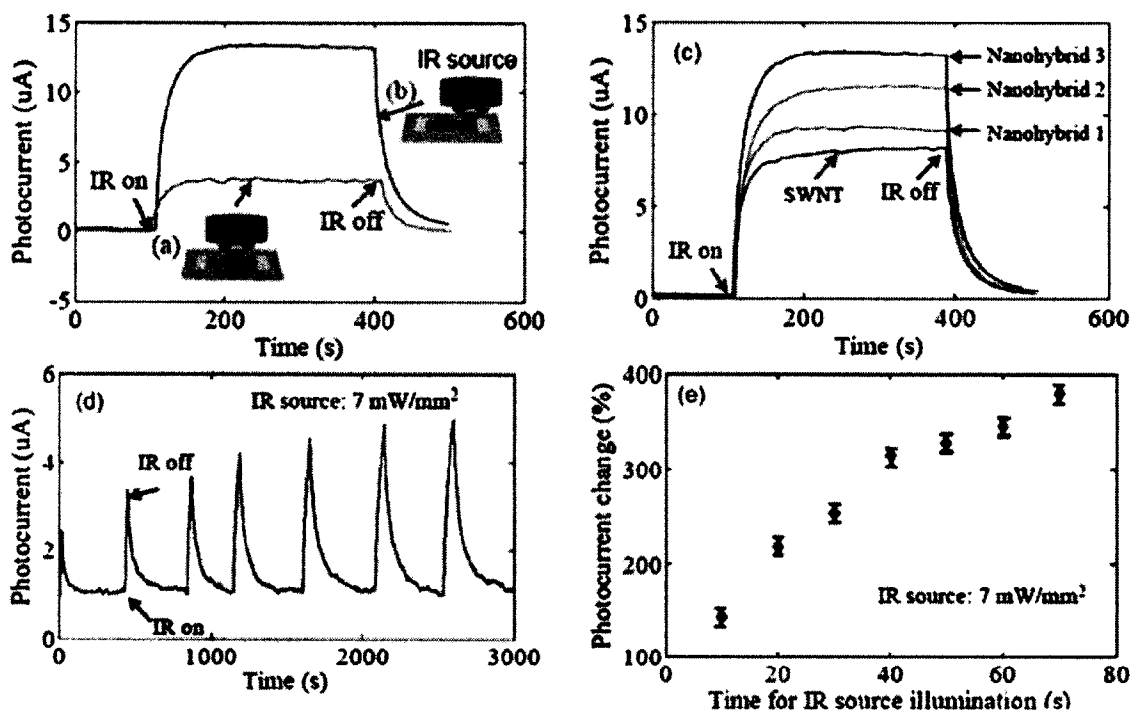


Figure 4-2 IR testing schemes: (a) shows symmetric illumination and (b) shows asymmetric illumination on a thin film IR sensor fabricated from Nanohybrid 3. (c) shows photocurrents for four different devices fabricated with pure SWNT and 3 different nanohybrids. For all cases, no voltage is applied on the IR sensor. (d) shows one representative photocurrent measurement before and after the IR light is on with different IR exposure times (10, 20, 30, 40, 50 sec, 60 s, 70 s). A voltage of 0.2mV is applied on the IR sensor and the IR light intensity is 7mW mm^{-2} . (e) shows the maximum photocurrent change under different IR light exposure times.

In the asymmetric illumination scheme, only the part of the IR sensor including one Cu-wire electrode is illuminated by the IR source, as shown in the inset in Figure 4-2(b). As can be seen, under asymmetric illumination, the photocurrent is much larger, which can be up to one order of magnitude larger, than that under symmetric illumination. As a result, the sensitivity of the IR sensor can be dramatically improved. This

observation suggests that this IR illumination strategy can be used for enhancing the IR sensor's performance.

The physical mechanism behind this enhancement can be explained as follows: when the IR sensor is under symmetric IR illumination, the photocurrent generated is only due to the photovoltaic and thermovoltaic effect of the nanohybrid thin film, since no temperature difference exists between the two junctions formed between the nanohybrid thin film and the two Cu-wire electrodes [84,45,90]. In contrast, if the IR sensor is under asymmetric IR illumination, a temperature difference is formed between the two junctions, as shown in Figure 4-2(b). The nanohybrid thin film is connected to these two Cu-wire electrodes, forming a simple circuit, which can generate a voltage due to the different Seebeck coefficients of the Cu wire and the hybrid nanomaterial thin film, provided that a temperature difference can be formed between the two junctions[94]. It is anticipated that the Seebeck coefficient of the hybrid nanomaterial is different from that of the Cu. For instance, the measured Seebeck coefficient of the carbon nanotube film is reported to be 10 to 50 mV K⁻¹ [91], which is different from that of the Cu wire/electrode of about 1.84 mV K⁻¹ [33]. Hence, if the thin film IR sensor is under asymmetric illumination, the thermoelectric voltage or current will be generated in addition to the photocurrent generated, due to the photovoltaic and thermovoltaic effect of the nanohybrid thin film. As a result, the total current will be larger than that under symmetric illumination. The photocurrents of four devices have been measured under asymmetric IR illumination and are shown in Figure 4-2(c). As can be seen, the photocurrents of the nanohybrid thin film devices are larger than those of the pure SWNTs thin film devices, as expected [45]. In addition, the more the amount of CuS NPs

attached to SWNTs, the larger the photocurrent generated. The physical mechanism for this observation can be explained as follows. The origin of the photocurrent involves the following process: absorption of photons, creation of excitons (electron-hole pairs) and transfer of charges [82]. The functionalization of the SWNTs with oleylamine molecules makes it an n-type material, thereby making the electrons the major carriers in the hybrid nanomaterials [55]. Specially, upon IR light illumination, excitons (electron and hole pairs) are generated in CuS NPs and SWNTs. While the holes would remain in the CuS NPs, the electrons will transfer to SWNTs. As a result, the enhanced photocurrent is achieved, as compared to the SWNTs thin film devices. In order to evaluate the percentage change of the photocurrent (i.e., the sensitivity) before and after the IR irradiance is available, a DC voltage of 0.2mV is applied to the IR sensor. One representative measurement is shown in Figure 4-2(d). For comparison with previously reported IR sensors [35], the IR light intensity is chosen to be 7mW mm^{-2} , while the illumination time is varied from 10 sec to 70 sec. The measured temperature difference between the two junctions of the IR sensor is about 20°C under this IR light intensity, which is monitored using a thermocouple (Omega HH306). All measurements show that the rapid IR response of the sensor and the IR response patterns under different IR illumination times are very consistent. As expected, the longer the illumination time, the larger the change of the photocurrent, as shown in Figure 4-2(e). Typically the change of the photocurrent is from 150% for 10 sec IR illumination to 380% for 70 sec IR illumination, which is much larger than those of the previously reported nanomaterial thin film sensors with an IR response change from 0.7% to 52.9% [82,35,37]. The relationship between photocurrent generation and the IR intensity has also been evaluated.

Representative photocurrent measurement under IR illumination with different intensities is shown in Figure 4-3(a) and (b), which shows good linearity, similar to those previously reported nanomaterial-based IR sensors. In addition, the measured response time of the IR sensors is in the range of 60–70 ms, which is similar to the carbon nanotube composite IR sensors and carbon nanoparticle IR sensors [82,35,37].

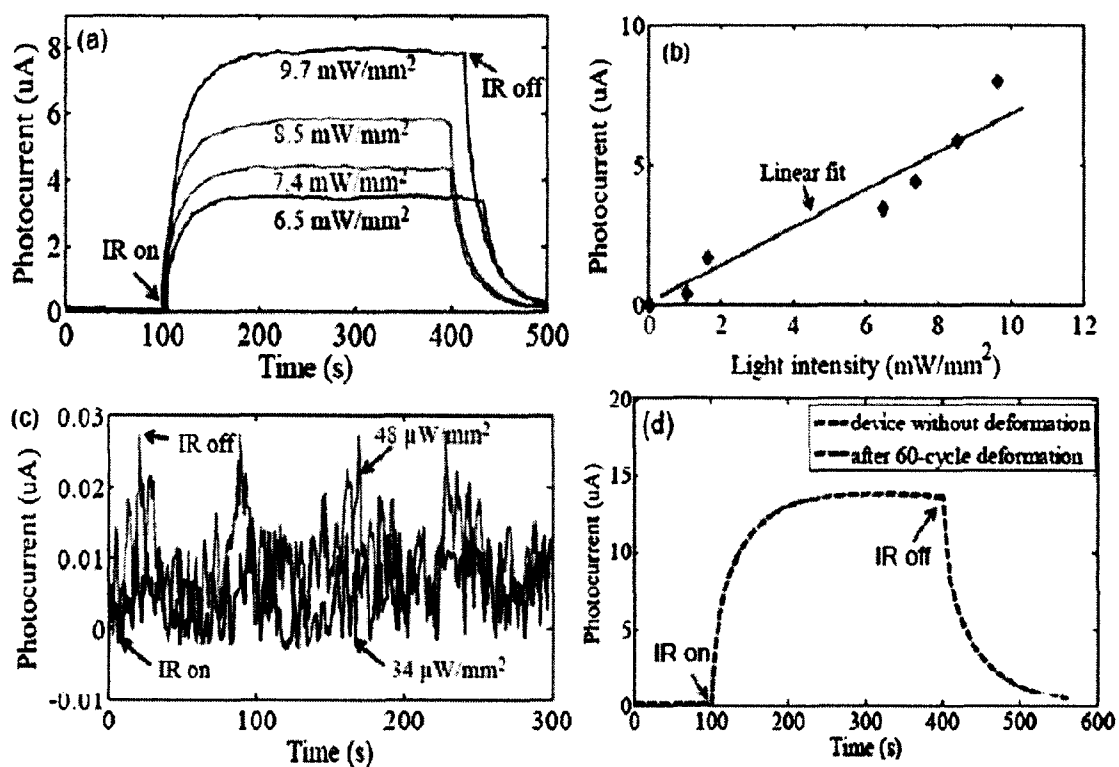


Figure 4-3 No voltage is applied on the IR sensor for all the measurements: (a) shows measured photocurrent under different intensities of the IR source. (b) shows relationship between measured photocurrent vs. IR source intensity for a nanohybrid thin film IR sensor fabricated from Nanohybrid 3, showing good linearity. (c) shows detection limit: a representative measurement of the photocurrent by reducing the IR light density to 48 mW mm², suggesting that the detection limit of the IR sensor is about 48 mW mm². (d) shows flexible IR nanosensor: measured photocurrent after different cycles of bending of the IR sensor.

The photocurrent measurements have been carried out by reducing the IR light intensity until the photocurrent due to IR illumination becomes non-distinguishable to

determine the detection limit of the IR sensor. Specifically, the measured photocurrents are regarded as distinguishable signals if they are at least two times the noise level of the test equipment (digital multimeter, Agilent U1253B). It has been found that the noise level of the test equipment is ~ 0.01 mA. As shown in Figure 4-3(c), the generation of photocurrent can be clearly observed at the IR intensity of 48mW mm^{-2} . However, when the IR light intensity reduces to 34mW mm^{-2} , the photocurrent generation becomes negligible, which indicates that the detection limit of the IR sensor is $\sim 48\text{mW mm}^{-2}$.

Flexible IR sensors using the same hybrid nanomaterial have been developed. The detailed fabrication process is described in the Experimental section. Photos of one flexible IR sensor embedded in PDMS and the deformed IR sensor are shown in Figure 4-1(c). The photocurrent responses of a fresh flexible IR sensor and after being deformed 60 cycles under IR illumination are given in Figure 4-3(d). It shows that the change of the photocurrent is essentially negligible as far as the nanohybrid nanomaterial thin film is not damaged. Experiments found that the photocurrent reduces if the thin film has some cracks after deformation.

4.4 Summary

IR sensors, based on SWNTs-CuS NP hybrid nanomaterials, have been successfully developed. The IR response in the photocurrent of the SWNTs-CuS NP hybrid thin film devices is significantly enhanced when the IR illuminates the thin film device asymmetrically. The change of photocurrent is up to 300%, which is ten times to 100 times larger than those of other reported nanomaterial-based IR sensors. The detection limit is as low as 48mW mm^{-2} , among the lowest of the previously reported IR nanosensors. In addition, the IR sensors embedded in polydimethylsiloxane (PDMS)

layers have been fabricated and tested, indicating their potential application as flexible IR sensors.

CHAPTER 5

**USING NANOMATERIALS FOR LOCAL
TEMPERATURE ENHANCEMENT
FOR THERMOELECTRIC
MICROGENERATORS**

5.1 Introduction

Due to technical progress, electronic devices have been developed to be more portable and smaller. How to supply light and continuous power to drive those devices has become an important issue [43]. Micro-size, green energy harvesting devices are the options to fabricate a small power source to supply low consumption devices. Different from consumption energies, such as petroleum, coal and nuclear energy, the green energies, such as wind, light, and heat, are clean, safe, and renewable, which indicates that green energies have the potential to be built as a micro-size energy generator. Recently, different green energy harvesting devices have been developed, and the thermoelectric generator is one of them [44].

Thermoelectric generators (TEGs) are based on the Seebeck effect to convert heat, specifically the temperature difference, into electricity [95]. This technology has been widely and successfully used for scavenging many types of thermal radiation energies, including the wasted heat from different sources [68]. In order to scale down

TEGs and thus make them easier to integrate with microdevices and microsystems, in recent years, different types of MEMS TEGs have been developed [44,96,97,98]. Even though the structural materials of the microdevices play a very important role in the heat-to-electricity conversion efficiency [68], another very important issue is how to efficiently dissipate the heat and thus create and maintain the temperature difference or gradient across the TEGs.

To this end, usually cooling or heat sinking elements are usually required and thus must be integrated to improve the conversion efficiency of TEGs [44,96,97,98], indicating the need for possible extra power consumption to maintain the temperature difference or gradient between the “hot” and the “cold” parts in the thermocouples. Evidently, the ideal case is that the temperature difference or gradient can be intrinsically generated and maintained by the TEGs themselves. In nanotechnology, many nanomaterials, such as carbon nanotubes (CNTs), graphene, and nanoparticles, have revealed their outstanding optical and thermal properties [24,35,36]. The nanomaterials can absorb the light and thermal radiation significantly, and efficiently convert them into heat [48,47,48,84]. In order to enhance their unique properties, the SWNTs can be functionalized with a chemical reagent, oleylamine, to attach CuS NPs on the surface of the SWNTs to form a hybrid nanomaterial. The hybrid nanomaterial exhibits wide and great optical wavelength absorption and directly transfers the absorbed energy into heat [45]. This new type of hybrid nanomaterial can be integrated with a thermoelectric microgenerator to enhance the local temperature causing a larger and continuous temperature difference or gradient in the microdevice. A clean and renewable source of electricity is generated.

Besides, an external tool, a tunable lens whose radius is adjustable, is fabricated and set on top of the SWNTs-CuS NPs nanohybrid thin film of the microgenerator. When light impinges on the microgenerator, the radius of the tunable lens can be adjusted to focus ambient light specifically on the thin film to increase the temperature difference on the microgenerator causing the enhancement of voltage generation.

5.2 Thermoelectric Microgenerators Embedded Hybrid Nanomaterial

5.2.1 Device and Its Operation Principle

The schematic of a thermoelectric microgenerator is shown in Figure 5-1. It is a layered-structure and consists of a layer of Au deposited on a p-type silicon substrate, a layer of silicon nitride, and a layer of Au deposited on silicon nitride. One region is coated with a SWNTs-CuS nanohybrid thin film, which is covered by SU8.

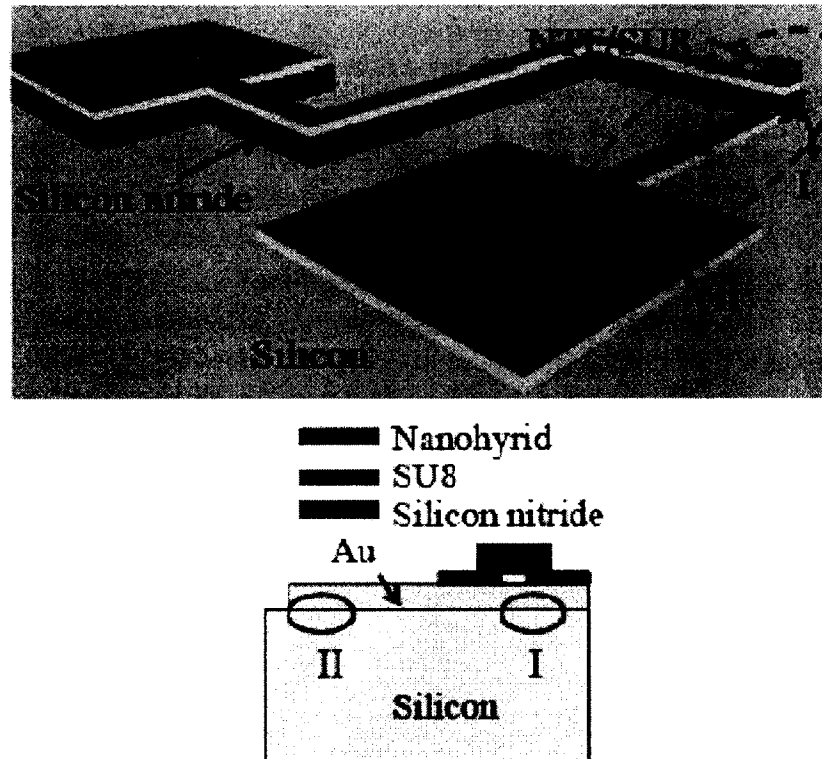


Figure 5-1 A sketch of a thermoelectric microgenerator with integrated nanohybrid thin film: (top) angled topside view; (bottom) cross-section showing the Junction I and II formed between silicon substrate and Au layer

Figure 5-2 shows a basic Seebeck effect structure, with two different materials connected to form two junctions. When the temperature is different between two junctions, an electrical voltage is generated with the microgenerator. Compared to Figure 5-1, the bottom Au layer forms the junctions between the p-type silicon. Specifically, Junction I and Junction II are labeled in the cross-sectional sketch of the thermoelectric microgenerator. The top Au layer is electrically isolated from the silicon substrate by the silicon nitride layer underneath, serving as a metal wire connection to Junction I. The Seebeck coefficient (S_{Si}) of the p-type Si doped with boron at a concentration in the range of 3×10^{18} to $2 \times 10^{19} \text{ cm}^{-3}$ is $\sim 300 \text{ } \mu\text{V/K}$, while the Seebeck coefficient (S_{Au}) of Au is $1.94 \text{ } \mu\text{V/K}$ [33]. If a temperature difference (ΔT_{I-II}) between Junction I and II exists, a

thermoelectric voltage between them will be generated between them, which is approximately given by:

$$V = (S_{Si} - S_{Au}) \times \Delta T_{I-II}, \quad (5-1)$$

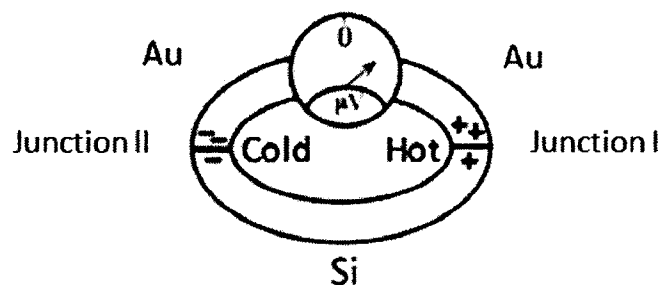


Figure 5-2 The basic structure of Seebeck effect device [103]

5.2.2 Fabrication Process for Thermoelectric Microgenerators

The fabrication process has two main steps: (i) synthesis of hybrid nanomaterials; (ii) integration of the nanomaterials with the microdevices.

Synthesis Procedure of Hybrid Nanomaterial. The SWNTs-CuS NPs hybrid nanomaterial is obtained by using a simple non-covalent bonding synthesis technique. Specifically, the hybrid nanomaterial is prepared by using the oleylamine as the linker molecules between SWNTs and CuS NPs [54]. A certain amount (1mg) of the SWNTs contained within a 10ml toluene solution containing 0.1% (v/v) oleylamine was sonicated in a nitrogen atmosphere and stirred overnight. Then, the oleylamine-functionalized SWNTs were isolated by centrifuge and rinsed with ethanol. The functionalized SWNTs were dispersed in 10ml toluene followed by adding a 30 μ l solution of CuS nanoparticles. The mixture was sonicated for 1.5 hours at room temperature. Then, the SWNTs-CuS NPs hybrid nanomaterials were precipitated by adding a small amount of methanol. Thin

films of both SWNTs-CuS NPs hybrid nanomaterials and SWNTs are prepared on a mixed cellulose ester (MCE) membrane using the vacuum filtration method [84]. Briefly, the nanohybrid and SWNTs suspension are vacuum-filtered through a mixed cellulose ester (MCE) filter, separately. The resulting thin film on the filter is rinsed twice with isopropyl alcohol and deionized water and then dried at 80°C for two hours to remove any remaining organic residues in the film. After drying, the film sheet can be either peeled off the filter or transferred onto a solid substrate.

The Microgenerator Fabrication and Integration. The fabrication process flow is illustrated in Figure 5.3. Specifically, starting from a p-type silicon wafer, using a lift-off process, the bottom 250nm thick Au layer is patterned on a silicon substrate with 200nm Ti as the adhesion layer. Then, a layer of 400nm thick silicon nitride is deposited and patterned. Using a lift-off process, the top Au layer of 250nm is deposited and patterned. Then, the thin film of the hybrid nanomaterial is transferred on to the top Au layer. SU8 is spin-coated and patterned as a mask, followed by the etching of the thin film of the hybrid nanomaterial. As a result, the hybrid nanomaterial is integrated in the Junction I region, as shown in Figure 5-3(f).

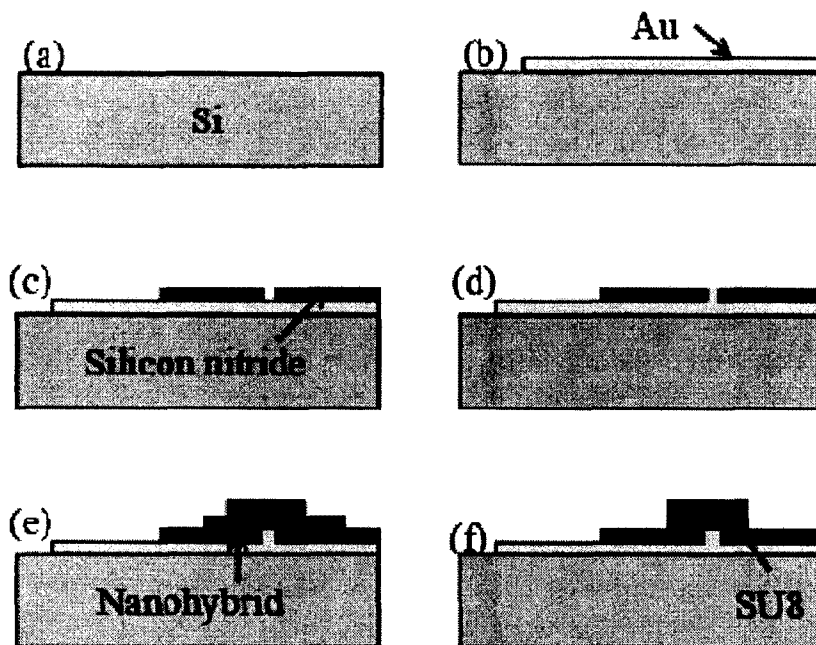


Figure 5-3 The fabrication process flow: (a) Start with ptype silicon wafer. (b) Au pattern is formed on the silicon substrate. (c) Silicon nitride is deposited and then patterned. (d) top Au pattern is formed. (e) SWNTs-CuS nanohybrid thin film is transferred on the substrate and SU8 layer is patterned. (f) the hybrid nanomaterial thin film is patterned using SU8 as a mask.

5.2.3 Experiment Setup and Measurements

A TEM image of SWNTs-CuS NPs hybrid nanomaterial is given in Figure 5-4(a). The SWNTs decorated with CuS NPs is clearly visible. A SEM image of the thin film of hybrid nanomaterial is shown in Figure 5-4(b). Again it is clear that the SWNTs are decorated with CuS NPs. A photo of a microdevice with integrated SWNTs-CuS NPs nanohybrid thin film in the Junction I region is shown in Figure 5-5.

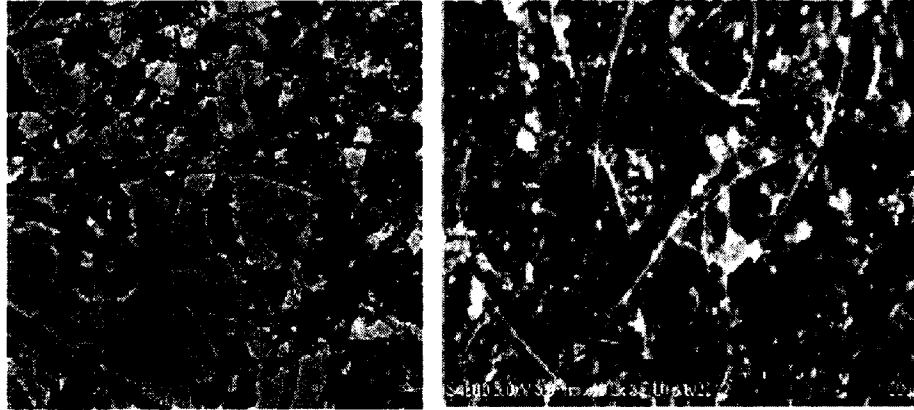


Figure 5-4 (left) the TEM image of SWNTs-CuS NPs hybrid nanomaterial; (right) the SEM image of the SWNTs- CuS NPs thin film.

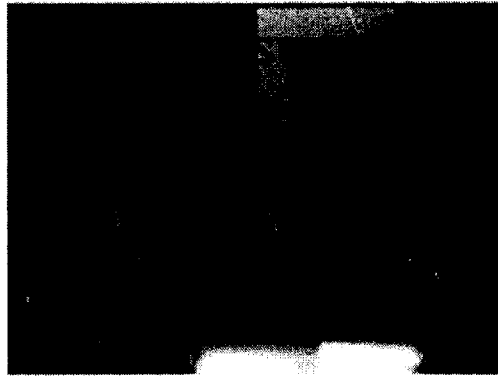


Figure 5-5 Photo of a fabricated thermoelectric microgenerator. The nanohybrid thin film was integrated in the Junction I region.

The experimental setup is shown in Figure 5-6. An Olympus TL-2 incandescent lamp was used to provide the light and thermal radiation source, while the measured voltages were recorded and stored in real time by a laptop computer.

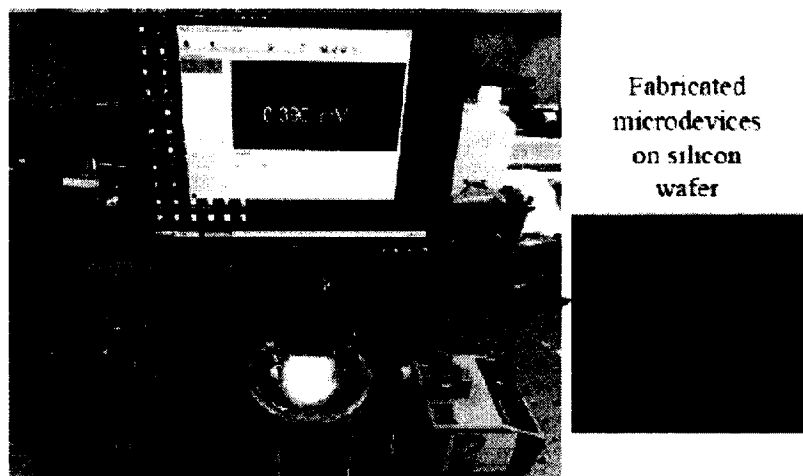


Figure 5-6 The experimental setup for the measurements of voltages and currents by the thermoelectric microgenerators.

As a comparison, for a microdevice without the integrated nanohybrid thin film, the measured open circuit voltage was about 0.01mV, as shown in Figure 5-7 under uniform illumination of the lamp. The uniform illumination means that all regions/parts of each microdevice were exposed by the lamp to uniform light intensity and heat radiation. Under the same experimental conditions, Figure 5-7 also gives the measured open circuit voltage of the microdevice with the integrated nanohybrid thin film. Its open circuit voltage was 0.08mV, which was eight times the voltage generated by the microdevice without nanohybrid thin film. As a reference, without turning on the lamp, the voltage was essentially zero. Evidently, the nanohybrid thin film enhances the local temperature in the Junction I region by absorbing the light and thermal radiation. Hence the temperature difference between the Junction I and the Junction II increases. As a result, the generated voltage increases as expected.

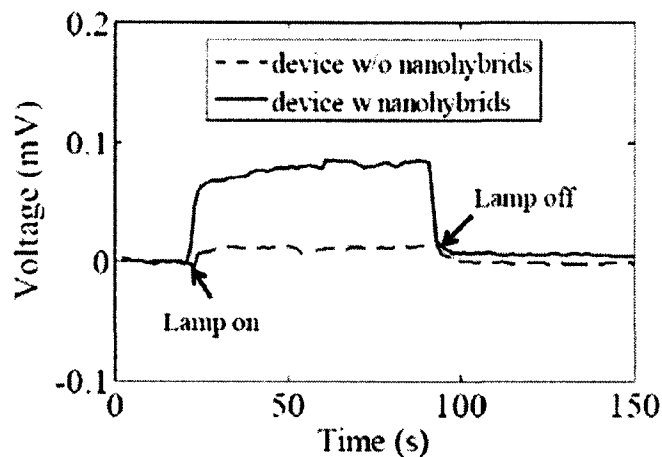


Figure 5-7 Measured open circuit voltage of a thermoelectric microgenerator with and without Nanohybrids under uniform lamp illumination

Figure 5-8 shows the measured open circuit voltages of these two types of devices when the lamp moves forward to illuminate the nanohybrid thin film region. As can be seen, the devices with the integrated nanohybrid thin film can generate larger voltages. This again confirms that the nanohybrid thin film enhances the local temperature of the Junction I region. Thus, the measured voltage is higher than that of the microdevices without the integrated nanohybrid thin film.

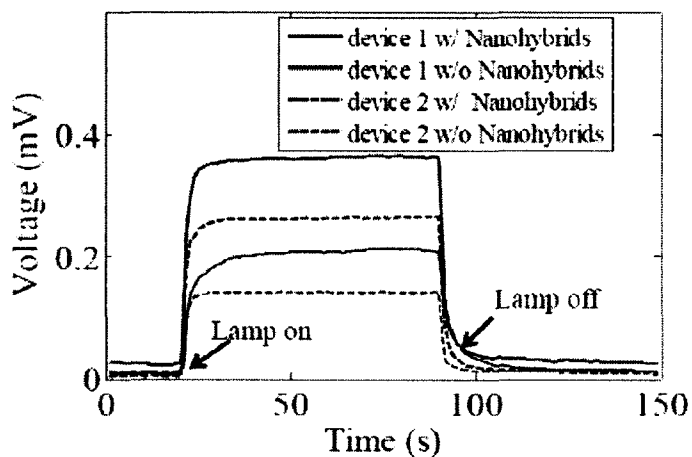


Figure 5-8 Measured open circuit voltage when the lamp illumination is only on the Nanohybrids region compared to a device without the integrated Nanohybrids

Finally, the output power of the microdevice has been measured. In this case, the light intensity and heat radiation was varied by changing the distance between the lamp and the microdevice. The lamp illuminated the Junction I region. Figure 5-9 gives the measured peak power by a microdevice under different light intensity and heat radiation. The output power was in the range to several or tens of nanowatts.

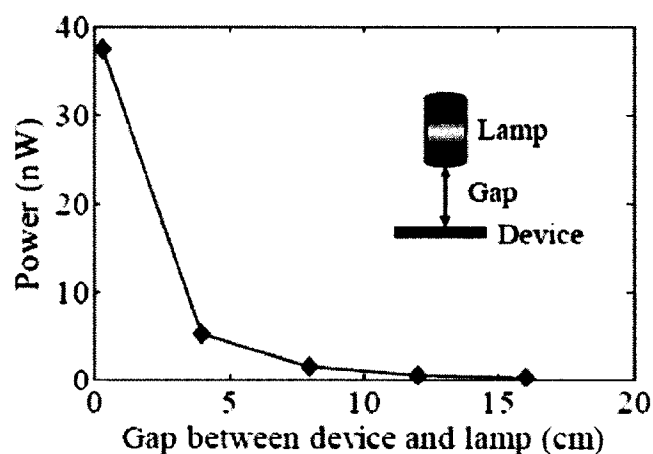


Figure 5-9: Measured peak power by the thermoelectric microgenerator under different light intensity and temperature of the lamp by changing the gap between the device and the lamp

All above measurements suggest that the NTF plays an important role in the enhanced local temperature and thus the power generation. Specifically, as evidenced in the measured results in Figure 5-7, the intrinsic temperature difference or gradient between Junction I and Junction II was generated and maintained in the microdevice with the integrated nanohybrid thin film even though the microdevice was illuminated uniformly by the lamp, which offers us a new route to design thermoelectric generators. It was anticipated that by optimizing the optical and thermal properties of the nanohybrid thin film, the generated voltage and power can be improved for each single device.

Furthermore, the output voltage and output power can be further improved by fabricating hundreds of this type of microdevices and electrically connecting them together.

5.3 Tunable Lens Fabrication and the Measurement Results

Figure 5-10 shows a tunable lens in which blue water was injected into the chamber. A two layer SU-8 pattern on a silicon wafer was built to form the tunable lens. The first SU8 layer used SU8-10 negative photoresist to form a about a 20 μ m thickness channel pattern which is shown in Figure 5-11(a). The second layer used SU8-2050 negative photoresist to build a about 200 μ m thickness chamber pattern which is shown in Figure 5-11(b). Before exposing the pattern to 365nm UV-light, the pattern was put on a flat table for 30 min until photoresist was uniformly coated on the silicon wafer. After the pattern was ready to be used, polydimethylsiloxane (PDMS) was stirred with a curing agent in the ratio of 10:1 and poured on the pattern which is shown in Figure 5-11(c). Then the wafer with the PDMS was baked at 65°C for 1.25 hours in an oven to dry it out. After the baking, the dried PDMS membrane, with channel and chamber patterns, was peeled off from the pattern. Then, an oxygen treatment bonding process was used to bond the PDMS membrane on a glass substrate which is shown in Figure 5-11(e). Two thicker PDMS anchors were bound on the two ends of the PDMS channel panel and two channels are punched through the PDMS anchors (Figure 5-11(b)) and membrane for pumping oil or solutions into the chamber to create the tunable lens which is shown in Figure 5-11(f).

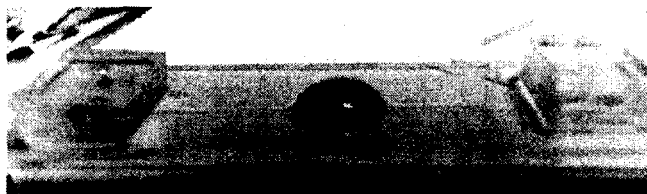


Figure 5-10 A tunable lens which the radius is 45mm with blue dyed water in the chamber.

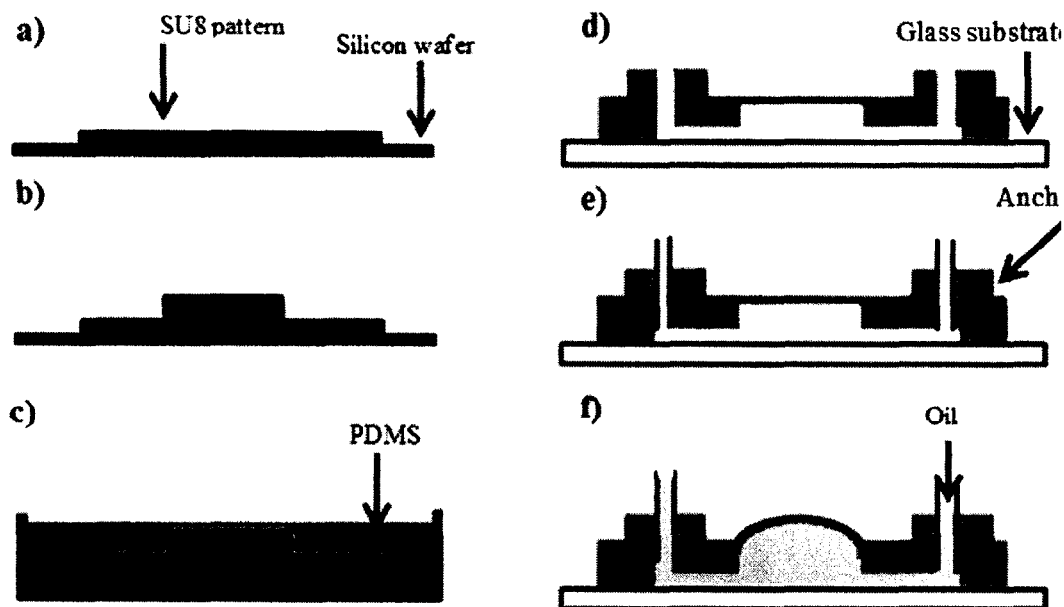


Figure 5-11 The tunable lens fabrication steps.

5.3.1 Measurement Setup and Results

Figure 5-12 shows the experimental setup with a tunable lens positioned between a lamp and the devices. A pump was used to push a syringe and inject oil into the tunable lens to increase the angle of the tunable lens and to specifically focus light on the nanohybrid thin film specifically. Optical contact angle equipment (Future Digital Scientific, OCA 15/20 Static Contact Angle Measurement) was use to observe the angle change between the flat region and then bulged region on the tunable lens. When oil was pumped into the chamber of the tunable lens, the PDMS membrane was expanded and

bulged up, resulting in the angle of the tunable lens becoming larger. The measurement result is shown in Figure 5-13. Oil was pumped into the lens chamber from 0 μ l to 140 μ l. The angle of the tunable lens was increased from 0° to 59.9°.

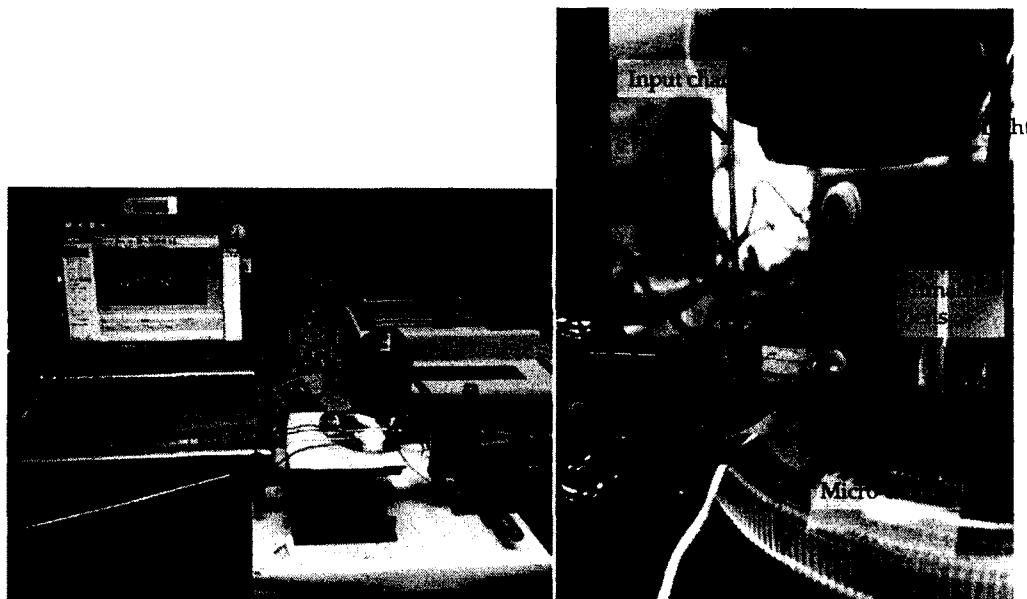


Figure 5-12 The experimental setup with a tunable lens between a lamp and devices for the measurement of voltages and currents. A channel was connected with the syringe and the tunable lens, Oil flowed through the channel into the tunable lens.

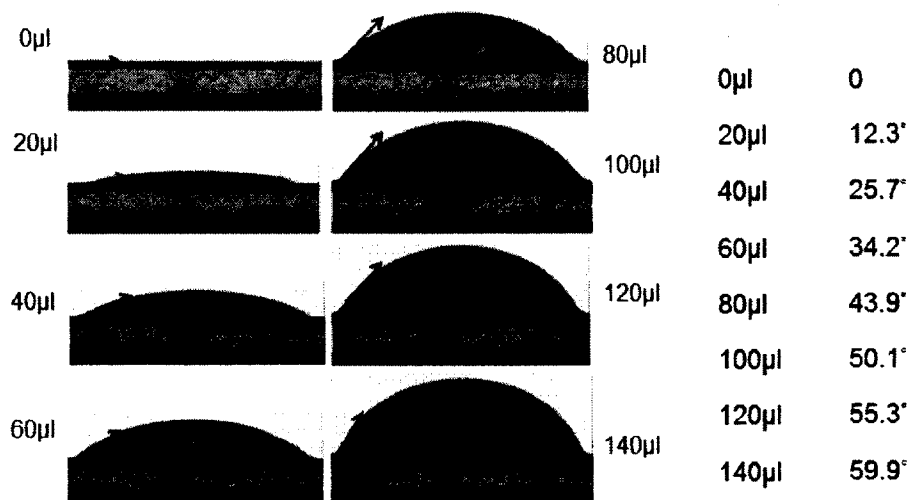


Figure 5-13 A contact angle measurement, when more oil is injected into the lens chamber, the angle of the tunable lens is increased.

For the measurements of the generated voltages and currents with the thermoelectric microgenerators with a tunable lens, six tests were completed with different amounts of oil in the lens chamber (0, 30, 60, 90, 120, 150μl). As can be seen from Figure 5-14, the microdevice without oil in the tunable lens showed that the lowest open circuit voltage is ~0.17mV under uniform illumination of the lamp. Uniform illumination means that all regions of the microdevice are assumed to be exposed by the lamp to uniform light intensity and heat radiation. Under the same experimental conditions, Figure 5-14 also gives the measured open circuit voltage of the microdevice with different amounts of oil in the tunable lens. The highest open circuit voltage was ~0.27mV (150μl of oil in the tunable lens). The open circuit voltage of the microdevice with 150μl of oil in the tunable lens is increased over 58% than the microdevice with 0μl of oil in the tunable lens. When oil started to be pumped into the tunable lens, the generated open circuit voltage became larger. The surrounding light was collected and focused specifically on the hybrid nanomaterial thin film region resulting in an increasing

temperature difference between two junctions. Therefore, the open circuit voltage of the microdevice was increased by the tunable lens.

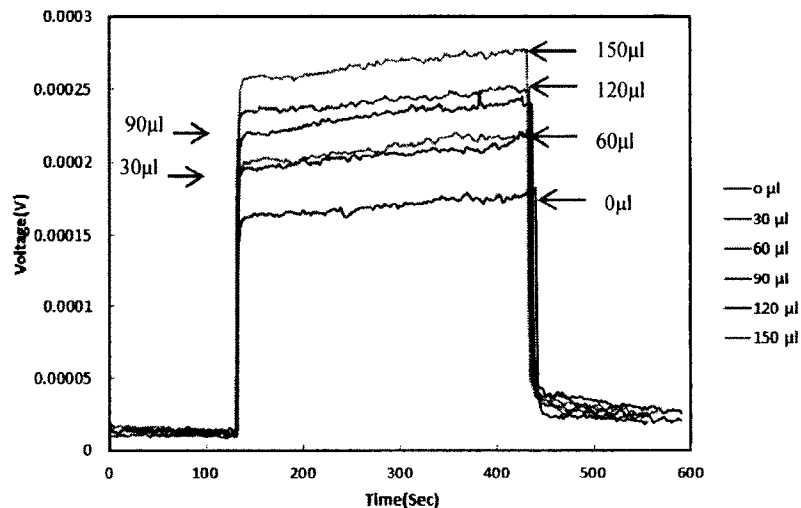


Figure 5-14 A Measured open circuit voltage when the lamp illumination is only on the hybrid nanomaterial thin film region with different amount of oil in the lens chamber.

5.4 Array of Thermoelectric Microgenerator Fabrication and The Measurement Results

In this dissertation, a single microgenerator can generate $\sim 0.08\text{mV}$ under uniform illumination. However, the voltage could be increased by changing the structure of the microgenerator and even arraying many microgenerators together. New structures of microgenerators were fabricated to analyze and optimize the efficiency of series or parallel connected microgenerators.

For the fabrication process, a silicon layer on an insulator (SOI) wafer where the thickness of the silicon layer is $\sim 1\mu\text{m}$, was used for the substrate of the new microdevices. An SiO_2 insulating layer was used to isolate each microgenerator independently. The silicon layer was etched using an inductively coupled plasma etching system (Alcatel, A601E Inductively Coupled Plasma (ICP) etcher.). ICP is one type of the dry etching

equipment which provides great etching quality and side-wall protection. The silicon material can be etched with SF₆ gas, the etching rate being ~0.9μm/min using the etching recipe SF₆: 40, pressure: 20%, source: 1000W, and substrate: 30W. The SOI wafer was put in the ICP to etch for 40 sec to etch one μm thickness silicon to form many pieces of rectangle shaped silicon structures which become the substrates for the microdevcies. Before etching, a 1.7μm thickness of 1813 positive photoresist was used to protect the silicon layer of the microdevices. The etching rate of the photoresist was ~0.086μm/min. Therefor, the photoresist could protect the silicon layer of the microdevices because the photoresist would not be etched away before the target region etched out. After the first layer of the microdevices was formed, the second layer was the electrode layer. The lift-off process was used to form the electrodes of the microdevices and 20nm Cr and 2.3μm Al were directly deposited on the SOI wafer using e-beam deposition equipment (CHA, four-pocket, electron beam deposition system.). The 20nm Cr was used for surface adhesion enhancement. The junctions of the thermoelectric microgenerators were created between the Al and silicon layers. The basic structures for series or parallel microdevices were fabricated. Next, was to fabricate the hybrid nanomaterial thin film and bond it on one junction region of each microgenerator. About a two μm thickness of hybrid nanomaterial thin film on the MCE filter were fabricated and the thin film side was put in contact with one junction region. A 3.5 liter beaker full of water as a weight was placed on the thin film and the wafer in an oven at 65°C all night. A surface tension offers a sufficient adhesion to directly transfer the hybrid nanomaterial thin film to the junction region. After that, the thin films were bound to the microdevices and the MCE filter could be dissolved out with acetone. Finally, the hybrid nanomaterial thin films were

protected with an SU8 layer and the redundant hybrid nanomaterial thin films were etched out with ICP dry etching for 50 minutes. Because the main structure of the thin films were SWNTs, SWNTs can be etched out by O_2 gas and the etchant rate is $\sim 0.047\mu/\text{min}$. Figure 5-15 shows the fabrication steps for the thermoelectric microgenerators in series and Figure 5-16 shows the fabrication steps for the thermoelectric microgenerators in parallel.

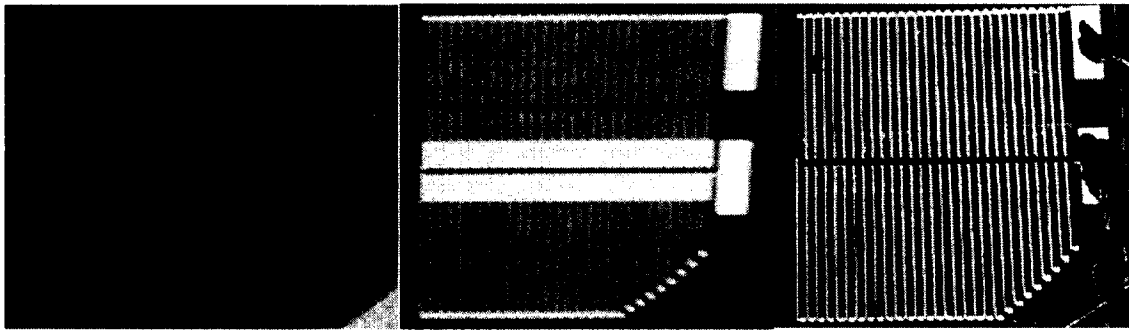


Figure 5-15 Top view of the fabrication steps for the thermoelectric microgenerators in series. a) 58 pieces of rectangle silicon sticks were formed on the top of the SiO_2 layer. b) an Al layer was deposited on the silicon sticks to form the electrodes and connect all microdevices together in series. c) After the deposition of the Al electrodes, the hybrid nanomaterial thin films were directly bound on a junction and an SU8 layer was coated on the top of the thin film to protect the thin films.

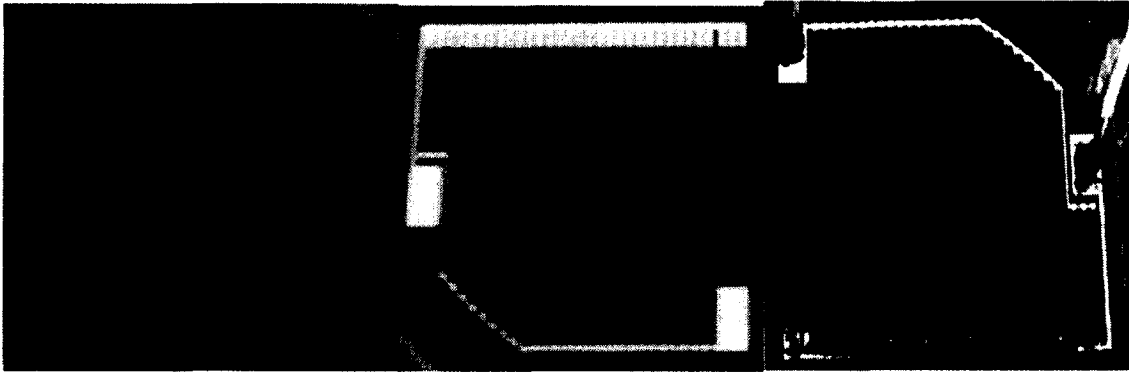


Figure 5-16 Top view for the fabrication steps for the thermoelectric microgenerators in parallel. a) 32 pieces of rectangle shape silicon sticks were formed on top of the SiO₂ layer. b) An Al layer is deposited on the silicon sticks to form the electrodes and connect all microdevices together in series. c) After deposition of the Al electrodes, the hybrid nanomaterial thin films were directly bound on a junction and a SU8 layer was coated on the top of the thin film to protect the thin films.

5.4.1 Measurement Results and Analysis

The array of thermoelectric microgenerators in series and parallel was fabricated to form energy harvesting devices. The measurement setup was similar to Figure 5-6. An Olympus TL-2 incandescent lamp was used to provide the light and thermal radiation source, while the measured voltages or current were recorded and stored in real time by a laptop computer. For the open circuit voltage measurements, Figure 5-17 shows a comparison of the devices in series with and without the hybrid nanomaterial thin film. As can be seen, the device in series without a thin film can generate ~50 mV when the light source illuminates a junction region. Moreover, when the thin film was attached on the junction region, the device could generate ~72mV, which is 44% higher than the device without the thin film under the same conditions. On the other hand, Figure 5-18 shows a comparison of the devices connected in parallel with and without the hybrid nanomaterial thin film. The device in parallel without a thin film can generate ~1.14mV and the device with the thin film can generate ~2.2mV when the light source illuminates

a junction region which has the thin film on top. The efficiency of the device in parallel was also improved over 92% with the thin film. Comparing the device in parallel to the device in series, the device in parallel shows much lower generated voltage. However, the device in parallel can be used to improve the current generation. Figure 5-19 shows the comparison of the single device and the devices in parallel. The device in parallel can generate much higher current than the device in series.

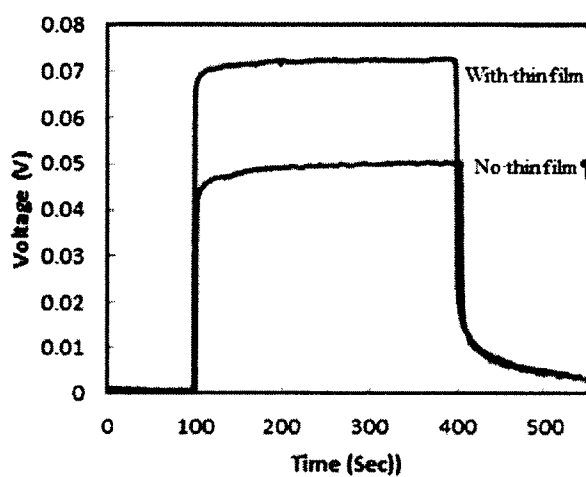


Figure 5-17 An open circuit voltage measurement when the light source only illuminated the hybrid nanomaterial thin films region compared to a device in series without the hybrid nanomaterial thin films.

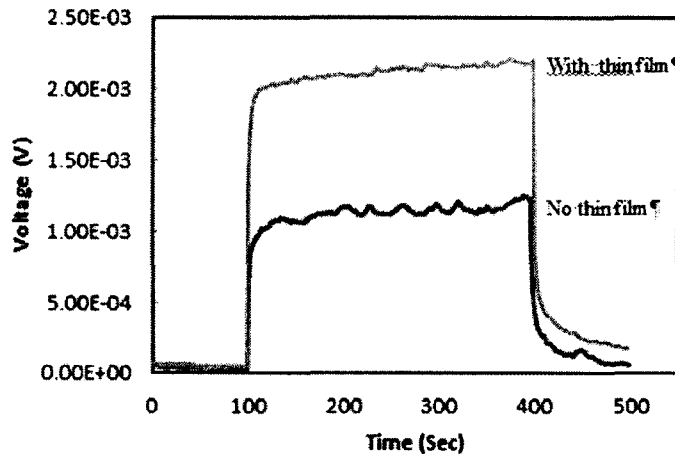


Figure 5-18 An open circuit voltage measurement when the light source only illuminated on the hybrid nanomaterial thin films region compared to a device in parallel without the hybrid nanomaterial thin films.

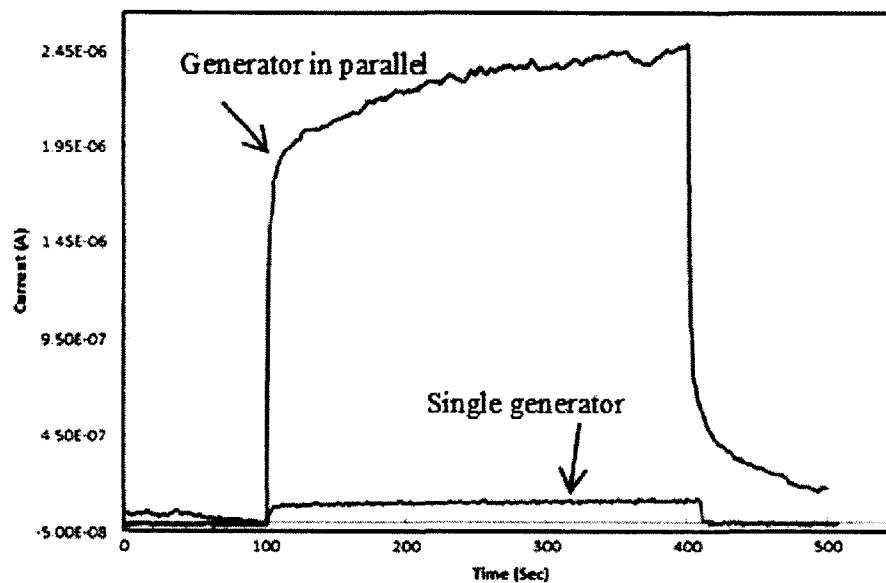


Figure 5-19 A current measurement of a single thermoelectric generator and thermoelectric generators in parallel.

The device in series was also used to measure open circuit voltage with sunshine and a commercial lens was used to enhance the efficiency of the device. Figure 5-20(a) shows the outdoor measurement setup as sunshine was focused on the thin film region with the lens. Figure 5-20(b) shows the measured result. This measurement has two parts,

Part I was the measurement without a lens and Part II was the measurement with a lens to focus the sunshine on the junction region. In the beginning, the device was covered to provide a dark reference and the measured voltage was almost zero. When the cover was taken off, a voltage was generated without the lens and sunshine was uniformly illuminated on the device. The surface temperature of the device was 30°C and the generated voltage was $\sim 11\text{mV}$ (Part I). After the device was covered again, the measured voltage returned back to almost zero. Further, when the cover was taken away again and the lens was used to focus sunshine on the one junction region, the generated voltage was increasing and reaching to $\sim 0.2\text{V}$ (Part II) which is 18 times greater than the device without the lens and the temperature changed from 30°C to 85°C . During the measurement with the lens (part II), the measured voltage decreased in the beginning because the focus point was not well directed on to the junction region. When the sun was moving, the voltage was decreasing.

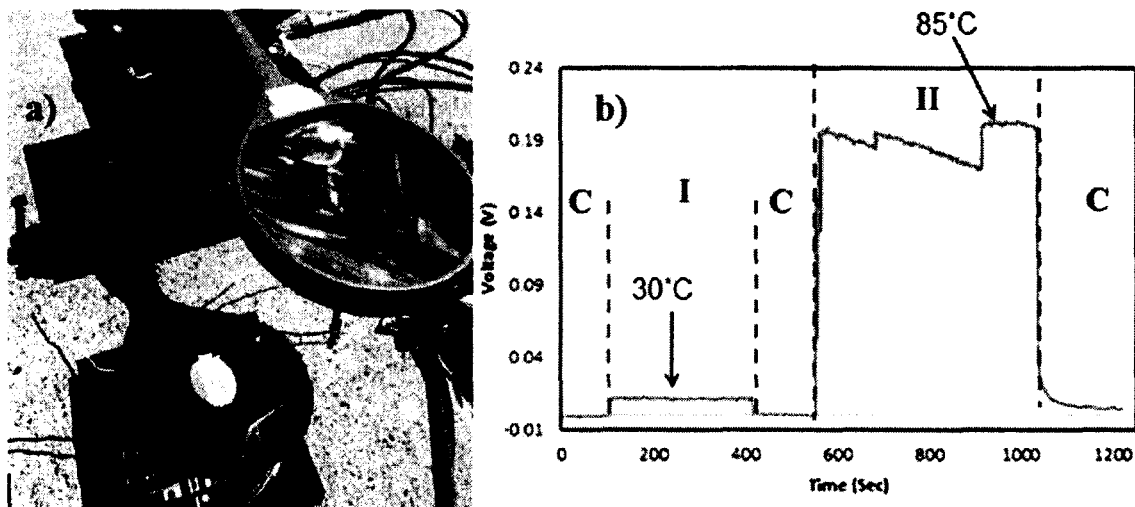


Figure 5-20 a) shows the measurement setup. b) shows voltage measurement with and without a lens on the device (outdoor temperature was 30°C).

5.5 Summary

A new type of thermoelectric microgenerator has been fabricated and tested. The new feature of this type of microdevice is that the nanohybrid thin film was integrated with the microdevices, serving as a local temperature enhancer. As a result, when these microdevices were exposed to light and thermal radiation, an intrinsic temperature difference or gradient across the thermoelectric microgenerator can be formed and maintained, resulting in continuous power generation even without integrating some specific heat sinking or cooling elements with the microdevices, which offers a new approach to design thermoelectric power generation devices. Moreover, a tunable lens was also fabricated to enhance the efficiency of the microdevices. The focus of the tunable lens can be adjusted by pumping oil into the lens chamber to focus light directly on the NTF region and increase the temperature difference between two junctions. For enhancing the generated voltage or current, two types of arrayed of microgenerators, devices in series and parallel, were fabricated. The device in series can generate higher voltage than the device in parallel. Due to the parallel structure, the generated voltage of the device in parallel is equal to one single microgenerator. Therefore, the generated voltage is lower than the device in series, but the device in parallel can generate higher current flow. For future applications, the microgenerators could be integrated in series and parallel together to optimize the device and generate higher output power.

CHAPTER 6

CONCLUSIONS AND FUTURE WORK

6.1 Conclusions

In this dissertation, a hybrid nanomaterial and its applications and a new type of hybrid nanomaterial, SWNTs-CuS NPs, were developed and analyzed for two applications: IR sensing and energy harvesting. Further more, a SWNTs-CuS NPs-Based thin film IR sensor and a SWNTs-CuS NPs enhanced thermoelectric generator were fabricated and tested. This hybrid nanomaterial exhibits specific wavelength absorption peaks at NIR radiation range which can be used to build an ultrasensitive IR sensor. Moreover, the hybrid nanomaterial shows excellent optical and thermal properties which can be used to enhance local temperature to generate electricity by a thermoelectric generator.

In recent years, many nanomaterials, such as fullerenes and nanoparticles, have been synthesized and analyzed. Due to their small dimensions and particular properties, SWNTs have attracted much intense interest to study their particular properties, such as crystal structure and mechanical, electrical, thermal and optical properties for many applications. For optical application, SWNTs have the potential for optical sensing and optical energy harvesting due to high optical absorption and electronic properties.

When the sizes of metal and semiconducting particles are reduced below 100nm, the small particles are called nanoparticles and they exhibit size-dependent properties.

For various applications, different metal and semiconducting nanoparticles have been synthesized. CuS NPs are one of the semiconducting nanoparticles which have outstanding optical absorption from 400nm to 1100nm and specific optical absorption peaks at in the NIR range. Due to these attractive properties, CuS NPs show the potential to combine with SWNTs to create a new type of hybrid nanomaterial, SWNTs-CuS NPs, for optical applications, such as IR sensing and energy harvesting.

SWNTs-CuS NPs is a new type of hybrid nanomaterial. SWNTs and CuS NPs can be bound together by a chemical reagent, oleylamine. It is used to functionalize the surface of the CNTs to attract CuS NPs to tightly attach to the surface of SWNTs. This binding method is called a non-covalent bond. After the synthesis, the electron structures of SWNTs and CuS NPs still kept the same properties because the two targets are bound together by opposite electric charges attracting rather than exchanging electrons or sharing electrons. Therefore, the unique properties of SWNTs and CuS NPs are still kept in the SWNTs-CuS NPs nanomaterial. In order to analyze and test the optical, electronic and thermal properties of the SWNTs-CuS NPs nanomaterial, the hybrid nanomaterial can be formed as a thin film by the vacuum filtration method.

For analysis and testing the hybrid nanomaterial, three different concentrations of the hybrid nanomaterial thin films have been prepared which are 10mg of SWNTs with 100, 200, and 300 μ l of CuS NPs solution. After the vacuum filtration processes, the thickness of the thin films was \sim 25 μ m and the thin films were cut into 10mm \times 15mm rectangles. The hybrid nanomaterial thin films were anchored on the glass substrates for testing and two conductive wires are bonded at two ends of each of the thin films to form prototype devices. As can be seen from the measurement results, the hybrid nanomaterial

thin film devices exhibit clearly enhanced optical and thermal switching characteristics, optical absorption, photocurrent and thermocurrent generation under light illumination or/and thermal radiation. Moreover, high concentrations of the hybrid nanomaterial thin films show better optical absorption and higher electrical current generation which indicate that the CuS NPs are effective for enhancing the efficiencies of SWNTs. For the applications, the thin films also exhibit great NIR radiation absorption which can be applied to enhance the sensitivity to NIR radiation to build an ultra-sensitive sensor. Moreover, a prototype thermoelectric generator enabled by the hybrid nanomaterials has been designed and demonstrated, providing a new route to obtain thermoelectricity without any cooling or heat-sink components. Measurements also found that the hybrid nanomaterial thin film devices exhibit a clear optical and thermal switching effect, which can be further enhanced up to ten times by asymmetric light illumination and thermal radiation on the thin film devices instead of symmetric illumination.

IR sensing is an important technology with applications in renewable energy, environmental science and medical engineering. Herein, environment-friendly IR sensors, based on the SWNTs-CuS NPs hybrid nanomaterials, were fabricated. The IR response in the photocurrent of a SWNTs-CuS NP hybrid thin film sensor is significantly enhanced when the IR light illuminates the thin film device asymmetrically. Measurement results show the change rate of photocurrent is up to 80%, which is larger than those of other reported nanomaterial-based IR sensors[35-37]. The detection limit can be as low as 48mW mm^2 , which is lower than the previously reported IR nanosensors. The dramatically enhanced sensitivity and detection limit are due to the temperature difference between the two junctions formed by the nanohybrid thin film and Cu-wire

electrodes under asymmetric IR illumination, and the difference between the effective Seebeck coefficient of the nanohybrid thin film and that of the Cu wire. The IR sensor embedded in flexible polydimethylsiloxane (PDMS) layers was fabricated and tested, indicating its potential application as a flexible IR sensor.

For energy harvesting application, a new type of thermoelectric microgenerator enabled by SWNTs-CuS NPs hybrid nanomaterial thin film was fabricated. The thermoelectric microgenerator is based on the Seebeck effect to convert the heat, specifically the temperature difference, directly into electricity. Moreover, a SWNTs-CuS NPs nanomaterial thin film which can absorb light and heat is attached to one side of the microgenerator. The thin film will enhance the local temperature and thus cause and maintain an intrinsic temperature difference or gradient which does not require any cooling or heat sinking element across the microgenerator, thereby directly converting light or heat into electricity. For testing microgenerators, three different concentrations of SWNTs-CuS NPs (100, 200, and 300 μ l) with the same amount of SWNTs were formed as three different thin films and attached to the three microgenerators. When the same light source illuminates on each of the thin films, the high concentration thin film can generate higher voltage, which means the high concentration thin film can absorb more energy to generate a bigger temperature gradient in the microgenerator. This result also proves that CuS NPs can effectively enhance the efficiency of SWNTs.

In addition, a tunable lens was fabricated and used to focus incoming light on the thin film region to increase the temperature difference on the microgenerator. The tunable lens was built with a soft and flexible polymer, Polydimethylsiloxane (PDMS) which was used to form a chamber with a membrane on top [41]. Oil or other solutions can be

injected into the chamber to control the curvature of the lens resulting in the focus change. After injecting about 140 μ l of oil into the lens, the efficiency for generating voltage was enhanced over 76% in the microgenerator with the SWNTs-CuS NPs thin film.

6.2 Future Work

The synthesis of SWNTs-CuS NPs has been successfully used for IR sensing and energy harvesting applications. For the energy harvesting application, the fabricated thermoelectric microgener still has room for improving the efficiency of voltage generation.

In order to generate higher electrical voltage with a thermoelectric generator, some important parameters, such as the Seebeck coefficient of the materials and the temperature gradient, have to be considered for future work. According to the Seebeck effect, a basic thermoelectric generator can be built with two different materials connected together to form two junctions at the two end sides of the materials. When the generator has a larger Seebeck coefficient difference for the two materials or a larger temperature gradient between the two junctions, the generator can generate higher voltage. For the microgenerator with a SWNTs-CuS NPs thin film, p-type silicon and Au were used to form the basic Seebeck structure, the Seebeck coefficients of the two materials are $\sim 300\mu\text{V/K}$ and $\sim 1.94\mu\text{V/K}$. Respectively, the Seebeck coefficient difference is ~ 298.06 , which is a large amount for a Seebeck device. Therefore, how to increase the temperature gradient has become an important issue for efficient enhancement.

The interest in the idea of embedding a thermal isolator into the thermoelectric microgenerator is growing. The thermal isolator can be fabricated between two junctions,

which is shown in Figure 6-1, to restrict the hot/cold region diffusion to the cold/hot region.



Figure 6-1 A thermoelectric generator with a thermal isolator (SiO_2). Silicon and Au (red color) are used to form the generator. SWNTs-CuS thin film is used to enhance local temperature, and SU-8 layer is for protecting the thin film.

The isolator should use a material, such as SiO_2 (0.014W/cm-K) or SiN_4 [42] which has extremely low thermal conductivity. In order to understand the efficiency of a thermoelectric generator after adding the isolator between two materials, the COMSOL software was used to simulate the thermoelectric generator with the thermal isolator. A simulated prototype thermoelectric generator was shown in Figure 6-2. For the simulation, a thermoelectric effect module was built to simulate three prototype thermoelectric generators: a generator without thermal isolator, a generator with a 200nm thick thermal isolator, and a generator with a 500nm thick thermal isolator. Two temperature parameters are set at the two ends of each generator and three temperature differences (10°C, 20°C, 30°C) between the two ends were applied. The simulation results were shown in Table 6.1. As can be seen, when the temperature differences were applied to the generators, electrical voltages were generated between the two ends of each generator. Moreover, if the generator with the thicker thermal isolator was embedded in the generator, the voltage difference became larger.

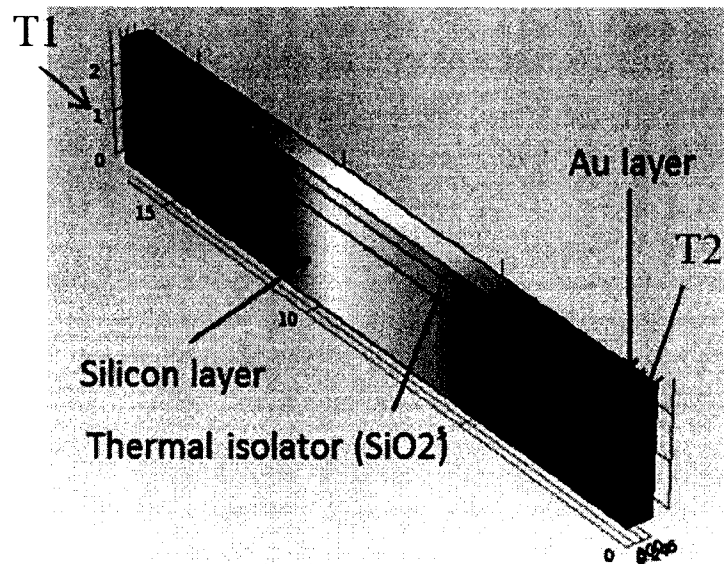


Figure 6-2 A prototype thermoelectric generator with embedded thermal isolator.

Table 6-1 Simulation results of different thickness of isolator layer in thermoelectric generators

Thermoelectric generator	0°C	10°C	20°C	30°C
Without a thermal isolator (μV)	0	154.3	308.7	463
With a 200nm thick thermal isolator (μV)	0	196	391.9	584.7
With a 500nm thick thermal isolator (μV)	0	311	621.5	931.7

In this research, the thermoelectric microgenerator with SWNTs-CuS thin film could generate $\sim 0.01\text{mV}$ which is not quite enough to drive high consumption devices. However, the microgenerator is very small and has the potential to build hundreds and thousands of microgenerators together in parallel or series to enhance current or voltage generation. In addition, some other potential future work is to study the fundamental physics and modeling for the thin film IR sensor and the thermoelectric generator. The

understanding of fundamental physics will help to optimize and redesign the next generation of the hybrid nanomaterial-based applications.

REFERENCES

- [1] L. Shaoxin and P. Balaji, "Optically driven nanotube actuators," *Nanotechnology*, vol. 16, pp. 2548, 2005.
- [2] W. Hoenlein, et al., "Carbon nanotube applications in microelectronics," *Components and Packaging Technologies, IEEE Transactions on*, vol. 27, pp. 629-634, 2004.
- [3] J. Jiang and J. Wang, "Joule heating and thermoelectric properties in short single-walled carbon nanotubes: Electron-phonon interaction effect," *Applied Physics*, vol. 110, 2011.
- [4] P. R. Somani, et al., "Application of metal nanoparticles decorated carbon nanotubes in photovoltaics," *Applied Physics Letters*, vol. 93, pp. 033315-3, 2008.
- [5] Reilly, Raymond M. "Carbon nanotubes: potential benefits and risks of nanotechnology in nuclear medicine," *Nuclear Medicine*, pp. 1039-1042, 2007.
- [6] M. Endo, T. Hayashi, Y. Kim, M. Terrones and M. Dresselhaus, "Applications of carbon nanotubes in the twenty-first century," *Philosophical Transactions of the Royal Society A*, vol. 362, pp. 2223-2238, 2007.
- [7] X. Wang, et al., "Fabrication of ultralong and electrically uniform single-walled carbon nanotubes on clean substrates," *Nano Letters*, vol. 9, pp. 3137-3141, 2009.
- [8] J. Salvetat, et al., "Mechanical properties of carbon nanotubes," *Applied Physics*, vol. 69, pp. 255-260, 1999.
- [9] L. Rui, et al., "Fabrication of platinum-decorated single-walled carbon nanotube based hydrogen sensors by aerosol jet printing," *Nanotechnology*, vol. 23, pp. 505301, 2012.
- [10] R. S. Ruoff, et al., "Mechanical properties of carbon nanotubes: theoretical predictions and experimental measurements," *Comptes Rendus Physique*, vol. 4, pp. 993-1008, 2003.
- [11] Popov, Valentin N. "Carbon nanotubes: properties and application," *Materials Science and Engineering*, 2004.

- [12] M. S. Dresselhaus, et al., "Electronic, thermal and mechanical properties of carbon nanotubes," *Philosophical Transactions of the Royal Society of London. Series A*, vol. 362, pp. 2065-2098, 2004.
- [13] Zhang, Wei, et al. "Chirality dependence of the thermal conductivity of carbon nanotubes," *Nanotechnology*, 2004.
- [14] C. H. W. Michael and H. Jang-Yu, "Thermal conductivity of carbon nanotubes with quantum correction via heat capacity," *Nanotechnology*, vol. 20, pp. 145401, 2009.
- [15] Z. Yonggang, et al., "Carbon nanotubes and thermal properties," *Laser Physics and Laser Technologies*, pp. 72-75, 2010.
- [16] Li, Yuebin, et al. "Copper sulfide nanoparticles for photothermal ablation of tumor cells," *Nanomedicine*, pp. 1161-1171, 2010.
- [17] G. Schmid. "Nanoparticles," *Wiley-Vch Weinheim*, 2003.
- [18] T. Huang and X.-H. N. Xu, "Synthesis and characterization of tunable rainbow colored colloidal silver nanoparticles using single-nanoparticle plasmonic microscopy and spectroscopy," *Materials Chemistry*, vol. 20, pp. 9867-9876, 2010.
- [19] B. D. Dickerson, "Organometallic synthesis kinetics of CdSe quantum dots," *Virginia Polytechnic Institute and State University*, 2005.
- [20] Zhang, Lei Z., Wei Sun, and Peng Cheng. "Spectroscopic and theoretical studies of quantum and electronic confinement effects in nanostructured materials," *Molecules*, pp. 207-222, 2003.
- [21] K. L. Kelly, et al., "The optical properties of metal nanoparticles: the influence of size, shape, and dielectric environment," *Physical Chemistry B*, vol. 107, pp. 668-677, 2003.
- [22] Pop, Eric, Vikas Varshney, and Ajit K. Roy. "Thermal properties of graphene: fundamentals and applications," *MRS Bulletin*, 2012.
- [23] C. N. R. Rao, A. Jay K. Sood, "Graphene: synthesis, properties, and phenomena," *John Wiley & Sons*, pp. 19-25, 2004.
- [24] H. Si. Nalwa. "Nanostructured materials and nanotechnology," *Academic Press*, pp. 329-357, 2002.
- [25] Mizuno, Kohei, et al. "A black body absorber from vertically aligned single-walled carbon nanotubes," *Proceedings of the National Academy of Sciences*, pp. 6044-6047, 2009.

- [26] Leonhardt. "Optical metamaterials: invisibility cup," *Nature Photonics*, pp. 207-208, 2007.
- [28] Mody, Vicky V., et al. "Introduction to metallic nanoparticles," *Pharmacy and Bioallied Sciences*, 2010.
- [29] Keyes, Robert James. "Optical and infrared detectors," *Contemporary Physics*, vol 19, 1980.
- [30] Manbachi, Amir, and Richard SC Cobbold. "Development and application of piezoelectric materials for ultrasound generation and detection," *Ultrasound*, pp. 187-196 2011.
- [32] Ulaby, Fawwaz T., Eric Michielssen, and Umberto Ravaioli. "Fundamentals of applied electromagnetics," *Prentice Hall*, 2010.
- [33] Kasap, Safa O. "Principles of electronic materials and devices," *New York, NY: McGraw-Hill*, vol. 3, 2006.
- [34] "Thin-film's share of solar panel market to double by 2013," renewableenergyworld.com, 2010.
- [35] Pradhan, Basudev, et al. "Carbon nanotube-polymer nanocomposite infrared sensor," *Nano Letters*, pp. 1142-1146, 2008.
- [36] Itkis, Mikhail E., et al. "Bolometric infrared photoresponse of suspended single-walled carbon nanotube films," *Science*, pp. 413-416, 2006.
- [37] Yuan, Longyan, et al. "Self-cleaning flexible infrared nanosensor based on carbon nanoparticles," *ACS Nano*, pp. 4007-4013, 2011.
- [38] Shockley, William, and Hans J. Queisser. "Detailed balance limit of efficiency of p-n junction solar cells," *Applied Physics*, pp. 510-519, 2004.
- [39] J. Nelson. "The physics of solar cells," *Imperial College Press*, 2003.
- [40] R.T. Ross and A.J. Nozik, "Efficiency of hot-carrier solar energy converters," *Applied Physics*, vol. 53, 3813-3818, 1982.
- [41] Chronis, Nikolas, et al. "Tunable liquid-filled microlens array integrated with microfluidic network," *Optics Express*, pp. 2370-2378, 2003.
- [42] S.M. Sze. "Physics of semiconductor devices," *John Wiley & Sons*, 1981.
- [43] Kao, Pin-Hsu, et al. "Fabrication and characterization of CMOS-MEMS thermoelectric micro generators," *Sensors*, pp. 1315-1325, 2010.

- [44] Huesgen, Till, Peter Woias, and Norbert Kockmann. "Design and fabrication of MEMS thermoelectric generators with high temperature efficiency," *Sensors and Actuators A: Physical*, pp. 423-429, 2008.
- [45] Tseng, Yi-Hsuan, et al. "Optical and thermal response of single-walled carbon nanotube–copper sulfide nanoparticle hybrid nanomaterials," *Nanotechnology*, 2012.
- [46] Gong, Zhongcheng, et al. "A micromachined carbon nanotube film cantilever-based energy cell," *Nanotechnology*, vol. 23, 2012.
- [47] Kotipalli, Venu, et al. "Light and thermal energy cell based on carbon nanotube films," *Applied Physics Letters*, vol. 97, 2010.
- [48] Gong, Zhongcheng, et al. "Studies of self-reciprocating characteristic of carbon nanotube film-based cantilevers under light and thermal radiation," *Nanoscience and Nanotechnology*, vol. 12, pp. 350-355, 2012.
- [49] Eder, Dominik. "Carbon nanotube-inorganic hybrids," *Chemical Reviews*, vol. 110, pp. 1348-1385, 2010.
- [50] Chen, Jian, et al. "Solution properties of single-walled carbon nanotubes," *Science*, vol. 282, pp. 95-98, 1998.
- [51] Zhang, Jun, et al. "Visible light photocatalytic H₂-production activity of CuS/ZnS porous nanosheets based on photoinduced interfacial charge transfer," *Nano Letters*, vol. 11, pp. 4774-4779, 2011.
- [52] Lee, Mikyung, and Kijung Yong. "Highly efficient visible light photocatalysis of novel CuS/ZnO heterostructure nanowire arrays," *Nanotechnology*, vol. 23, 2012.
- [53] Zhan, Zhaoyao, et al. "Photoresponse of multi-walled carbon nanotube–copper sulfide (MWNT–CuS) hybrid nanostructures," *Physical Chemistry Chemical Physics*, vol. 13, pp. 20471-20475, 2011.
- [54] Olek, Maciej, et al. "Quantum dot modified multiwall carbon nanotubes," *the Physical Chemistry B*, vol. 110, pp. 12901-12904, 2006.
- [55] Li, Xianglong, Yi Jia, and Anyuan Cao. "Tailored single-walled carbon nanotube–CdS nanoparticle hybrids for tunable optoelectronic devices," *ACS Nano*, vol. 4.1, pp. 506-512, 2009.

- [56] Shim, Moonsub, et al. "Polymer functionalization for air-stable n-type carbon nanotube field-effect transistors," *The American Chemical Society*, vol. 123, pp. 11512-11513, 2001.
- [57] Ratanatawanate, Chalita, Amy Chyao, and Kenneth J. Balkus Jr. "S-nitrosocysteine-decorated PbS QdS/tio₂ nanotubes for enhanced production of singlet oxygen," *The American Chemical Society*, vol. 133, pp. 3492-3497, 2011.
- [58] HE, Jin-Song, et al. "Thermodynamics, kinetics, and structure chemistry," *Acta Phys Chim Sin*, vol. 27, pp. 2499-2504, 2011.
- [59] Li, Yuebin, et al. "Copper sulfide nanoparticles for photothermal ablation of tumor cells," *Nanomedicine*, vol. 5, pp. 1161-1171, 2011.
- [60] Lakshmanan, Santana Bala, et al. "Local field enhanced Au/CuS nanocomposites as efficient photothermal transducer agents for cancer treatment," *Biomedical Nanotechnology*, vol. 8.6, pp. 883-890, 2012.
- [61] Kasap, Safa O. "Principles of electronic materials and devices," vol. 3. *New York, NY: McGraw-Hill*, 2006.
- [62] Wang, Xue-ying, Zhen Fang, and Xiu Lin. "Copper sulfide nanotubes: facile, large-scale synthesis, and application in photodegradation," *Nanoparticle Research*, vol. 11, pp. 731-736, 2009.
- [63] Wu, Zhuangchun, et al. "Transparent, conductive carbon nanotube films," *Science*, vol. 30, pp. 1273-1276, 2004.
- [64] Salleh, Faiz, et al. "Seebeck coefficient of ultrathin silicon-on-insulator layers," *Applied Physics Express*, vol. 2.7, 2009.
- [65] Zeng, Nan, and Anthony B. Murphy. "Heat generation by optically and thermally interacting aggregates of gold nanoparticles under illumination," *Nanotechnology* vol. 20, 2009.
- [66] Moon, Hye Kyung, Sang Ho Lee, and Hee Cheul Choi. "In vivo near-infrared mediated tumor destruction by photothermal effect of carbon nanotubes," *ACS Nano*, vol. 3, pp. 3707-3713, 2009.
- [67] Zhang, Y., and S. Iijima. "Elastic response of carbon nanotube bundles to visible light," *Physical Review Letters*, vol. 82, 1999.
- [68] Snyder, G. Jeffrey, and Eric S. Toberer. "Complex thermoelectric materials," *Nature Materials*, vol. 7, pp. 105-114, 2008.

- [69] Kind, Hannes, et al. "Nanowire ultraviolet photodetectors and optical switches," *Advanced Materials*, vol. 14, 2002.
- [70] Itkis, Mikhail E., et al. "Bolometric infrared photoresponse of suspended single-walled carbon nanotube films," *Science*, vol. 312, pp. 413-416, 2006.
- [71] Yuan, Longyan, et al. "Flexible solid-state supercapacitors based on carbon nanoparticles/MnO₂ nanorods hybrid structure," *ACS Nano*, vol. 6, pp. 656-661, 2011.
- [72] Snyder, G. J. "Thermoelectric power generation: efficiency and compatibility," *Macro to Nano*, 2006.
- [73] Crosbie, Michael J., ed. "The passive solar design and construction," *John Wiley & Sons*, 1998.
- [74] Pejic, Bobby, Matthew Myers, and Andrew Ross. "Mid-infrared sensing of organic pollutants in aqueous environments," *Sensors*, vol. 9, pp. 6232-6253, 2009.
- [75] Flavin, Kevin, Helen Hughes, and Peter McLoughlin. "The development of a novel smart mid-infrared sensing methodology for residual solvents," *Environmental and Analytical Chemistry*, vol. 87.1, pp. 29-42, 2007.
- [76] Tsai, C. F., and Ming-Shing Young. "Pyroelectric infrared sensor-based thermometer for monitoring indoor objects," *Review of Scientific Instruments*, vol. 74, pp. 5267-5273, 2003.
- [77] Maldague, X. P. V., et al. "Chapter 2: Fundamentals of infrared and thermal testing: part 1. principles of infrared and thermal testing," *Nondestructive*, vol. 3, 2001.
- [78] Bertozzi, Massimo, et al. "Pedestrian detection for driver assistance using multiresolution infrared vision," *Vehicular Technology, IEEE Transactions on*, vol. 53, pp. 1666-1678, 2004.
- [79] Masek, J., et al. "Monolithic photovoltaic PbS-on-Si infrared-sensor array," *Electron Device Letters, IEEE*, vol. 11, pp. 12-14, 1990.
- [80] Gorbunov, V., et al. "Biological thermal detection: micromechanical and microthermal properties of biological infrared receptors," *Biomacromolecules*, vol. 3, pp. 106-115, 2001.
- [81] Henini, Mohamed, and Manijeh Razeghi, eds. "Infra-red detection technologies," *Elsevier*, 2002.

- [82] Itkis, Mikhail E., et al. "Bolometric infrared photoresponse of suspended single-walled carbon nanotube films," *Science*, vol. 312, pp. 413-416, 2006.
- [83] Zhang, Jiangbo, et al. "Design, manufacturing, and testing of single-carbon-nanotube-based infrared sensors," *Nanotechnology*, vol. 8, pp. 245-251, 2009.
- [84] Gong, Zhongcheng, et al. "A micromachined carbon nanotube film cantilever-based energy cell," *Nanotechnology*, vol. 23, 2012.
- [85] Kometani, Noritsugu, et al. "Preparation and optical absorption spectra of dye-coated Au, Ag, and Au/Ag colloidal nanoparticles in aqueous solutions and in alternate assemblies," *Langmuir*, vol. 17, pp. 578-580, 2001.
- [86] Link, Stephan, and Mostafa A. El-Sayed. "Spectral properties and relaxation dynamics of surface plasmon electronic oscillations in gold and silver nanodots and nanorods," *Physical Chemistry B*, vol. 103, pp. 8410-8426, 1999.
- [87] HE, Jin-Song, et al. "Thermodynamics, kinetics, and structure chemistry," *Acta Phys Chim Sin*, vol. 27, pp. 2499-2504, 2011.
- [88] A. L. Rogach, et al., "Synthesis and characterization of a size series of extremely small thiol-stabilized CdSe nanocrystals," *Physical Chemistry B*, vol. 103, pp. 3065-3069, 1999.
- [89] L. Qi, et al., "Synthesis and characterization of CdS nanoparticles stabilized by double-hydrophilic block copolymers," *Nano Letters*, vol. 1, pp. 61-65, 2000.
- [90] Yoshino, Taiki, et al. "Three-dimensional photomobility of crosslinked azobenzene liquid-crystalline polymer fibers," *Advanced Materials*, vol. 22, pp. 1361-1363, 2010.
- [91] B. Wan, W. Wang, K. Liao and J. Lu, Int. J. Mod," Seebeck effect in carbon nanotube films," *Modern Physics B*, vol. 19, pp. 643-645, 2005.
- [92] D. Eder, "Carbon nanotube inorganic hybrids," *Chemical Reviews*, vol. 110, pp. 1348-1385, 2010.
- [93] Nath, Manashi and Teredesai, Pallavi V and Muthu, DVS and Sood, AK and Rao, CNR, "Single-walled carbon nanotube bundles intercalated with semiconductor nanoparticles," *Current Science*, vol. 85, pp. 956-960, 2003.
- [94] Jeffrey Snyder, G. "Combination of large nanostructures and complex band structure for high performance thermoelectric lead telluride," *Energy & Environmental Science*, vol. 4, pp. 3640-3645, 2011.
- [95] G. S. Nolas, et al. "Thermoelectrics: basic principles and new materials developments," *Physics and Astronomy*, vol. 45, 2001.

- [96] G. J. Snyder, J. R. Lim, C. Huang, and J. Fleurial, "Thermoelectric microdevice fabricated by a MEMS-like electrochemical process," *Nature Materials*, vol. 2, pp.528-531, 2003.
- [97] C. Gould and N. Shamma, "A review of thermoelectric MEMS devices for micro power generation, heating and cooling applications," *InTect*, 2009.
- [98] Bottner, Harald, et al. "New thermoelectric components using microsystem technologies," *Microelectromechanical Systems*, vol. 13, pp. 414-420, 2004.
- [99] Silva, Gabriel A. "Introduction to nanotechnology and its applications to medicine," *Surgical Neurology*, vol. 61, pp. 216-220, 2004.
- [100] G. Schmid. "Nanoparticles," *Wiley-Vch Weinheim*, 2004.
- [101] H. Budzier and G. Gerlach, "Thermal infrared sensors: theory," *Optimisation and Practice*, pp. 149-251, 2011.
- [102] A. Rogalski, "Infrared detectors: CRC Press," 2010.
- [103] S. O. Kasap. "Principles of electronic materials and devices," *New York, NY: McGraw-Hill*, vol. 3, 2006.